MODELING, CONTROL AND PARAMETER ESTIMATION FOR THE MAIN COOLING SYSTEM OF A SEAWATER-COOLED CHP PLANT

Authors: Jens Jørgen Møller Nielsen
                Pablo Fernández López

Supervisors: Palle Andersen
                Tom S. Pedersen

Control and Automation, Spring 2014

BREAKING NEW GROUND

AALBORG UNIVERSITY

AALBORG UNIVERSITY

DENMARK

Synopsis:

Title:

Modeling, Control and Parameter Estimation for the Main Cooling System of a Seawater-Cooled CHP Plant.

Project period:
Control and Automation
4. semester, Spring 2014

Project group:
1030

Group members:
Jens Jørgen M. Nielsen
Pablo Fernández López

Supervisors:
Palle Andersen
Tom S. Pedersen

Pages: 133

Appendix: 6

Project finished:
04/06/2014

This project has been proposed by Rambøll Danmark A/S to improve the control strategy of the main cooling system in the Studstrup power plant, operated by DONG Energy. The project first analyses the current control of the pumps which supply seawater to the steam condenser of the power plant. The current project assesses the feasibility of improving the strategy by finding the main states involved in the plant operation.

Models are derived for both the hydraulic and the thermodynamic parts of the main cooling system. The model has a focus on simulating the observed outputs based on the most relevant parameters of the plant operation. Furthermore, a more reliable way to estimate the flow of seawater in the system has been proposed. The ultimate goal of the control strategy proposed in this project is to take the plant to its best efficiency point for the current conditions, which will be given by the condensation pressure. Therefore, the control structure aims to achieve and maintain the reference pressure in the steam condenser.

Additionally, the solution must respect a set of constraints imposed by the environmental policy and the physical limits of the machinery. The theoretical models have been fitted to operational data from Studstrup, but general nature of the method makes it applicable to other power plants without major modifications.

In order to fulfill these requirements, two solutions have been proposed: a first approach based on an inner and outer loop control using PI and integral regulators and a second solution based on Model Predictive Control.

AALBORG UNIVERSITY

DENMARK

Titel:

Modellering, Kontrol og Parameterestimering for Hovedkølesystemet i et Havvandskølet Kraftvarmeværk.

Projekt periode:

Kontrol og Automation
4. semester, Forår 2014

Projekt gruppen:

1030

Gruppens medlemmer:

Jens Jørgen M. Nielsen
Pablo Fernández López

Vejleder:

Palle Andersen
Tom S. Pedersen

Sider: 133

Bilag: 6

Projekt færdigt:

04/06/2014

Synopsis:

Dette projekt er foreslået af Rambøll Danmark A/S for at forbedre kontrolstrategien af hovedkølesystemet i Studstrup kraftvarmeværk, styret af DONG Energi. Projektet analyserer først den nuværende kontrol af pumperne som leverer havvand til dampkondensatoren i kraftvarmeværket. Det aktuelle projekt vurderer mulighederne for at forbedre strategien ved at finde de vigtigste tilstande, der er involveret i driften af værket. Modeller er afledt for både den hydrauliske og termodynamiske del af hovedkølesystemet. Modellens fokus er at simulere de observerede resultater af relevante parameter for anlæggets drift. Desuden er der foreslået en mere pålidelig måde at estimere havvands gennemstrømningen i systemet. Det ultimative mål for kontrol strategien foreslået i dette projekt, er at få værket til det mest effektive arbejdspunkt under de givne forhold, hvilket er givet ved kondensator trykket. Derfor har kontrolstrukturen til formål at opnå og fastholde referencetrykket i dampkondensatoren. Derudover skal løsningen overholde en række begrænsninger pålagt af miljøregler og fysiske grænser af maskinerne. De teoretiske modeller er blevet tilpasset operationelle data fra Studstrup, men den generelle fremgangsmåde muliggør samme anvendelse ved andre kraftværker uden større modifikationer. For at opfylde disse krav er to løsninger blevet foreslået: den første fremgangsmåde er baseret på en indre og ydre sløjfe styring ved brug af en PI og integrerede regulatorer og den anden løsning er baseret på model prædiktiv kontrol.

Acknowledgements

The authors would like to thank their supervisors Tom S. Pedersen and Palle Andersen for their support, ideas and feedback during the development of the project.

Special thanks to Lukas Hanspach for proposing the project and answering questions related to its operation, as well as introducing the CHP plant along with Kai C. Jensen

Preface

This thesis has been proposed by the engineering consulting company Rambøll Danmark A/S in order to investigate possible improvements on the control of the main cooling system for the Studstrup CHP plant, run by DONG Energy. The project was proposed by Lukas F. Hanspach, who is working at Rambøll as SCADA (Supervisory Control and Data Acquisition) engineer.

The documentation of the project is written in English and is a research report. It documents the chronology, methods, results and conclusions. A nomenclature is made to explain terms and abbreviations of words, that might be unclear to the reader. References to documentation are made according to the Harvard-method, where a link is made in the text pointing to a specific source in the bibliography. On the CD attached references to electronic documents, references and various other material can be found. The 💿 symbol will tell when there is material to be found on the cd.

Jens Jørgen Møller Nielsen	Pablo Fernández López

Nomenclature

Abbreviations

AAU	Aalborg Universitet
BEP	Best Efficiency Point
CHP	Combined Heat and Power
DH	District Heating
EKF	Extended Kalman Filter
FOPDT	First Order Plus Dead Time
IMC	Internal Model Control
LKF	Linear Kalman Filter
LMTD	Log Mean Temperature Difference
LQG	Linear Quadratic Gaussian
MSE	Minimum Squared Error
MPC	Model Predictive Control
NPSH	Net Positive Suction Head
PI	Proportional Integral
PID	Proportional Integral Derivative
SISO	Single-Input-Single-Output

Contents

Part I

Introduction

Introduction 1

As part of Europe's effort to achieve a more efficient and environment-friendly way to meet energy demand, a 2004 EU directive [European Directive 2004/8/EC, 2004] was introduced (which took effect in 2007) promoting the use of cogeneration in its Member States. Every year, Member States are obliged to produce reports on the state of cogeneration in the country and the state efforts to promote it. Denmark is one of the leaders in Europe in combined heat and power production.

1.1   Energy in Denmark

As for 2010, 38.6 TWh of electricity were produced in Denmark [International Energy Agency, 2011], of which 44% came from coal; 20% from gas; 20% from wind power and 13% from biofuels, as shown in Figure 1.1. Other sources account for the remaining 3% of the energy supply.

Energy Production in Denmark, by source
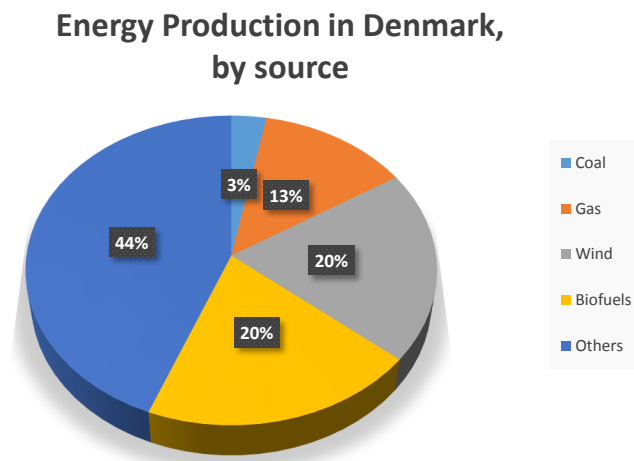
Figure 1.1. Sources of energy production in Denmark in 2010. Elaborated from data in [International Energy Agency, 2011].

In addition to electricity, it is necessary to provide District Heating to the approximately 2.5 million households in Denmark that receive heat from the public heat supply. According to data retrieved from the Danish Energy Agency [Danish Energy Agency, 2014b], the heat is supplied from the sources shown in Figure 1.2.

Heat Production in Denmark, by source

- CHP - Large cities
- Oil
- CHP - small and medium cities
- Natural gas
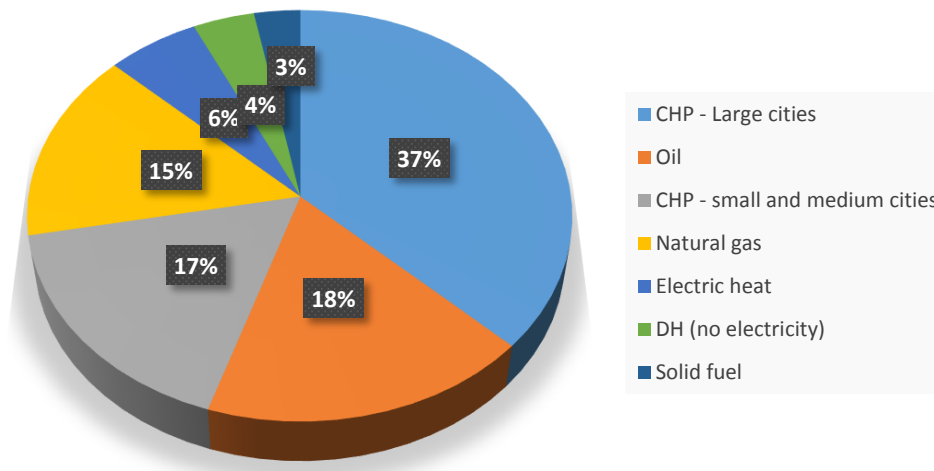- Electric heat
- DH (no electricity)
- Solid fuel

Figure 1.2. Current sources for heat supply in Denmark. Elaborated from data in [Danish Energy Agency, 2014b].

Combined Heat and Power (CHP) plants provide District Heating (DH) at the same time as electricity (a process also known as cogeneration). Compared to the separate production of electricity and heating, it is estimated that fuel consumption is reduced by 30% ([Danish Energy Agency, 2014b]).

1.2 CHP in Denmark

In Denmark district heating (DH) is either supplied from a heating plant or a combined heat and power plant (CHP). Public heat supply DH plants are either centralised or decentralised, where the centralised plants are in the area of the larges cities and the decentralised plants are in the area of the smaller cities. In Denmark there are 16 centralised CHP plants, 285 decentralised CHP plants and 130 decentralised heating plants that supply public heating. One third of the decentralised heating plants and one seventh of the decentralised CHP plants are using environmentally friendly fuels such as wood chips, wood pellets, straw, biogas or waste, where the rest of the decentralised plants are using natural gas [Danish Energy Agency, 2014a].

1.2.1 CHP by DONG Energy

In Denmark the largest supplier of DH is DONG Energy, where one third of the markets heating is delivered by DONG [DONG Energy, 2014b]. In Figure 1.3 the location of the different power plants in Denmark owned by DONG Energy is shown. One of the central CHP plants owned by DONG Energy is Studstrupværket. It uses both straw and coal in the process of heating and power production. In the start-up of the plant as well as in some special operating situations fuel oil is used. Studstrupværket is producing heat and power, but can, if necessary, produce power without heat production. In order to handle periodically high demand of district heating, a storage tank is filled at suitable times.

Figure 1.3. Power plants in Denmark owned by DONG Energy [DONG Energy, 2014a].

Studstrup Power Plant 2

In this chapter general information about the Studstrup power plant will be presented. The cooling system in the power plant will be examined, where the steam flow estimation, seawater flow estimation and pump control will be explained.

2.1 General Information

Studstrup power plant was in 1968 established in Kalø Bay. Today the power plant is composed by a unit 3 and unit 4, where both units has been in operation since 1984 and 1985. In 1998 and 1999 the units 1 and 2 were scrapped. The maximum net power that can be produced in the two units is 350 MW and maximum heat production is 455 MJ/s [DONG Energy, 2014a]. There are two factors that determine the production of power, the first one is the supply and demand for power on the Nordic power market and the second one are the power and fuel prices. The heat produced for DH is either stored in a storage tank or sent into the DH grid. The storage tank at Studstrupværket is the largest pressurised storage tank in the world. The size of the storage tank makes it possible to generate heat and power at all time and thereby get the optimum economic and environmental use of the fuel. Studstrupværket is selling the produced heat to the municipal DH companies in Aarhus. In Figure 2.1 the DH network near Aarhus is shown.
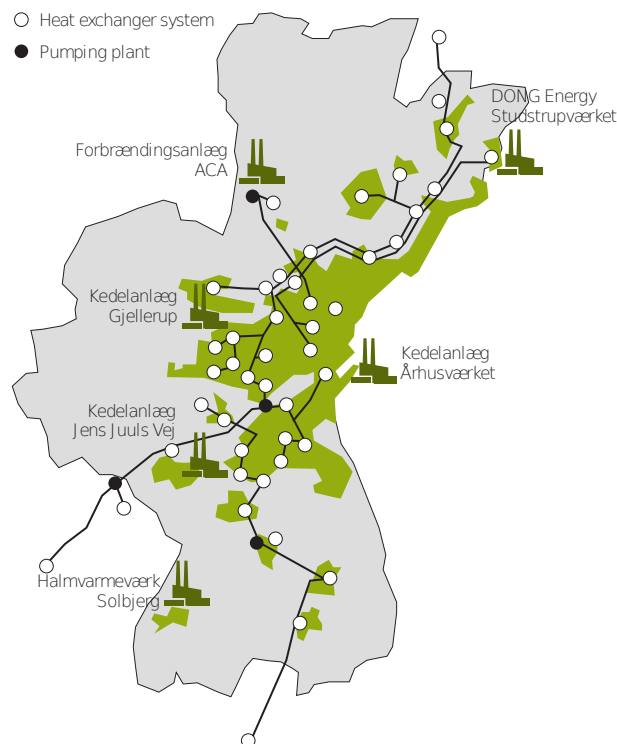

Figure 2.1. Transmission system in Aarhus [DONG Energy, 2014a].

2.2 Overview of The Power Plant

In Figure 2.2 the work flow of Studstrupværket is shown. The water to the boiler is demineralised water. The water is heated in the furnace and is in that process converted into steam. The steam is leaving the boiler with a temperature of 540°C and flows to the first part of the turbine, where the pressure is 250 bar. The turbine is divided in three parts. In the first part of the turbine some of the energy in the steam is converted into electrical energy. The steam is then led back to the boiler to be reheated. The second part of the turbine is converting some of the energy in the steam from the reheater to electrical energy. The third part of the turbine is using some of the steam from the second part of the turbine to generate electrical energy. The rest of the steam from the second part of the turbine is used to generate heat for DH. There are two district heat exchangers at the power plant, where the steam is cooled and returned to the boiler. The steam from the third part of the turbine is led to a condenser, where seawater is used to cool the steam. The condenser consists of more than 15000 pipes, where the seawater passes through. In the cooling process the steam becomes water again, where the water is led back to the boiler [DONG Energy, 2014a].

1. Coal
2. Coal silos
3. Coal mill
4. Air and coal dust
5. Burners
6. Furnace
7. Boiler walls
8. Turbine
9. Generator
10. District heat exchanger
11. Condenser
12. Storage tank
13. Bottom ash
14. DeNOx plant
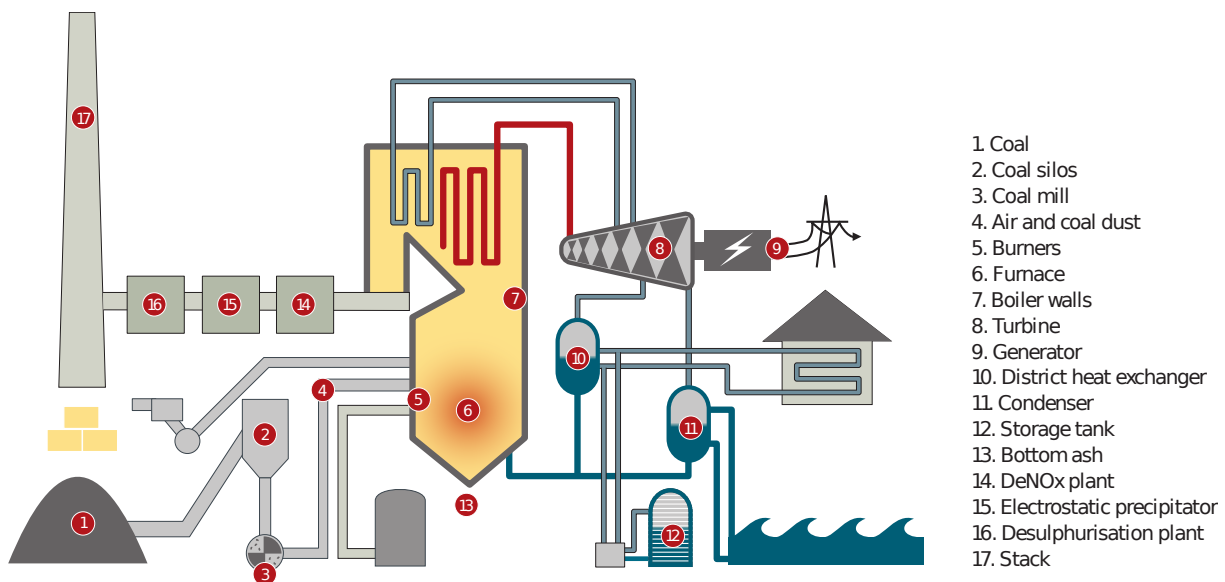15. Electrostatic precipitator
16. Desulphurisation plant
17. Stack

Figure 2.2. Overview of the Studstrup power plant [DONG Energy, 2014a].

2.3 Cooling of The Steam

In Figure 2.3 the sensors related to the monitoring of the steam is shown. The measured steam flow to the reheater and the measured energy to the DH are used to calculate the amount of steam to the condenser. The calculation of the steam is shown in Equation 2.1. The case one is used, when the high pressure preheating is switched off and the case two is used, when it is switched on. The static values in the equation have been found heuristically by DONG.

$$\dot{m}_{con} = \begin{cases} 1.1 \cdot K_1 \cdot \dot{m}_{HP} - K_2 \cdot P_{DH} & \text{Case 1} \\ K_1 \cdot \dot{m}_{HP} - K_2 \cdot P_{DH} & \text{Case 2} \end{cases} \tag{2.1}$$

where:

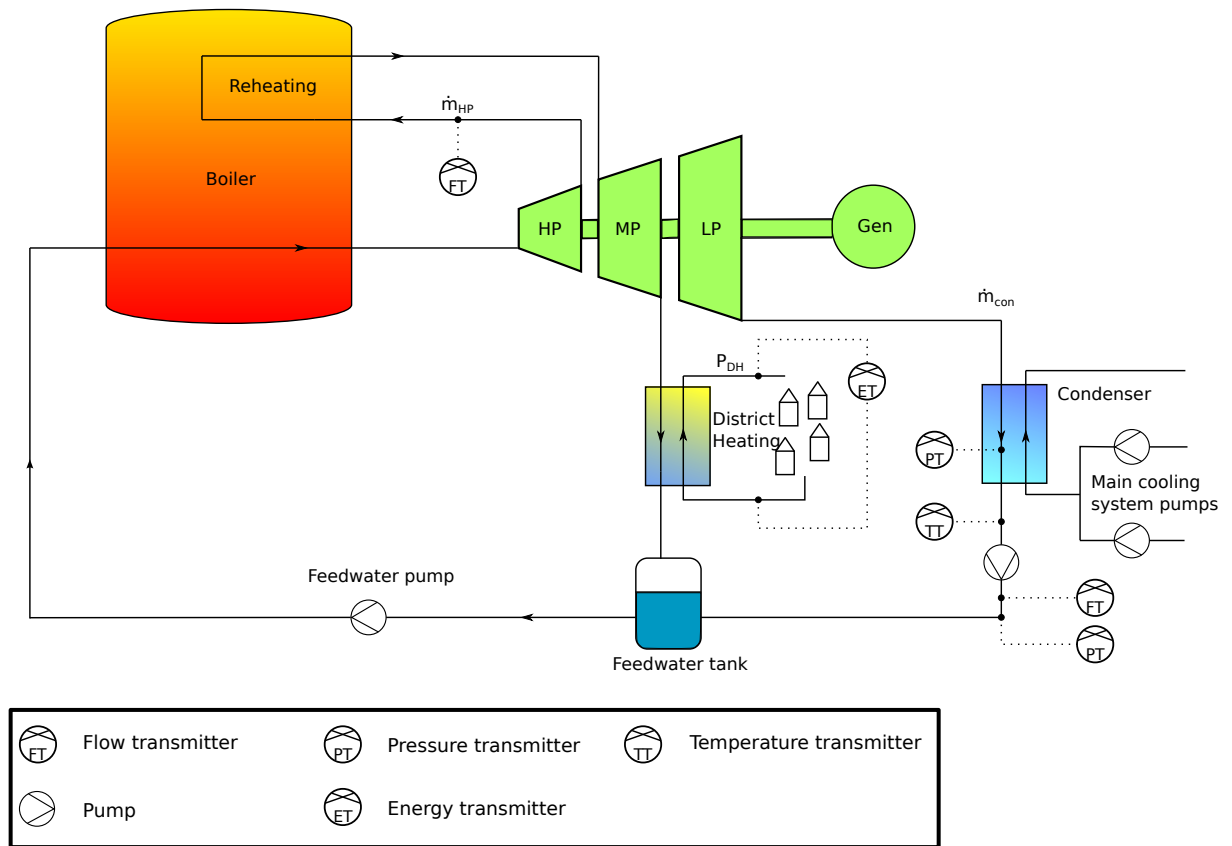|		
$\dot{m}_{con}$	Mass flow of the steam to the condenser	[kg/s]
$\dot{m}_{HP}$	Mass flow of the steam from the high pressure turbine	[kg/s]
P_{DH}	The amount of energy to the DH	[MJ/s]
K_1	Constant and is 0.334	[-]
K_2	Constant and is 0.16	[-]

Figure 2.3. Schematic of the Studstrup power plant.

From the calculated steam flow to the condenser, the needed revolutions per minutes (RPM) in the main cooling pumps can be found. At Studstrup the RPM is found through heuristic functions. There are a number of functions, where the function that will be used is depending on the temperature of the seawater. In Figure 2.4 this is depicted by the function number n, that is chosen from the seawater temperature. From the steam flow a reference value is found by the function. This reference value is used in another function to find the RPM needed in the pumps to cool the steam. The RPM is not allowed to change more than 15 RPM per second.
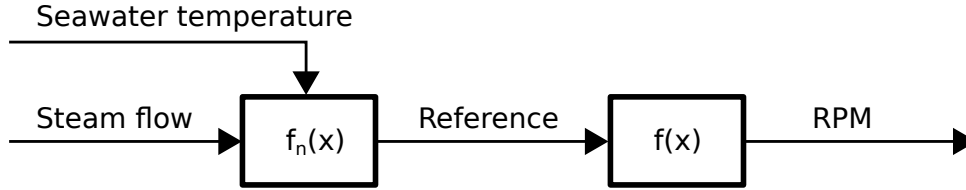

Figure 2.4. From steam flow to RPM, where the function number n is chosen from the seawater temperature.

There are two condensers in the main cooling system, where only one of them is shown in Figure 2.5. The other condenser is connected to the first one and they are identical. The strainer in the diagram is a part of a pipe cleaning system. The seawater contains different kind of impurities that will accumulate in the pipes if not removed. The cleaning system uses cleaning balls to clean the pipes in the condenser, where the balls are injected into the seawater at the inlet of the condenser. The balls are distributed in the pipes, where they clean the condenser. At the outlet of the condenser, the balls are collected in the strainer and pumped back to the inlet of the condenser [TAPROGGE, 2014]. The mass flow of the seawater is calculated by Equation 2.2, where the equation had been made heuristically by DONG. The equation uses the quadratic relationship between the pressure and flow in a pipeline.

$$\dot{m}_{seawater} = 18690 \cdot \sqrt{\Delta P_{con1} + \Delta P_{con2}} \qquad (2.2)$$

where:
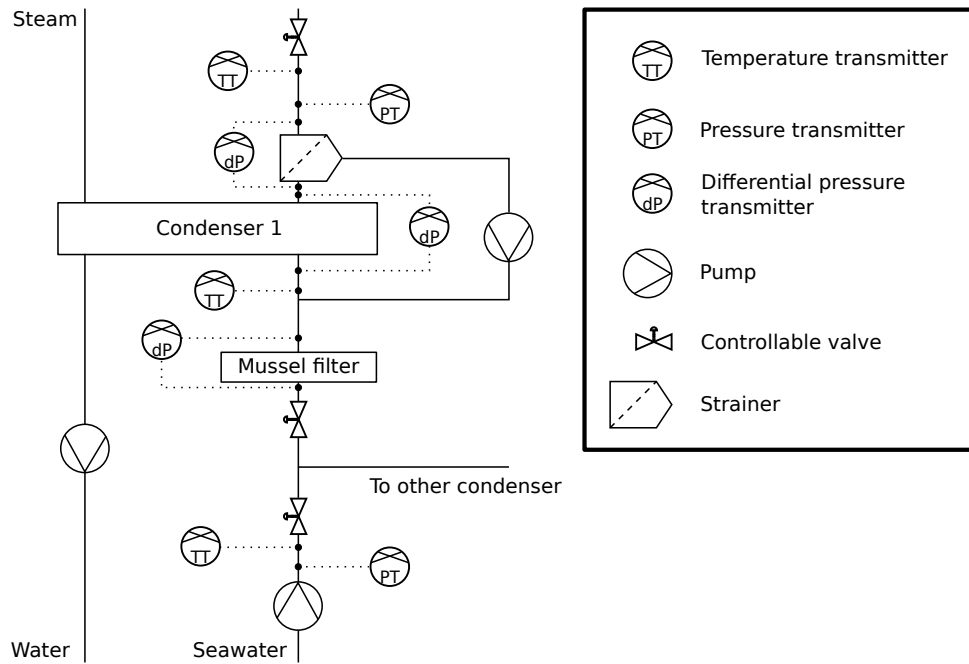|		
$\dot{m}_{seawater}$	Mass flow of the seawater to the condenser	[kg/s]
ΔP_{con1}	Pressure loss across the condenser number 1	[bar]
ΔP_{con2}	Pressure loss across the condenser number 2	[bar]

Figure 2.5. Seawater circuit diagram.

In Figure 2.6 the seawater intake and outlet is shown. The seawater is pumped from the bottom of a basin, where the water level of the basin is depending on the water level of the sea. As there is an offset in the measurements due to sensor placement, the water level from the pump placement is calculated by Equation 2.3.
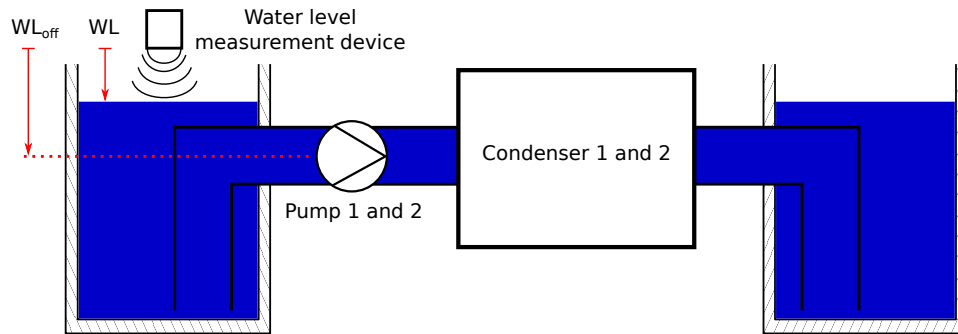
Figure 2.6. Seawater inlet and outlet, where WL is the water level measured from the sensor placement to the water surface and WL_{off} is the offset given by the length from the sensor placement to the pump placement.

$$WL_{pump} = WL_{off} - WL \tag{2.3}$$

where:

WL_{pump}	Water level from the pump placement	[m]
WL	Water level measured by sensor	[m]
WL_{off}	Offset in the water level measurement, which is 2.58	[m]

Working principle of a CHP plant 3

CHP or cogeneration plants are capable of providing both heat and electrical power simultaneously. In order to do so, they typically use a Rankine cycle with reheating and/or regenerative preheating. This chapter will introduce the general principles involved in the working principle of a power plant and its cooling system.

3.1   The Rankine cycle

The Rankine cycle models the process by which steam-operated engines generate power. Its most basic type consists of 4 basic steps, as it can be seen in Figure 3.1:

- 1-2: expansion in the turbine. The steam loses pressure and causes the rotation of the blades of the turbine. This is ideally and isentropic process and thus it is represented by a vertical line on the T-s diagram.
- 2-3: condensation of the steam until the liquid is in saturated conditions. This step takes place in the condenser, where the working fluid releases its heat towards the coolant.
- 3-4: the pressure of the sub-cooled water is increased by the feedwater pump. There is a slight increase of temperature during this process.
- 4-1: the fluid is heated in the boiler at a constant pressure (isobaric). In the figure the fluid only reaches saturation conditions. Heating beyond this point is known as superheating.
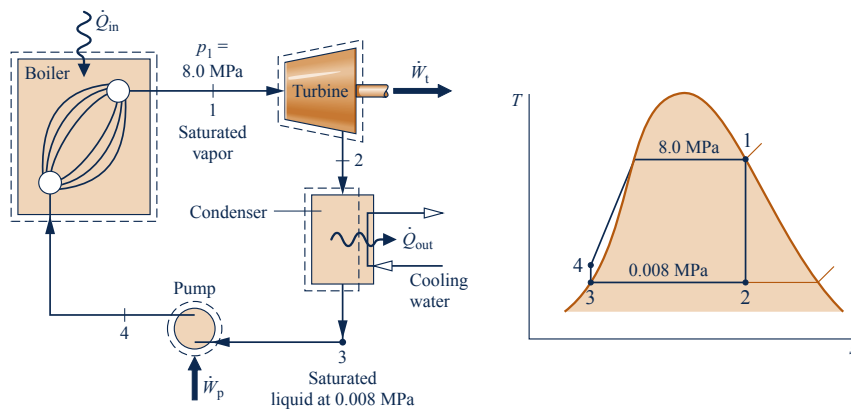

Figure 3.1. Basic Rankine cycle and corresponding T-s diagram [Michael J. Moran, 2005]

3.1.1 Superheating, reheating and regeneration

The aforementioned cycle is the most simple realization, and further improvements are necessary for it to be implementable in a real system. In Figure 3.1, the fluid was only heated until its saturation point. However, this implies that when it is expanded in the turbine, an increasing fraction of liquid will be present within the mixture. The water droplets may impact against the spinning blades of the turbine at great speed, causing additional strain on the blades and shaft and erosion on the surface of the blades. It is therefore of interest that the outlet of the turbine is saturated vapour with high quality (very low or no content of liquid).

Figure 3.2 shows a Rankine cycle where the steam is superheated at the output of the boiler (1). After the first expansion in the high pressure turbine (2), the steam is sent back to the boiler and reheated (3). At this point, the pressure of the steam is lower than in (1), and the steam will undergo a second expansion in the low pressure turbine (4). The remaining steps (condensation 4-5 and pump 5-6) are identical to the previous case. The point (4') is the theoretical state that would be reached if there was no reheating between the expansion in the high pressure turbine and the low pressure turbine.
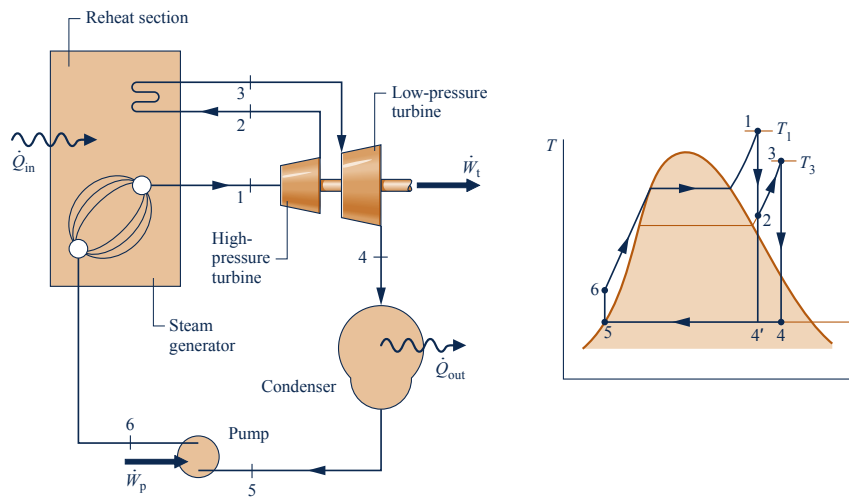

Figure 3.2. Rankine cycle with superheating and reheating [Michael J. Moran, 2005].

An additional method for improving the performance of a vapour power cycle is regenerative feedwater heating. It consists in preheating the fluid before it enters the boiler using an extraction from the turbine. Figure 3.3 shows a Rankine cycle with regeneration. A small amount of fluid (y) is extracted after the high pressure stage of the turbine (2) in order to preheat the water from (5) to (6). The points (2s) and (3s) represent the final state of the fluid if the expansion in the turbine was ideal (i.e., isentropic). However, this is not the case in a real cycle. An increase of entropy will always occur due to the irreversibility of the expansion process (Second Law of Thermodynamics), so the final states after the expansion will actually be (2) and (3). The heater represented in Figure 3.3 is open, meaning that the fluids are in direct contact and are therefore required to have the same pressure. A closed heat exchanger allows the streams of fluid to be at different pressures during the preheating.
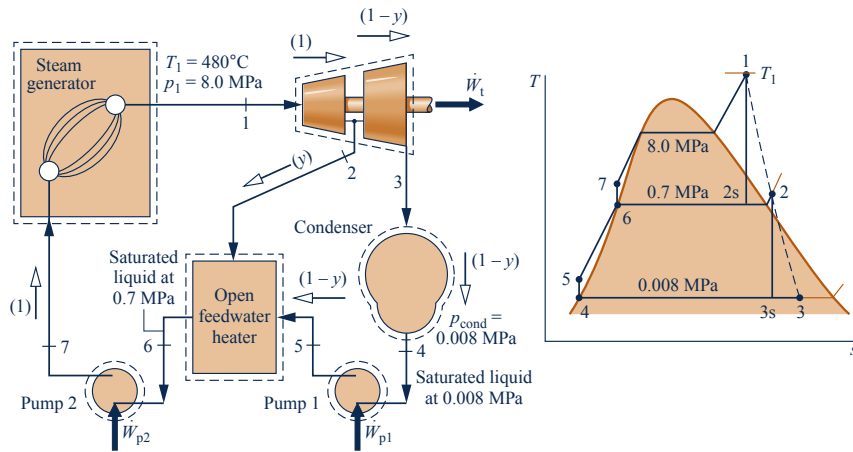

Figure 3.3. Rankine cycle with regeneration [Michael J. Moran, 2005]

3.1.2 The supercritical cycle

If the working fluid is heated beyond the critical point (above the saturation curve of the fluid), it will become supercritical fluid. An example of a supercritical cycle with reheating is shown in Figure 3.4.
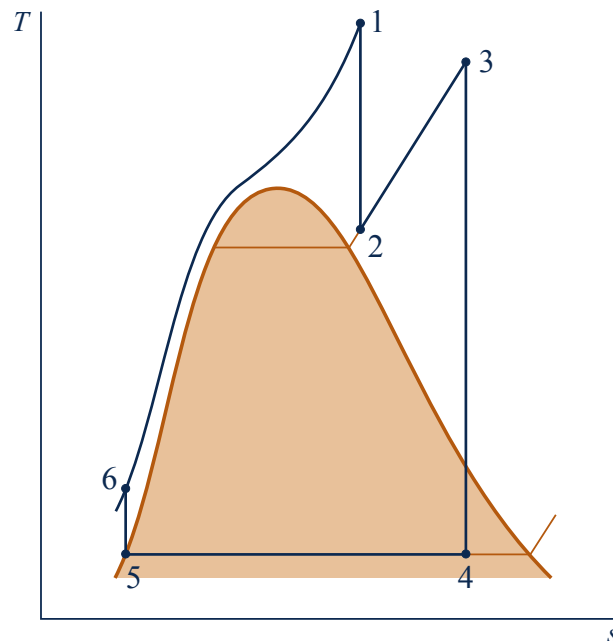

Figure 3.4. Supercritical Rankine cycle [Michael J. Moran, 2005].

3.1.3 District Heating

The distinctive feature of CHPs is that they not only deliver electricity to the grid, but they also provide DH. The DH heat exchanger acts as a medium temperature condenser, where the heat of the steam before its final expansion in the low pressure turbine takes place. An example of such cycle is shown in Figure 3.5. It can be summarized in the following steps:
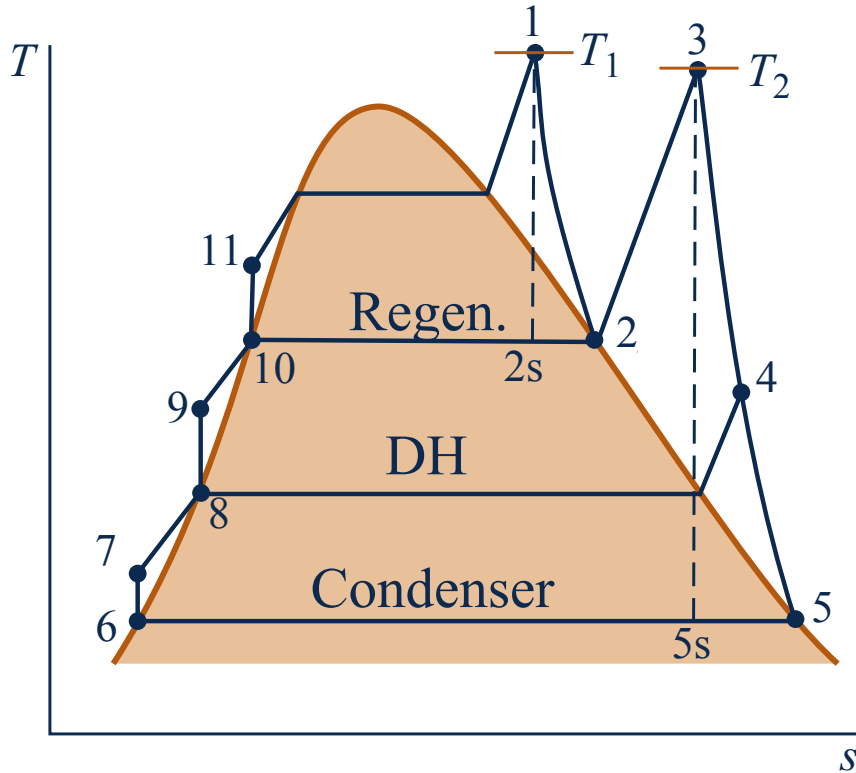

Figure 3.5. Regenerative Rankine cycle of a CHP plant with reheating.

- **1-2:** Expansion in the high pressure stage of the turbine. 2s represents the hypothetical point that would be reached in an isentropic expansion.
- **2-3:** The steam at the outlet of the high pressure stage of the turbine is led back to the boiler and reheated to a temperature T_2.
- **2-10:** An amount of fluid is extracted after the high pressure turbine for the regeneration. There can be several regenerative extractions at different points of the medium and low pressure turbine stages.
- **3-4:** Expansion in the medium pressure stage of the turbine.
- **4-5:** Final expansion in the low pressure stage of the turbine.
- **4-8:** Extraction after the medium pressure stage. This extraction will be used for DH and its volume will therefore determine what percentage of heating and electricity is provided.
- **5-6:** The steam is condensed to water in the condenser.
- **6-7:** A pump raises the pressure of the condensed fluid until the pressure of the DH.
- **7-8:** The condensed fluid is mixed with the fluid coming from the DH exchanger.
- **8-9:** A pump raises the pressure of the mixture to match that of the regenerative extraction after the high pressure turbine.
- **9-10:** The fluid is preheated before entering the boiler (regeneration)
- **10-11:** Circulation pump before the boiler.
- **11-1:** The fluid is superheated in the boiler until a temperature T_1.

3.2 Seawater Cooling

The flow of steam that is not used for DH and is expanded in the low pressure stage of the turbine needs to be condensed. There are several ways this cooling can be achieved. The plant may use a closed circuit system with cooling tower or use water taken directly from the sea. The Studstrup plant uses seawater as coolant for the condenser, which needs to be circulated by two hydraulic pumps. The usage of seawater eliminates the need for a cooling tower, but there are several aspects that need to be considered when using seawater for cooling the steam.

One of the biggest issues encountered when using seawater is the formation of fouling. Fouling is defined as the attachment of living organisms (biofouling) and non-living inorganic or organic substance in the equipment exposed to seawater. The result of fouling buildup in the walls of any heat exchanger is that the effectiveness of the heat transfer will deteriorate. A classic solution to avoid the formation of fouling is to add sodium hypochlorite in the intake, which is highly toxic to the aquatic environment. Since its usage for this purpose is no longer allowed in Denmark for environmental reasons, this is not a suitable solution.

Another important factor that needs to be considered when using water from the sea is the possible environmental impact of such practice. If the temperature of the return water is much higher than the temperature of the sea, it can affect the fauna and flora of the surrounding ecosystem. Therefore, there is an environmental limit to the increase in the temperature of the seawater used in the process. There is both a limit on the inlet-outlet temperature difference and on the absolute return temperature of the water that need to be regarded. These limits depend on the local legislation. As a consequence, a larger flow of seawater may be needed to achieve the same cooling power in the condenser.

The cooling power that needs to be provided is not constant throughout the year. During summer, it is not necessary to provide as much heating, only electricity. Therefore, all the steam flow will be directed to the low pressure turbine and condensed. Thus, in summer the load on the condenser (the amount of heat it needs to extract from the work fluid) will be maximal.

3.2.1 Seawater pump

In order to circulate the necessary seawater required for the cooling, one or several pumps are required. It is desirable to operate where the pumps are more efficient and there is no risk of cavitation (formation of bubbles in the inlet of the pump due to the low pressure of the liquid).

Efficiency of a pump

The efficiency of a pump can be defined in relation to the following parameters [Massoud, 2005,P. 754]:

- **Hydraulic horsepower.** It is the power transferred to the fluid to deliver a flow rate $\dot{V}$ with a head H. It can be expressed as:

$$\dot{W}_{hyd} = \rho g H \dot{V} \; = \; \dot{m} g H \tag{3.1}$$

where:

$\dot{W}_{hyd}$	Hydraulic horsepower	$[W]$
ρ	Density of the fluid	$[kg/m^3]$
H	Head provided by the pump	$[m]$
$\dot{m}$	Mass flow	$[kg/s]$

- **Brake horsepower.** It is the power that is necessary to deliver to the pump by the prime mover. It can be expressed as:

$$\dot{W}_{bhp} = \omega T \tag{3.2}$$

where:

$\dot{W}_{bhp}$	Brake horsepower	$[W]$
ω	Rotational speed of the pump shaft	$[rad/s]$
T	Shaft torque delivered by the prime mover	$[N \cdot m]$

Then the pump efficiency can be defined as:

$$\eta = \frac{\dot{W}_{hyd}}{\dot{W}_{bhp}} \tag{3.3}$$

Cavitation

Cavitation is defined as the formation, via vaporization, and subsequent collapse (through condensation), of vapor bubbles in a liquid. The bubbles are formed at regions with low pressure, and once the pressure of the fluid is increased, they collapse, causing erosion and pitting in the pump components.

Cavitation occurs when the pump suction is under low-pressure conditions and the liquid vaporizes at the eye of the impeller, to later collapse violently at the discharge side of the pump. This causes progressive wear on the materials.

It is therefore of great interest to avoid cavitation in the pumps, since it will drastically reduce the lifespan of the pump. The requirement to avoid cavitation is that the available Net Positive Suction Head (NPSH) is at least equal to the required NPSH, which is specified by the pump manufacturer. The available NPSH is defined as [Massoud, 2005,P. 753]:

$$NPSH_A = \frac{p_i}{\rho g} + \frac{v_i^2}{2g} - \frac{p_v}{\rho g} \tag{3.4}$$

where:

p_i	Inlet pressure	[Pa]
v_i	Inlet velocity of the fluid	[m/s]
p_v	Vapour pressure of the liquid	[Pa]

It is recommendable that the available NPSH is 2 or 3 meters above the required NPSH [Kreith, 1986].

The Pump Efficiency Curve

There are constraints on the maximum and minimum flow a pump can handle. A flow that is too low may cause cavitation in the impeller. The flow of the pump should at all times be higher than the minimum continuous stable flow. In contrast, a flow too high will cause vibration in the system, cavitation and the head provided by the pump will be very low. This point is called the maximum flow point or "run-out". The ideal point to operate is called the Best Efficiency Point (BEP), where the hydraulic losses of the pump are at their lowest.
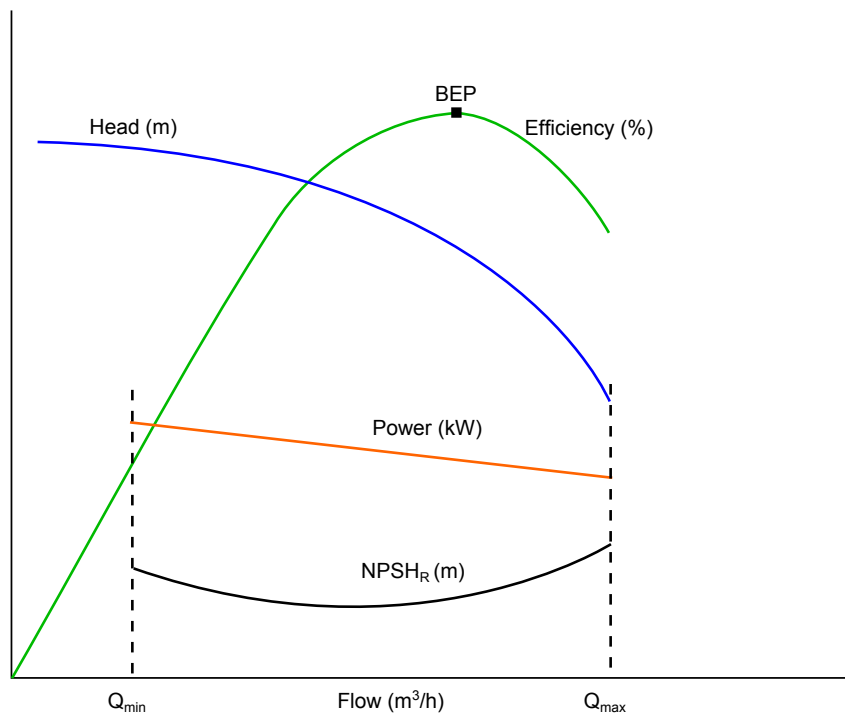

Figure 3.6. Example of a pump efficiency curve for a fixed rotational speed.

An example of a pump effiency curve is shown in Figure 3.6. All the curves therein are given for a fixed rotational speed n. It can be seen that the head decreases with the flow and the efficiency reaches an absolute maximum at the BEP. The NPSH required is low around the BEP

but high when the flow is close to the maximum or minimum flow. Both the NPSH and the head are measured in meters of water column.

Operating point

It is necessary that the pump matches the requirements of the system it operates on. For each singular system, the head requirement varies as a function of the flow. The correlation between the head requirement and the flow in a hydraulic system is called the system curve.

The head requirement consists of two components [Steve Wilson, Grundfos A/S]: the independent head and the friction head. The independent head consists of the pressure requirements that do not depend on the flow: the static head (the height the fluid needs to be lifted) and the head required at the end of the system. The friction head is the pressure loss due to friction within the piping of the system. The sum of both heads results in the head-flow curve of the system.

The decreasing head characteristic curve of the pump (for a given speed) crosses the increasing head characteristic curve of the system at the operating point. Since different speeds result in different characteristic curves, there will be a different operating point for each velocity setpoint of the pump. This is illustrated in Figure 3.7. For the same system, given by its characteristic curve, a pump rotating at n_1 rpm will provide a head of H_1 and a flow of Q_1 at the operating point OP_1. However, if a higher flow is required, the rotational speed of the pump can be increased to n_2. In that case, the head required by the system is higher, but the pump can also provide a greater flow.
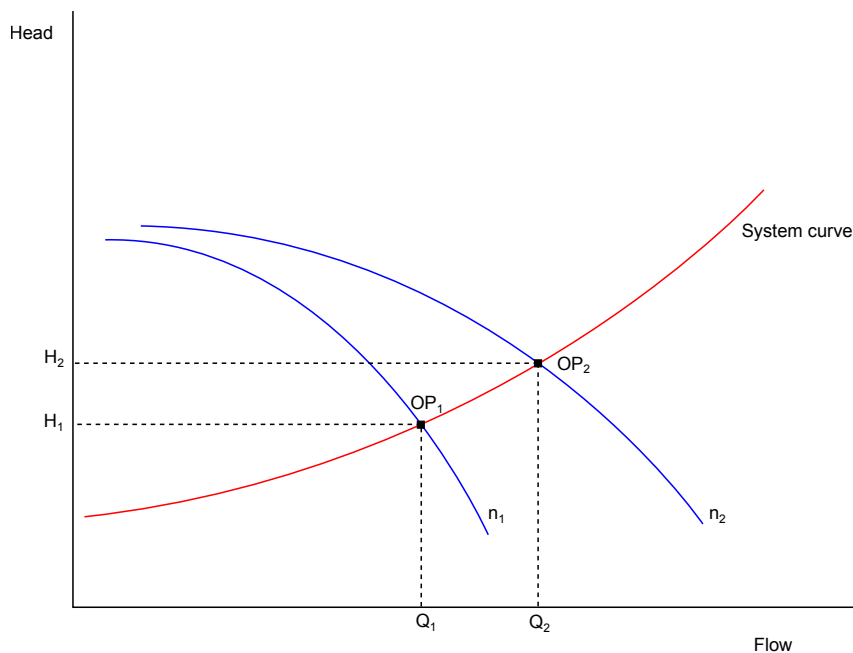
Figure 3.7. Operating point of one pump for two different rotational speeds.

However, an individual pump may not have the capability to reach the desired operating point. If the pump cannot provide enough head for the system, a possible solution is to place two or more pumps in series. If, on the other hand, it is the flow demand that cannot be met, this can be solved by arranging the pumps in a parallel configuration. It may as well be possible to operate with one or with both pumps under some circumstance. As it will be explained later in chapter 2, the main cooling system of the plant that will be studied uses two pumps running

in parallel. The case where two pumps run in parallel is illustrated in Figure 3.8. Previously, a single pump was providing a flow Q_1 at OP, represented by the blue curve on the left side of the picture. As a larger flow is required (that is denoted as Q'), there are two possible scenarios.
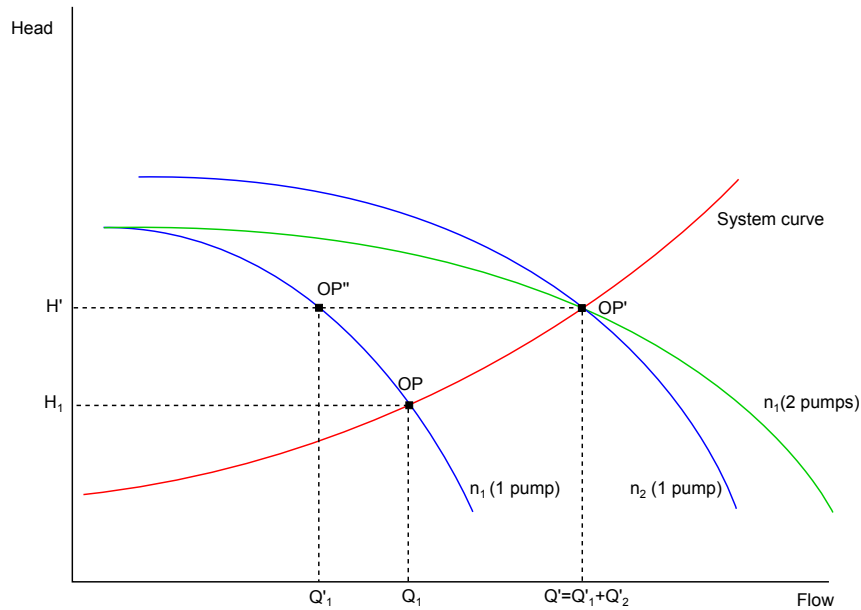

Figure 3.8. Operating point when two pumps are run in parallel, as opposed to the case where only one pump is used.

In both of the cases, the operating point is the same (OP'). The first scenario is identical to the previous case: the number of rpm of the pump is increased until the operating point is met. The second scenario is based on the parallel operation of several pumps. The green curve represents the case when the two pumps are arranged in a parallel configuration. In that case, both pumps are operating at a lower speed than if only one pump was operating. The flow provided by each of the pumps is Q'_1 and Q'_2, respectively, but both need to provide the same head, since their outputs are directly connected. A substantial difference in the output head of the pumps could cause regression of the flow and should therefore be avoided. In the particular case where both pumps are identical (which is the case in Studstrup) $Q' = 2Q'_1$, and each pump provides half of the required flow. The operating point for each of the pumps would then be OP'', with H' and $Q'_1 = Q'/2$.

Problem Definition 4

As explained in Chapter 2, Studstrup currently uses a number of heuristic functions in order to determine the setpoint for the pumps driving the main cooling system. There are, however, accuracy and reliability issues associated to this method, meaning that the functions often need to be manually adjusted in order to correct the operating point of the pumps.

The approach used to calculate the flow of seawater has some reliability issues, as fouling in the condenser will lead to higher differential pressure and the flow is then computed to be higher than the actual flow.

There is a limit to the allowed change in the seawater temperature from intake to outlet and the steam outlet of the turbine is not allowed to contain liquid droplets. The cooling process therefore needs to operate within certain boundaries. Furthermore, the speed of the pumps will be limited by cavitation.

The present project aims to develop a control strategy to automatize the control of the pumps. The solution should fulfill the following primary requirements:

Primary requirements

- Estimate the flow of seawater in a more accurate and reliable way.
- Automatically generate the appropriate setpoints for the pumps without needing continuous human supervision.
- A control strategy that respects the limitations of the turbine.
- A control strategy that respects the limitations of the seawater temperature.
- A control strategy that respects the limitations of the pump speed.
- The control should be designed with a focus on robustness.

The project aims for robustness rather than performance, but performance would be appreciated. It should be possible to use the same control approach on other power plants with only minor adjustments. Therefore the project should contain ideas to fulfill the following secondary requirements:

Secondary requirements

- A control strategy that takes the plant to the maximum efficiency.
- The control of the power plant should be portable to other power plants.

Part II

Modeling and Estimation

Modeling 5

This chapter will present models for the main components involved in the main cooling system of Studstrup. This includes the two seawater pumps and the condenser. The seawater and the steam are always separated such that they will never mix. Throughout the chapter it will be distinguished between a seawater part and a steam part, where the seawater part is all the pipes, valves, pumps, filters and the condenser where the seawater is going through. The steam part is the condenser, where the steam is.

5.1 Overview of the model

The model of the main cooling system of the Studstrup plant consists of a hydraulic part, which contains the seawater pumps, valves, pipeline, mussel filter, TAPPROGGE filter and the condenser pipes; and a thermodynamic part, which models the condenser, where the heat is exchanged between the seawater and the steam.

The hydraulic model analyzes the seawater part without taking into account any thermal effects. Inside the condenser, which is shown in Figure 5.1, it can be seen that the condenser works as a closed heat exchanger, and therefore the only connection between the two parts is the energy transfer. The hydraulic properties of the seawater part are assumed to be unaffected by the steam part. It can therefore be modeled independently of the steam part.

On the other hand, the thermodynamic model studies the heat transfer between the seawater side and the steam side that takes place in the condenser, and how the different parameters will affect the pressure level in the condenser. The inside of the condenser can be seen in Figure 5.1. The steam is entering the condenser in the top, where the steam is condensed into water. The water is collected in the bottom of the condenser (the hotwell). The seawater is pushed through small pipes, where the energy from the steam is absorbed.
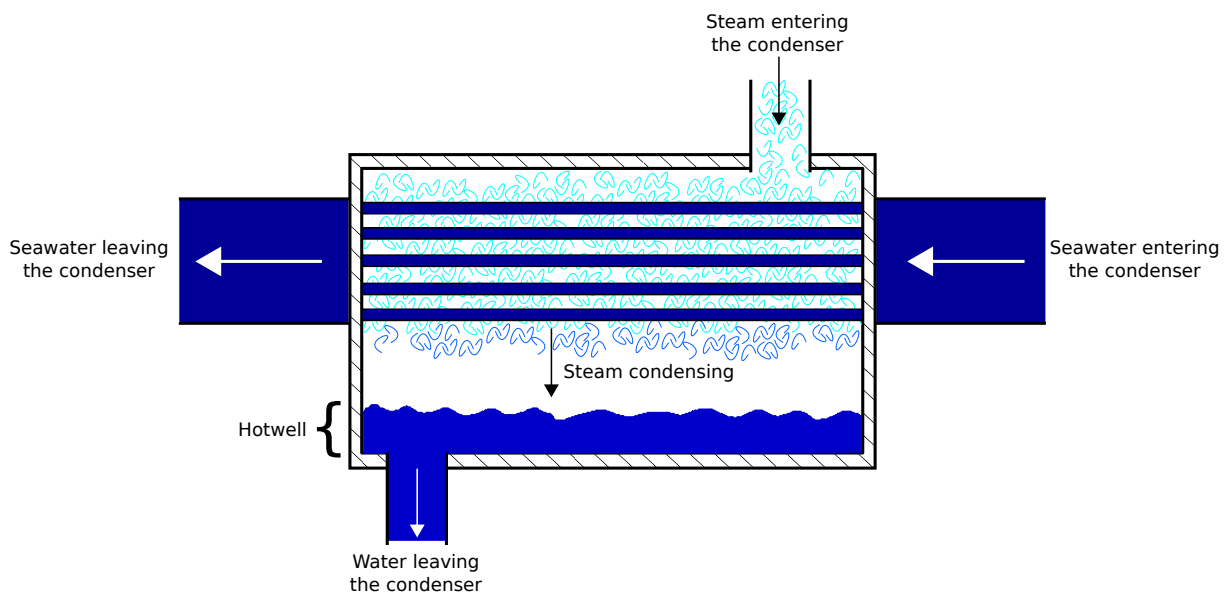

Figure 5.1. The inside of the condenser. The steam is turned into water, where, the water is collected in the bottom of the condenser.

A scheme showing the overall model, including both the hydraulic and the thermodynamic parts, is shown in Figure 5.2. The rotational speed of the pumps is the input to the model, and the pressure level in the condenser is the output. The inlet temperature of seawater collected from the basin and the flow of steam to the condenser are regarded as measurable disturbances in the model. The model of the condenser includes a model for the outlet temperature of the seawater and the mean temperature difference between the steam side and the seawater side.
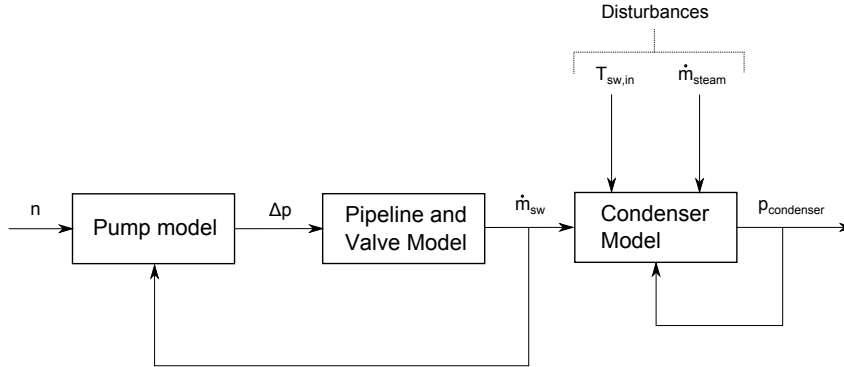

Figure 5.2. Overview of the complete model for the main cooling system.

The next sections will present the hydraulic and the thermodynamic models separately. Each of the models will be fitted and tested against real validation data from the plant operation.

5.2   Hydraulic Model

The flow through the pipeline system is analyzed in the same manner as the current in electronic circuit. The sum of mass flow to a pipeline is the sum of the mass flow leaving the pipeline. Pressure in the pipeline system is analyzed in the same manner as voltage in electronic circuit. The total pressure difference between the inlet and outlet of two pipelines in series is the sum of the pressure difference between the inlet and outlet from each of them. In Figure 5.3 the hydraulics of the seawater is shown. When both pumps are in use, the pressure difference Δp_m is assumed zero, as the RPM must be the same in both pumps for safety reasons and the pipeline system is assumed mirrored. When only one pump is operating and both condensers are in use, the mass flow from the pump will be divided into two, where one part of the mass flow will go through condenser one and the other part will go through condenser two. This will then produce a pressure difference in Δp_m.
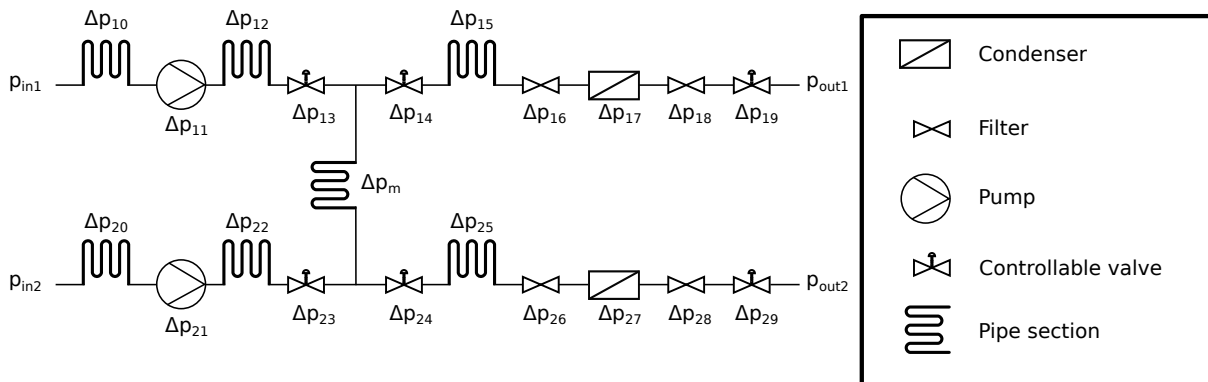

Figure 5.3. The hydraulics of the seawater part.

The inlet and outlet of the hydraulic system is assumed to be at the same level beneath the sea. The sum of pressure change through the hydraulic system is therefore zero.

5.2.1 Model of The Pipes and Valves

The model of a pipe and valve is assumed the same. The model of a pipe is derived in Appendix A using [Jovic, 2013]. In Equation 5.1 the dynamic model of a pipe is shown.

$$J \cdot \dot{q} \; = \; - K \cdot |q| \cdot q + \Delta p \tag{5.1}$$

where:

q	Volumetric flow	$[m^3/s]$
Δp	Pressure drop across the pipe	$[kg/m \cdot s^2]$
J	Fluid inertance in the pipe	$[kg/m^4]$
K	Fluid resistance coefficient in the pipe	$[kg/m^7]$

In Equation 5.1 the volumetric flow is not squared, but $(|q| \cdot q)$, as the flow can flow in both directions. Both the J and K are depending on the pipe dimensions. In case of fouling the pipe will be narrowed down and the parameters J and K will thereby change. The J value will increase, as the cross section area of the pipe will decrease. By studying Equation 5.1 in steady state, the K value will increase in case of fouling, as the same flow will give a higher pressure drop across the pipe.

5.2.2 Condenser pipe Model

In order to calculate the flow in each condenser instead of the total flow, which is done by using the flow estimation method given by Equation 2.2 on page 8, a model for each condenser is made. The pipe model of one condenser is made by using the pipe model given by Equation 5.1. As the flow in the condenser is only traveling in one direction at all time, the $(|q| \cdot q)$ is changed to (q^2). The dynamic condenser pipe model is given by Equation 5.2.

$$J_c \cdot \dot{q}_c \; = \; - K_c \cdot q_c^2 + \Delta p_c \tag{5.2}$$

where:

J_c	Fluid inertance in condenser pipe	$[kg/m^4]$
K_c	Fluid resistance coefficient in condenser pipe	$[kg/m^7]$
q_c	Volumetric flow through condenser	$[m^3/s]$
Δp_c	Pressure drop across the condenser	$[kg/m \cdot s^2]$

In Equation 5.3 the condenser pipe model is in steady state and the flow is isolated such that the flow is estimated by the pressure drop across the condenser.

$$q_c = \sqrt{\frac{\Delta p_c}{K_c}} \tag{5.3}$$

where:

K_c	Fluid resistance coefficient in condenser pipe	$[kg/m^7]$
q_c	Volumetric flow through condenser	$[m^3/s]$
Δp_c	Pressure drop across the condenser	$[kg/m \cdot s^2]$

The value of the K_c parameter is calculated by comparing the mass flow estimation given by Equation 2.2 on page 8 and the steady condenser pipe model given by Equation 5.3. The pressure drops across the two condensers are assumed to be the same and thereby $\sqrt{\Delta P_{con1} + \Delta P_{con2}} \approx \sqrt{2 \cdot \Delta P_{con1}}$. The K_c parameter is given by Equation 5.4, where the ρ is due to the difference in mass flow and volumetric flow and the $\sqrt{10^5}$ is due to conversion from bar to Pascal.

$$K_c = \left(\frac{2 \cdot \rho \cdot \sqrt{10^5}}{18690 \cdot \sqrt{2}} \right)^2 \tag{5.4}$$

where:

K_c	Fluid resistance coefficient in condenser pipe	$[kg/m^7]$
ρ	Density of fluid	$[kg/m^3]$

5.2.3   Pipeline Model

The pipelines of the seawater system is modeled by using the pipe model shown in Equation 5.1. In Figure 5.4 the pipeline model is simplified by collecting all the pipes and valves. In the line section part the filters, condenser, pipes and valves are collected and in the pipe section before and after each pump, the pipes and valves are collected.
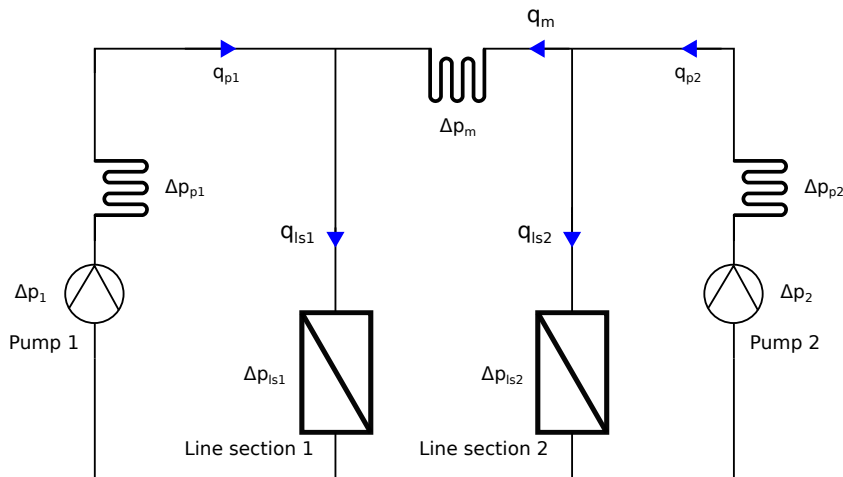

Figure 5.4. Simplified pipeline system, where the blue arrows indicates the flows.

The sums of pressures in Figure 5.4 are calculated by the equations from Equation 5.5 to 5.8.

$$\Delta p_1 - \Delta p_{p1} - \Delta p_{ls1} = 0 \tag{5.5}$$
$$\Delta p_2 - \Delta p_{p2} - \Delta p_{ls2} = 0 \tag{5.6}$$
$$\Delta p_1 - \Delta p_{p1} + \Delta p_m - \Delta p_{ls2} = 0 \tag{5.7}$$
$$\Delta p_2 - \Delta p_{p2} - \Delta p_m - \Delta p_{ls1} = 0 \tag{5.8}$$

where:

Δp_1, Δp_2	Pressure produced by pump	$[kg/m \cdot s^2]$
Δp_{p1}, Δp_{p2}	Pressure loss in pipes before and after pump	$[kg/m \cdot s^2]$
Δp_{ls1}, Δp_{ls2}	Pressure loss in line section 1 and 2	$[kg/m \cdot s^2]$
Δp_m	Pressure loss in the pipe between the two pumps	$[kg/m \cdot s^2]$

In order to minimize the number of states, the flow in the pipe between the two pumps (q_m) is calculated from the flows in the pipelines at the pumps (q_{p1}, q_{p2}) and the flows in the line sections (q_{ls1}, q_{ls2}). In Equation 5.9 and 5.10 the calculations of (q_m) are shown.

$$q_m = q_{ls1} - q_{p1} \tag{5.9}$$
$$q_m = q_{p2} - q_{ls2} \tag{5.10}$$

where:

q_m	Flow in the pipeline between the pumps	$[m^3/s]$
q_{p1}	Flow from pump 1	$[m^3/s]$
q_{ls1}	Flow in line section 1	$[m^3/s]$
q_{p2}	Flow from pump 2	$[m^3/s]$
q_{ls2}	Flow in line section 2	$[m^3/s]$

The sum of pressures given by the equations from 5.5 to 5.8 and the pipe model is used to make the model of the pipeline system given by 5.11. The λ_J function is a function of the derivative of the flows. The λ_{K1} function is a function of the flows in the pipelines, where the flows are only traveling in one direction at all time. The λ_{K2} function is a function of the flows in the pipelines, where the flows are traveling in two directions. The λ_p function is a function of the pressure from the pumps. The parameters J, K_1 and K_2 are related to the hydraulic properties of the pipes and valves.

$$\lambda_J(J, \dot{q}) = -\lambda_{K1}(K_1, q) - \lambda_{K2}(K_2, q) + \lambda_p(\Delta p) \tag{5.11}$$

The flows and pressures are, in Equation 5.11, in vector form and is given by:

$$q \; = \; \begin{bmatrix} q_{p1} \\ q_{p2} \\ q_{ls1} \\ q_{ls2} \end{bmatrix} \;\;,\; \Delta p = \begin{bmatrix} \Delta p_1 \\ \Delta p_2 \end{bmatrix}$$

where:

q_{p1}	Flow in pipeline at pump 1	$[m^3/s]$
q_{p2}	Flow in pipeline at pump 2	$[m^3/s]$
q_{ls1}	Flow in line section 1	$[m^3/s]$
q_{ls2}	Flow in line section 2	$[m^3/s]$
Δp_1	Pressure produced by pump 1	$[m]$
Δp_2	Pressure produced by pump 2	$[m]$

The λ_J function is found by using the sum of pressures and the pipe model, where the only variable considered is the flow acceleration. The λ_J function is given by Equation 5.12.

$$\lambda_J(J, \dot{q}) \; = \; \begin{bmatrix} J_{p1} \cdot \dot{q}_{p1} + J_{ls1} \cdot \dot{q}_{ls1} \\ J_{p2} \cdot \dot{q}_{p2} + J_{ls2} \cdot \dot{q}_{ls2} \\ J_{p1} \cdot \dot{q}_{p1} - J_m \cdot (\dot{q}_{ls1} - \dot{q}_{p1}) + J_{ls2} \cdot \dot{q}_{ls2} \\ J_{p2} \cdot \dot{q}_{p2} + J_m \cdot (\dot{q}_{p2} - \dot{q}_{ls2}) + J_{ls1} \cdot \dot{q}_{ls1} \end{bmatrix} \tag{5.12}$$

By isolating the flow acceleration vector in the λ_J function, the J parameter is expressed as a matrix and is given by:

$$J \; = \; \begin{bmatrix} J_{p1} & 0 & J_{ls1} & 0 \\ 0 & J_{p2} & 0 & J_{ls2} \\ (J_{p1} + J_m) & 0 & -J_m & J_{ls2} \\ 0 & (J_{p2} + J_m) & J_{ls1} & -J_m \end{bmatrix}$$

The model of the pipelines is rearranged such that the model is in state space form and is given by Equation 5.13.

$$\dot{q} \; = \; -J^{-1}\lambda_{K1}(K_1, q) - J^{-1}\lambda_{K2}(K_2, q) + J^{-1}\lambda_p(\Delta p) \tag{5.13}$$

The λ_{K1} function is found in the same manner as the λ_J function, but as the flow is only traveling in one direction at all time, the $(|q| \cdot q)$ is changed to (q^2). The λ_{K1} function is given by Equation 5.14.

$$\lambda_{K1}(K_1, q) \;=\; \begin{bmatrix} K_{p1} \cdot q_{p1}^2 + K_{ls1} \cdot q_{ls1}^2 \\ K_{p2} \cdot q_{p2}^2 + K_{ls2} \cdot q_{ls2}^2 \\ K_{p1} \cdot q_{p1}^2 + K_{ls2} \cdot q_{ls2}^2 \\ K_{p2} \cdot q_{p2}^2 + K_{ls1} \cdot q_{ls1}^2 \end{bmatrix} \qquad (5.14)$$

The λ_{K2} function is found in the same manner as the λ_J function. The λ_{K2} function is given by Equation 5.15.

$$\lambda_{K2}(K_2, q) \;=\; \begin{bmatrix} 0 \\ 0 \\ K_m \cdot |q_{ls1} - q_{p1}| \cdot (q_{ls1} - q_{p1}) \\ -K_m \cdot |q_{p2} - q_{ls2}| \cdot (q_{p2} - q_{ls2}) \end{bmatrix} \qquad (5.15)$$

The λ_p function is found in the same manner as the λ_J function. The λ_p function is given by Equation 5.16.

$$\lambda_p(\Delta p) \;=\; \begin{bmatrix} \Delta p_1 \\ \Delta p_2 \\ \Delta p_1 \\ \Delta p_2 \end{bmatrix} \qquad (5.16)$$

The Values of The Fluid Resistance Coefficients

The fluid resistance coefficients are found by using data, where the seawater flow in the condensers are steady. By using the steady state model of a pipe, the fluid resistance coefficients is calculated by the flow in the pipe and the pressure across the pipe. The pressure across the pumps are calculated by the seawater level measurement and the pressure measurement after the pump. The pressure across the filters and condensers are measured directly. The pressure across the valves and pipes are not measured, but as the pipeline is modeled as being closed, the sum of pressures is zero. The pressure across the valves and pipes can thereby be calculated as being the pressure drop left. The sum of the fluid resistance coefficients by these valves and pipes can thereby be found. In Figure 5.5 the parts where the pressure is measured and the parts where the pressure is not measured is shown. The red parts indicates that the pressure is not measured and the green parts indicates that the pressure is measured. The pump and the pipe before the pump is not measured directly, but the seawater level and the pressure measurement after the pump is used to calculate the total pressure across both the pump and the pipe.
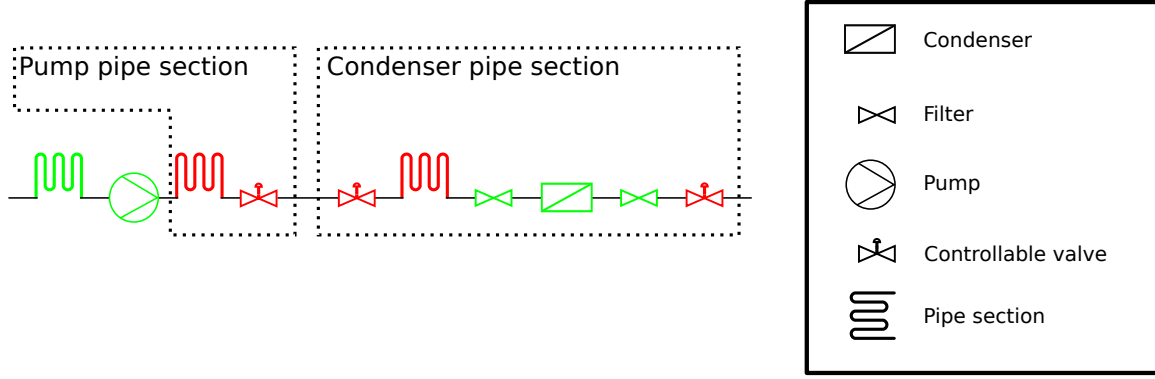
Figure 5.5. Pipeline system, where only one line is shown. The green parts indicates that the pressure can be measured. The red parts indicates that the pressure can not be measured.

By using data where both pumps and both condensers are operating with the same conditions each line can be handled individually. In Figure 5.6 to the left line 1 is shown. As both lines is assumed to have the same fluid resistance ($K_{p1} = K_{p2}$ and $K_{ls1} = K_{ls2}$), only one line needs to be analyzed. The total fluid resistance in line 1, when both pumps and both condensers are operating with the same conditions, is $K_{line1} = K_{p1} + K_{ls1}$. By using data where only pump one is active the values of K_{p1}, K_{ls1} and K_m can be found by knowing K_{line1}, the flows and the sum of pressures.
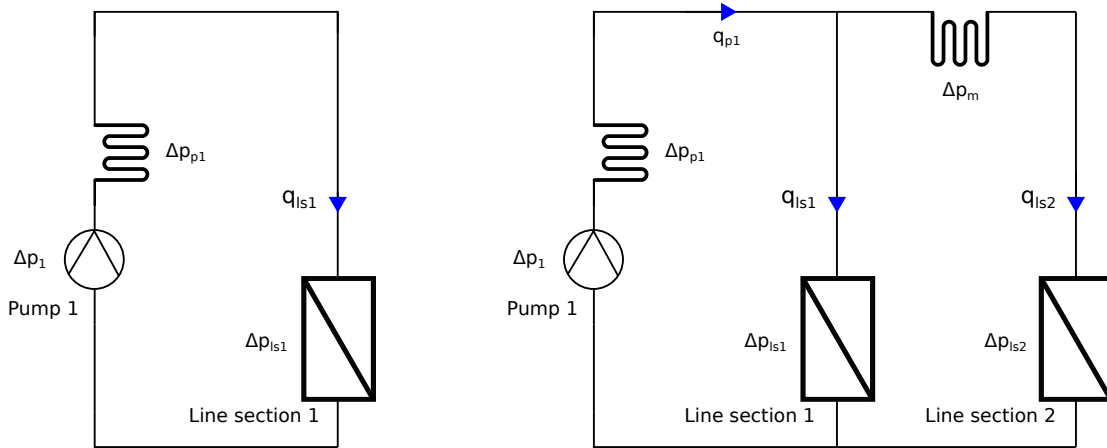

Figure 5.6. Two different setups, where the pipeline to the left is when both pumps and both condensers are operating with the same conditions and the pipeline to the right is when one pump and two condensers are active.

The value of K_{line1} is found by using steady state data where both pumps and both line sections are operating with the same conditions. The calculation is done by using Equation 5.17.

$$K_{line1} = \frac{\Delta p_1}{q_{ls1}^2} \tag{5.17}$$

The value of K_{ls1} is found by using steady state data where only pump one is active. The calculation is done by using Equation 5.18, where the sum of pressure is ($\Delta p_1 - \Delta p_{p1} - \Delta p_{ls1} = 0$).

$$K_{ls1} = \frac{\Delta p_1 - K_{line1} \cdot q_{p1}^2}{q_{ls1}^2 - q_{p1}^2} \tag{5.18}$$

The value of K_{p1} is found by using the values found in Equation 5.17 and 5.18. The calculation is done by using Equation 5.19.

$$K_{p1} = K_{line1} - K_{ls1} \tag{5.19}$$

The value of K_m is found by using steady state data where only pump one is active. The calculation is done by using Equation 5.20, where the sum of pressure is ($\Delta p_{ls1} = \Delta p_m + \Delta p_{ls2}$).

$$K_m = \frac{q_{ls1}^2 - q_{ls2}^2}{q_{ls2}^2} \cdot K_{ls1} \tag{5.20}$$

The values of the fluid resistance coefficients can be found in Appendix C on page 119.

The Values of The Fluid Inertance

The fluid inertance (J_{p1}) is assumed to be the same as (J_{p2}), the same is the case with (J_{ls1}) and (J_{ls2}). First ($J_{line1} = J_{p1} + J_{ls1}$) is found, as this can be found by using data, where the seawater flow is the same in both line sections and both pumps are running with the same speed. When the seawater flow is the same in both line sections and both pumps are running with the same speed, the flow in the pipe between the two pumps will be zero. Thereby the flow from pump number 1 is the same as the flow to line section 1. After the sum of (J_{p1}) and (J_{ls1}) is found, the values of (J_{p1}), (J_{ls1}) and (J_m) are found by using data, where only one pump is active. By knowing the value of (J_{line1}), only two values are changed in the fitting of the model, as ($J_{p1} = J_{line1} - J_{ls1}$).

The continuous time model of pipeline number 1 is given by Equation 5.21.

$$J_{line1} \cdot \dot{q}_{ls1} = -K_{line1} \cdot q_{ls1}^2 + \Delta p_1 \tag{5.21}$$

The discrete time model of pipeline number 1 is made using the forward Euler method. The model is given by Equation 5.22. By fitting the model to data, where he seawater flow is the same in both condensers and both pumps are running with the same speed, the value of (J_{line1}) can be found, as the rest of the parameters in Equation 5.22 is known.

$$q_{ls1}[k+1] = -\frac{Ts \cdot K_{line1}}{J_{line1}} \cdot q_{ls1}[k]^2 + \frac{Ts}{J_{line1}} \cdot \Delta p_1[k] + q_{ls1}[k] \tag{5.22}$$

The values of (J_{p1}), (J_{ls1}) and (J_m) are found by fitting the model given by Equation 5.13 to data where one pump is turned off. The values can be found in Appendix C.

The Pipeline Model Compared To The Data

In Figure 5.7 and 5.8 the fitted model is tested against the estimated flow from the condenser pressure, where Figure 5.7 shows the flow in line 1 and Figure 5.8 shows the flow in line 2. The data is from the 10th of February 2014 and the figures shows, that the model flow is close to the estimated flow from the condenser pressure.
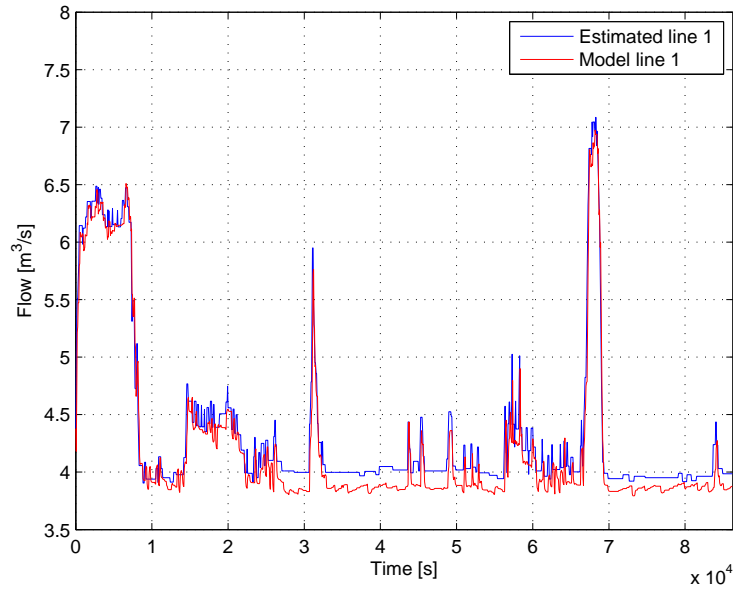

Figure 5.7. Flow in line 1, where the estimated flow is the flow estimated from the condenser pressure and the model flow is the fitted model.
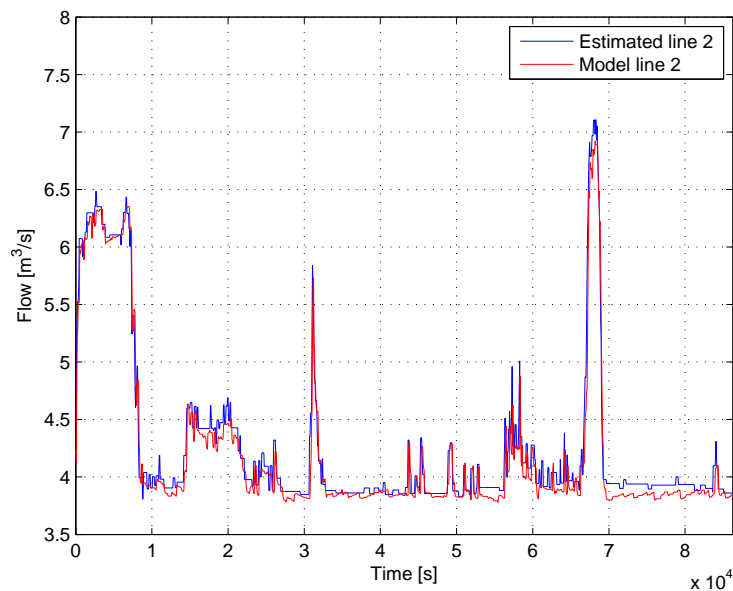

Figure 5.8. Flow in line 2, where the estimated flow is the flow estimated from the condenser pressure and the model flow is the fitted model.

In Figure 5.9 the relative error between the model flow and the flow estimated from the condenser pressure is shown.
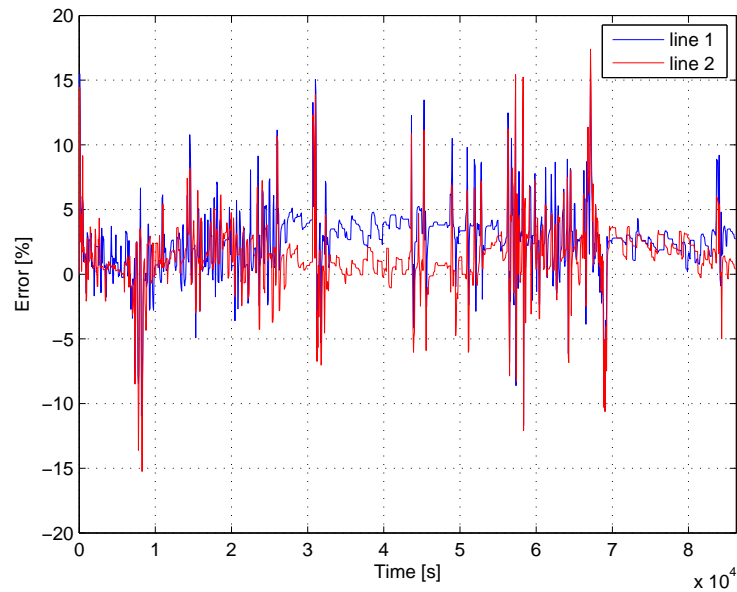
The relative error in Figure 5.9 stays below 5% for 89.14% of the time, the model is therefore considered to be a good representation of the system.

5.2.4   Model of The Pumps

The pump curves provided by the pump manufacturer, KSB, contains the information about the relationship between the RPM, volumetric flow, pump head, power consumption and the NPSH needed by the pump. The pump curves is divided into head, power and NPSH, where each is analyzed separately. From each curve a pump model is fitted, where the input to these models is flow and RPM and the output is head, power and NPSH. The models is tested on data from the 10th of February 2014. In Figure 5.10 the RPM of each pump and the flow through each condenser from the 10th of February 2014 is shown.
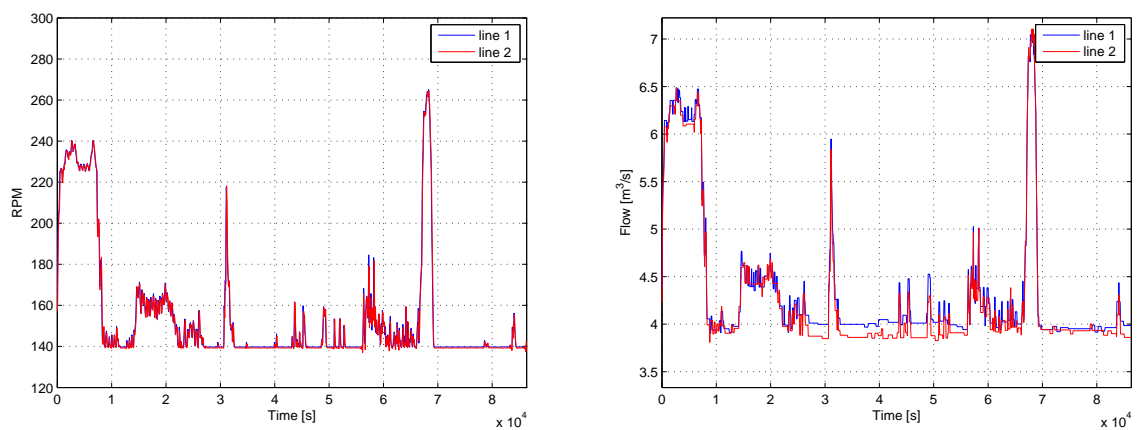

Figure 5.10. Data from the 10th of February 2014, where the graph to the left shows the RPM of each pump and the graph the the right shows the flow through each condenser.

31

Head

The curves shown in Figure 5.11 is showing the head provided by the pump for different flow values, where each curve represents a fixed rotational speed. It can be seen that the capacity to provide head decreases with the flow. A higher speed need to be chosen in order to meet a higher head requirement of the hydraulic system.

Figure 5.11. Pump head at different RPM.

In Figure 5.12 the curves from Figure 5.11 is fitted to a function of RPM and volumetric flow. The graph to the left is the points from the curves used in the fitting and the graph to the right is the fitted function. The function is a polynomial with a degree of five in each variable and can be found in Appendix C on page 119.

Figure 5.12. From RPM and flow to head, where the graph to the left shows the points from the data sheet and the graph to the right is the fitted curve.

In Figure 5.13 the fitted model is tested against the head measurement from the 10th of February 2014. The figure shows, that the model output is close to the measurement.

Figure 5.13. Pump head at line 1.

The relative error between the model and the measurement is in Figure 5.14 shown.
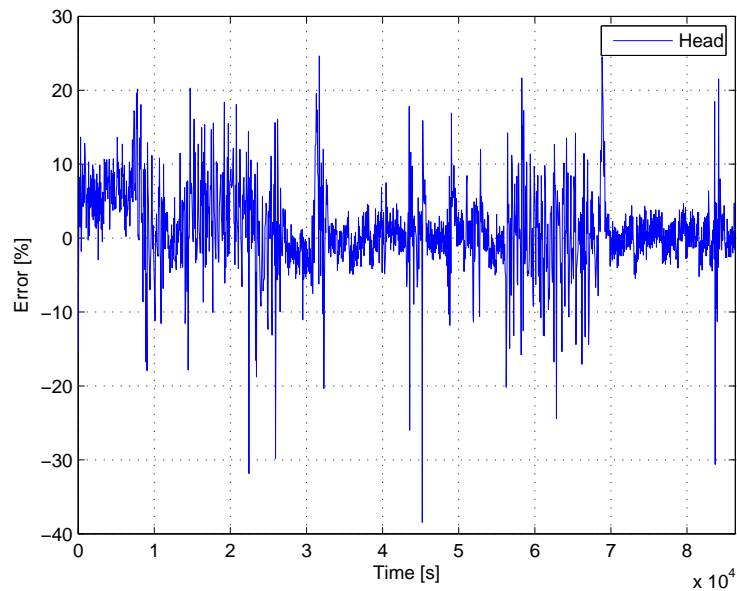
Figure 5.14. The error in pump head between model and measurement.

The relative error stays in 89.68% of the time belove 10%, therefore the model is considered a good representation of the pump pressure.

Power

In Figure 5.15 the curves of the power consumption at different volumetric flows are shown, where each curve represents a fixed rotational speed. It can be seen that the power consumption increases with less flow.
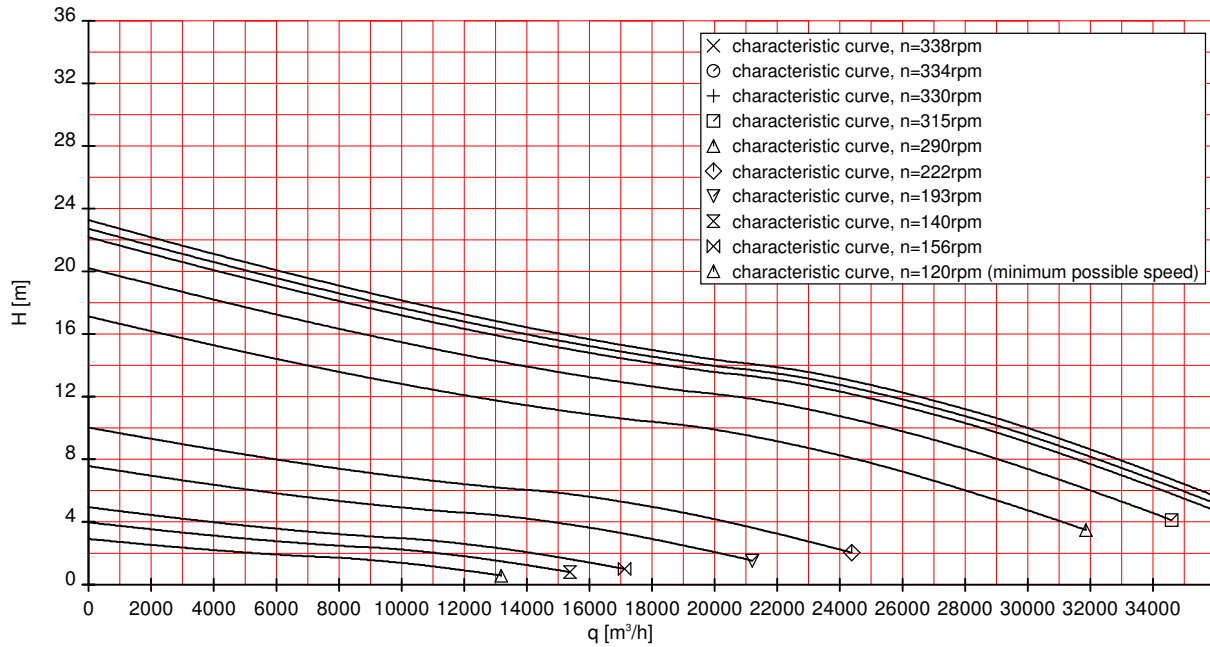

Figure 5.15. Power consumption at different RPM.

In Figure 5.16 the curves from Figure 5.15 is fitted to a function of RPM and volumetric flow. The graph to the left is the points from the curves used in the fitting and the graph to the right is the fitted function. The function is a polynomial with a degree of five in each variable and can be found in Appendix C on page 119.
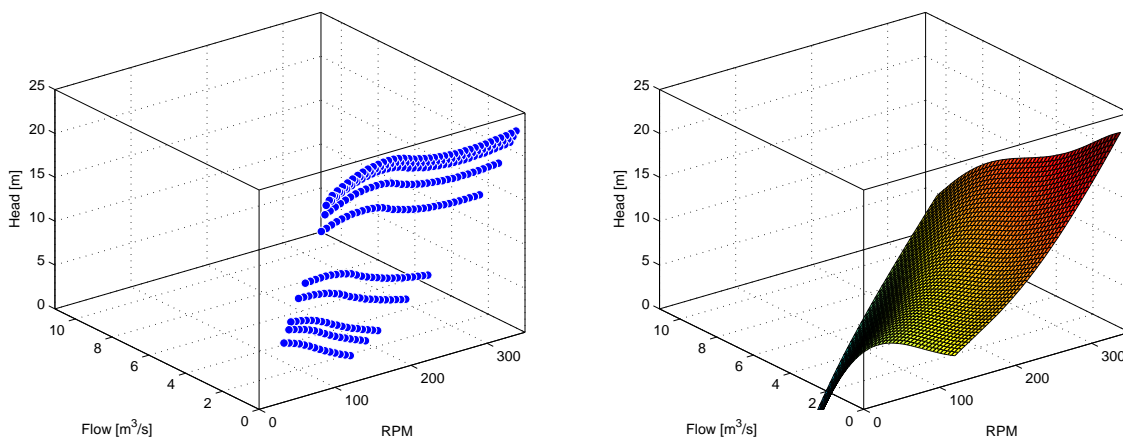

Figure 5.16. From RPM and flow to power, where the graph to the left shows the points from the data sheet and the graph to the right is the fitted curve.

In Figure 5.17 the fitted model is tested against the power measurement from the 10th of February 2014. The figure shows, that the model output is close to the measurement.
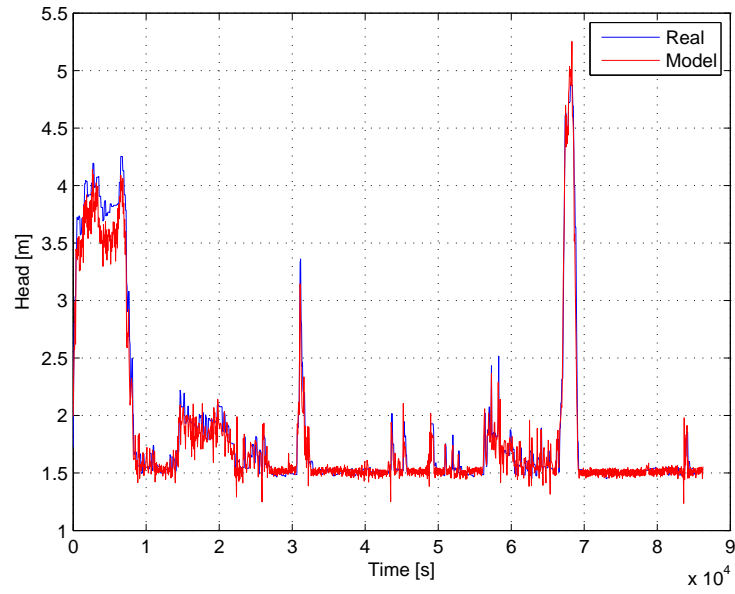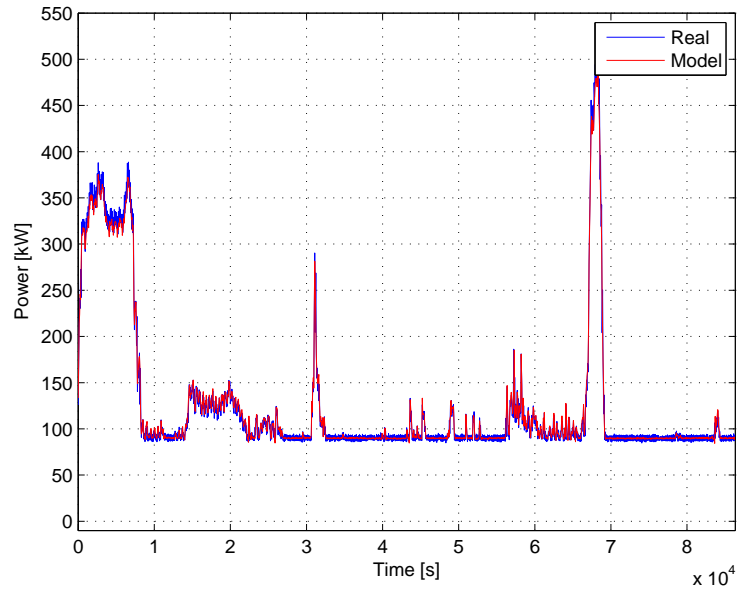

Figure 5.17. Pump power at line 1.

In Figure 5.18 the error between the model and the measurement is shown.
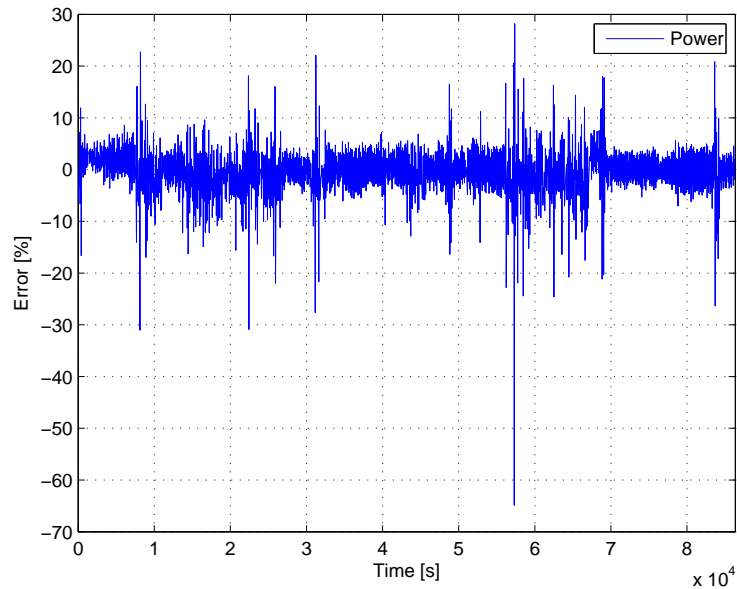
Figure 5.18. The error in pump power between model and measurement.

The relative error stays belove 10% for 92.81% of the time, the model is therefore considered a good representation of the pump power.

NPSH

Figure 5.19 shows the NPSH required by the pump as a function of the volumetric flow for different rotational speeds.
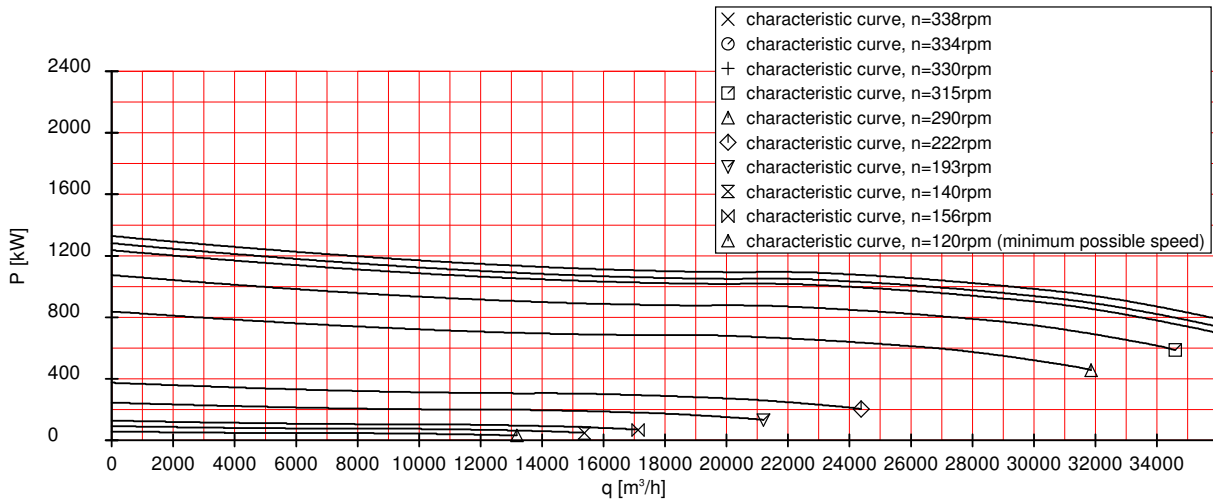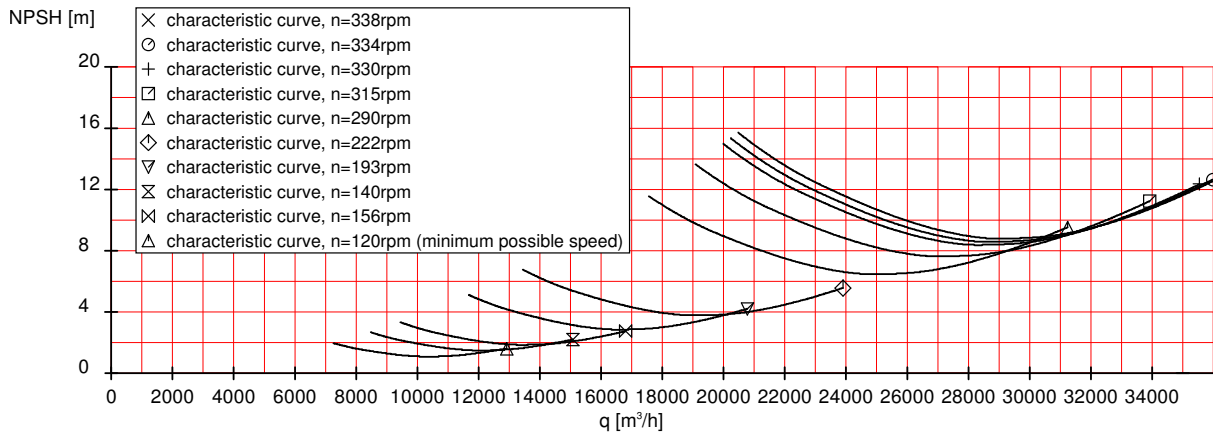

Figure 5.19. Pump NPSH vs. flow at different RPM.

In Figure 5.20 the curves from Figure 5.19 is fitted to a function of RPM and volumetric flow. The graph to the left is the points from the curves used in the fitting and the graph to the right is the fitted function. The function is a polynomial with a degree of two in each variable and can be found in Appendix C on page 119.
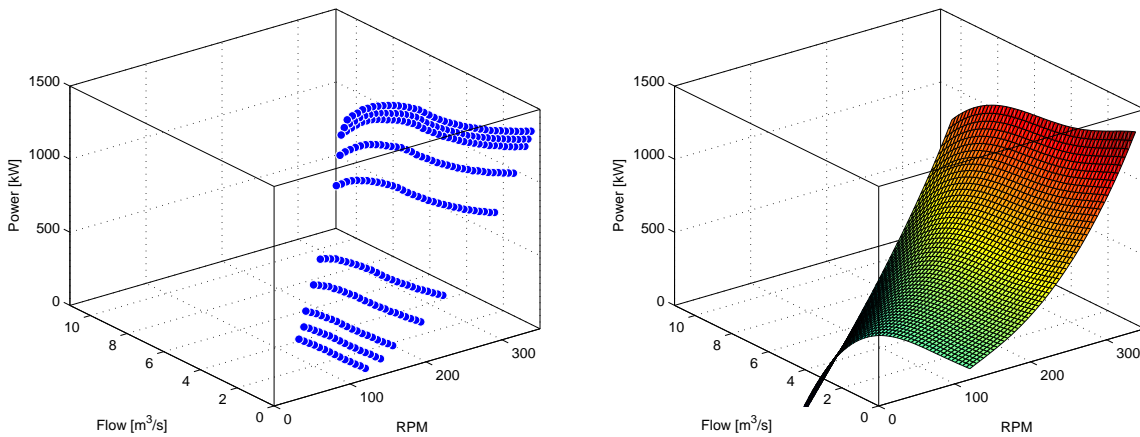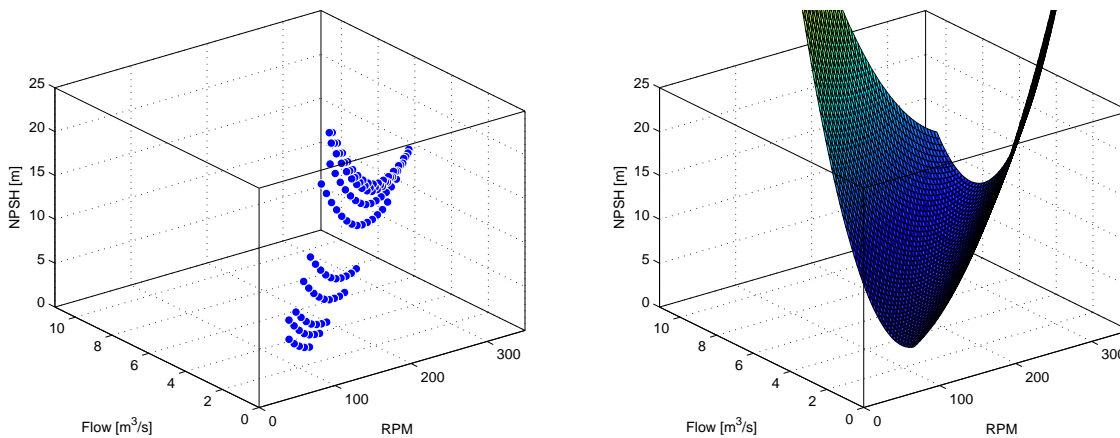

Figure 5.20. From RPM and flow to NPSH, where the graph to the left shows the points from the data sheet and the graph to the right is the fitted curve.

The equation used to calculate the available NPSH to the pump is derived in Appendix B on page 117 and is given by Equation 5.23.

$$NPSH_A = 12.2902 - WL \tag{5.23}$$

where:

$NPSH_A$	NPSH available for the pump	$[m]$
WL	Water level measured by sensor	$[m]$

5.3   Thermodynamic Model of the Condenser

The goal of the condenser in a CHP power plant is to extract sufficient heat from the steam that has not been used for DH (and therefore has completed its expansion in the low pressure stage of the turbine) to condensate it into saturated liquid. This is achieved by using a cooling fluid (seawater) and allowing heat to be exchanged between both sides. Thus, a condenser is just a particular case of a heat exchanger, where the hot fluid undergoes condensation instead of just experiencing a drop in temperature.

This section will present a model of the thermodynamics involved in the condensation of the steam by means of a seawater condenser. A model of the condenser will be proposed, and the inclusion of fouling in the model will be discussed in this section.

Assumptions

In order to derive a model for the condenser, the following assumptions are made:

- Total condensation. It is assumed that the output of the low pressure turbine is saturated steam (two-phase fluid with a very high quality to avoid water droplets in the blades of the turbines) and the fluid at the output of the condenser is saturated liquid (subcooling will increase the energy that must be supplied to the fluid during the preheating and in the boiler). A more general model of a condenser would include a desuperheating and subcooling regions, but the input and output of the condenser will be as close to the saturation curve as possible in order to ensure a long lifetime of the equipment and a good efficiency for the cycle.
- There is no heat loss to the surroundings of the condenser. The totality of heat from the steam is transferred over to the seawater side.
- The specific heat capacity of the seawater is constant throughout the condenser. The variations of this parameter with the temperature are very small and their effect on the model is negligible.
- The temperature in each section of the condenser is approximated as constant along its length.
- There is no axial heat conduction, neither in the tubes nor within the fluids. Only radial conduction across the radius of the pipe is considered.
- Both parts of the condenser are identical in terms of seawater temperature, mass flow and heat transfer.

Neglecting heat losses to the environment, the source of heat will be the condensing steam coming from the last stage of the turbine, and the heat sink will be the seawater pumped by the main cooling system. The heat transfer between them will be subject to the overall heat transfer coefficient of the condenser (see Figure 5.21).
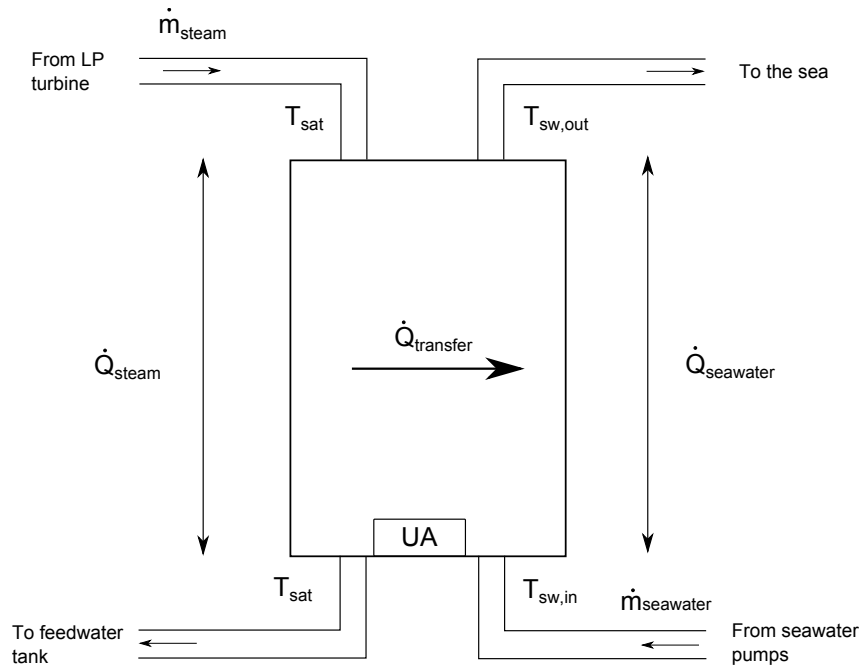
Figure 5.21. Heat balance in the condenser.

The condenser is modelled as a cross flow heat exchanger, where the heat yielded by the steam is due to its phase change, rather than to a change in temperature. The general theory of heat exchangers still applies, only the source of heat coming from the warmer fluid does not cause a drop in its temperature, but a change in its phase.

The models by [Arthur G.O. Mutambara, 1999] and [Guðmundsson, 2008] propose a lumped model of the heat exchanger with four zones in both the seawater and steam sides. Under the assumption of total condensation, the temperature across all four zones in the steam side of the condenser is constant, only the enthalpy may vary. It is possible to propose a model that divides the steam side in four zones and considers the enthalpies as states. However, this model still requires knowledge of the saturation temperature of the steam (through the mean temperature difference of the fluids, as will be seen later). But it must be considered that the aim of the control loop is to control the pressure inside the condenser, and this can be derived from the temperature as long as the fluid is in saturation conditions. Therefore, splitting the steam side does not contribute to a more accurate model and would only demand a higher order model.

The model proposed here is based on the previously mentioned models, but in this case, a number of n sections are considered. The condenser is physically divided in two parallel parts, but it is considered that both of the parts are identical in terms of temperature, flow and heat transfer. A schematic of how the proposed model is organized is shown in Figure 5.22.
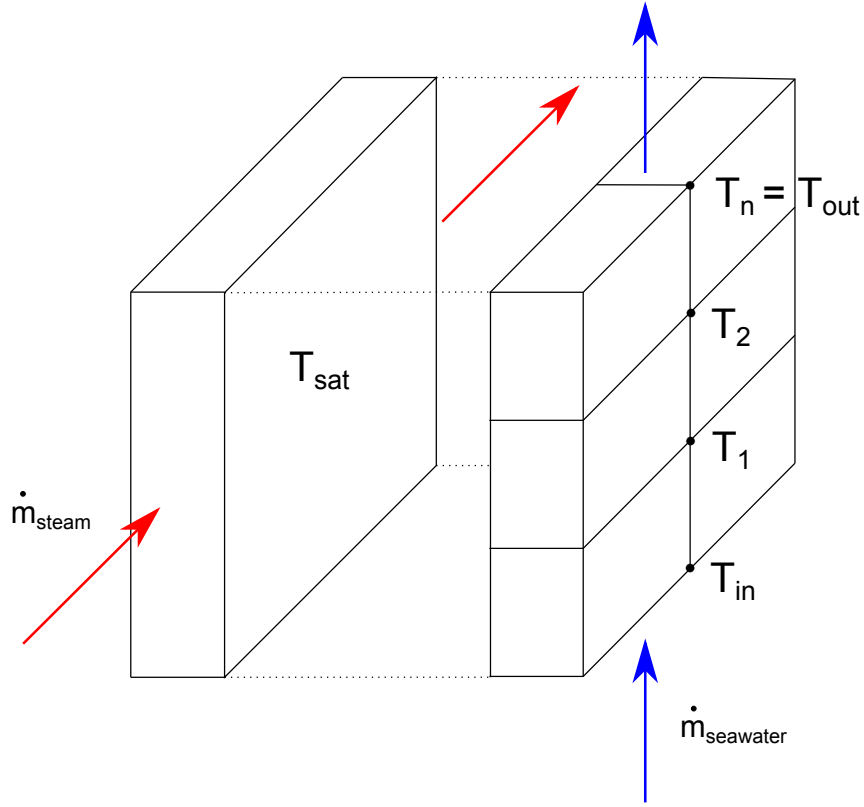
Figure 5.22. Model of the cross-flow condenser and its different regions.

In each of the sections of the condenser in the seawater side, the energy balance equation is given by 5.24.

$$M_{sw}c_{sw}\frac{dT_i}{dt} \;=\; \dot{m}_{sw}c_{sw}(T_{i-1} - T_i) - UAF\Delta T_i \tag{5.24}$$

where:

M_{sw}	Total amount of seawater in one condenser section	$[kg]$
c_{sw}	Heat capacity of the fluid in the section (assumed constant)	$[kJ/(kgK)]$
$\frac{dT_i}{dt}$	Temperature change of the fluid contained in section i	$[K/s]$
$\dot{m}_{sw}$	Mass flow of seawater through the section.	$[kg/s]$
$T_i - T_{i-1}$	Temperature change of the seawater across section i of the condenser	$[K]$
U	Overall heat transfer coefficient in one section	$[kJ/(m^2K)]$
F	Correction factor for non-counterflow heat exchangers	[-]
ΔT_i	Temperature difference between the ij cells and the steam side in the condenser.	$[K]$

In a heat exchanger with no phase change, the enthalpy difference is due exclusively to the change in the temperature of each fluid. In the case of a condenser, however, this is only the case in the seawater side. In the steam side, the enthalpy difference is due to the condensation, while the temperature remains at T_{sat} across the whole condenser. The total enthalpy drop across all the sections of the condenser in the steam side is equal to the latent heat of condensation of the steam. The energy balance in this case is given by Equation 5.25. The right side of the equation represents the heat that is exchanged between the steam (due to its condensation) and the seawater sides. The imbalance in this heat transfer will result in a variation of the saturation temperature of the steam-pipe ensemble, as expressed in the left side of Equation 5.25.

$$\underbrace{(M_{steam}c_{steam} + M_{tube}c_{tube})}_{\gamma}\frac{dT_{sat}}{dt} = \dot{m}_{steam}\lambda(T_{sat}) - U_{tot}AF\Delta T_{tot} \qquad (5.25)$$

where:

M_{steam}	Total amount of steam in the condenser	$[kg]$
c_{steam}	Heat capacity of the steam	$[kJ/(kgK)]$
M_{tube}	Total amount of the metal pipe	$[kg]$
c_{tube}	Heat capacity of the metal pipe	$[kJ/(kgK)]$
T_{sat}	Saturation temperature of the steam.	$[K]$
$\dot{m}_{steam}$	Mass flow of steam through the section.	$[kg/s]$
λ	Latent heat of condensation of the steam	$[kJ/kg]$
U_{tot}	Overall heat transfer coefficient for all sections	$[kJ/(m^2K)]$
F	Correction factor for non-counterflow heat exchangers	[-]
ΔT_{tot}	Overall temperature difference between both sides of the condenser.	$[K]$

Combining Equations 5.24 and 5.25, the resulting system will be:

$$\frac{dT_1}{dt} = \frac{1}{M_{sw}}(T_{in} - T_1)\dot{m}_{sw} - \frac{UAF}{M_{sw}c_{sw}}\Delta T_1 \qquad (5.26)$$

$$\frac{dT_2}{dt} = \frac{1}{M_{sw}}(T_1 - T_2)\dot{m}_{sw} - \frac{UAF}{M_{sw}c_{sw}}\Delta T_2$$

$$\vdots \qquad\qquad\qquad \vdots$$

$$\frac{dT_{out}}{dt} = \frac{1}{M_{sw}}(T_{n-1} - T_{out})\dot{m}_{sw} - \frac{UAF}{M_{sw}c_{sw}}\Delta T_n$$

$$\frac{dT_{sat}}{dt} = -\frac{U_{tot}AF}{\gamma}\Delta T_{tot} + \frac{\dot{m}_{steam}}{\gamma}\lambda(T_{sat})$$

These equations constitute a nonlinear dynamic system in the form:

$$\dot{x} = f(x,u) \qquad (5.27)$$
$$y = g(x) \qquad (5.28)$$

In this case, the parameter that needs to be controlled is the flow of seawater, that will be controlled through the speed setpoint of the pumps. Other parameters such as the inlet water temperature and the flow of steam are not controllable inputs and will be considered as disturbances in the model.

$$x = \begin{bmatrix} T_1 \\ T_2 \\ \vdots \\ T_i \\ T_{sat} \end{bmatrix}, \qquad \delta = \begin{bmatrix} T_{in} \\ \dot{m}_{steam} \end{bmatrix}, \qquad y = \begin{bmatrix} T_{sw,out} \\ T_{sat} \end{bmatrix}, \qquad u = \dot{m}_{sw} \qquad (5.29)$$

The correction factor F is needed in the heat transfer equation whenever the heat exchanger setup is not counter-flow (in that case $F = 1$). However, in the case of condensers, this factor will always have a value of 1, regardless of the configuration of the heat exchanger [Yanus A. Cengel, 2012,P.1047].

The most accurate value for $\Delta T_i(t)$ is the log mean temperature difference (LMTD) between the cells, which is given as:

$$\Delta T_i \;=\; \frac{(T_i - T_{sat}) - (T_{i-1} - T_{sat})}{ln\left(\frac{T_i - Tsat}{T_{i-1} - T_{sat}}\right)} \tag{5.30}$$

Simplifying:

$$\Delta T_i \;=\; \frac{T_i - T_{i-1}}{ln\left(\frac{T_i - Tsat}{T_{i-1} - T_{sat}}\right)} \tag{5.31}$$

where:

T_i	Temperature at the outlet of section i	[°C]
T_{st}	Steam temperature	[°C]
T_{sw}	Seawater temperature	[°C]

5.3.1 Discretized model

In order to implement and fit the model to the observations, it first needs to be discretized to the corresponding sampling time of the observations. The discretization method used is Euler forward discretization:

$$\dot{x} \;=\; \frac{x(t+1) - x(t)}{Ts} \tag{5.32}$$

$$x(t+1) \;=\; x(t) + Ts \cdot \dot{x} \tag{5.33}$$

5.3.2 The Overall Heat Transfer Coefficient

One of the parameters in Equation 5.25 is the overall heat transfer coefficient U (in the UAF term). This section will show how this parameter is estimated depending on the operating conditions of the condenser. Typically, the overall heat transfer coefficient experiences great variations in short amounts of time. Therefore, the mean value of U for steady state operation is considered in this section. Another factor to be taken into account in a seawater cooled condenser, as discussed previously, is the formation and buildup of fouling in the pipes. However, as the tubes in Studstrup are being continuously cleaned by the TAPROGGE system, this effect can be neglected.

The general expression of the overall heat transfer coefficient is:

$$\frac{1}{U} \ = \ \underbrace{\frac{1}{h_{sw}} + \frac{1}{h_{st}} + \frac{\Delta x}{k}}_{1/U_{clean}} + R_i \qquad (5.34)$$

where:

h_{sw}	Heat transfer coefficient from the seawater to the tube	$[W/(m^2 K)]$
h_{st}	Heat transfer coefficient from the tube to the steam	$[W/(m^2 K)]$
Δx	Thickness of the tube	$[m]$
k	Thermal conductivity of the metal tube	$[W/(mK)]$
R_i	Fouling resistance	$[m^2 K/W]$

However, the value for the overall heat transfer coefficient in a clean tube is not constant, it depends on the velocity of the fluid. From the expression of the Nusselt number:

$$Nu \ = \ \frac{hL}{k} \longrightarrow h = f(Nu) \qquad (5.35)$$

where:

Nu	Nusselt number	[-]
L	Characteristic length	[m]

$$Nu \ = \ cRe^a Pr^{1/3} \qquad (5.36)$$

where:

Re	Reynolds number	[-]
Pr	Prandtl number	[-]

$$Pr \ = \ \frac{\nu}{\alpha} \qquad (5.37)$$

where:

ν	Kinematic viscosity	$[m^2/s]$
α	Thermal diffusivity	$[m^2/s]$

$$Re \ = \ \frac{\rho v D_H}{\mu} \ = \ \frac{\dot{m} D_H}{\rho \nu A} \qquad (5.38)$$

where:

D_H	Hydraulic diameter	$[m]$
ρ	Density of the fluid	$[kg/m^3]$
μ	Dynamic viscosity	$[kg/(s \cdot m)]$
ν	Kinematic viscosity	$[m^2/s]$
A	Cross-section area	$[m^2]$

The overall heat transfer coefficient is a function of the Reynolds number and, therefore, of the mass flow of the fluid through the pipe. [Wilson, 1915] derived an expression that relates the transfer coefficient to the flow of coolant in the heat exchanger. This is known as the Wilson Plot theory.

$$\frac{1}{U} = C_1 + \frac{1}{C_2}v^{0.8} \tag{5.39}$$

where:
v Velocity of the coolant $[m/s]$
C_1, C_2 Constant parameters $[-]$

Since the heat exchange area in the condenser is constant, equation 5.39 can be re-expressed in terms of UA as:

$$\frac{1}{UA} = a + b \cdot \dot{m}_{sw}^{0.8} \tag{5.40}$$

In order to fit this equation to the condenser of interest, let us consider Equation 5.25 once again. In steady state, the equation becomes:

$$\gamma \cdot 0 = \dot{m}_{steam}\lambda(T_{sat}) - (UA)_{tot}\Delta T_{tot} \tag{5.41}$$

and therefore:

$$(UA)_{tot} = \frac{\dot{m}_{steam}\lambda(T_{sat})}{\Delta T_{tot}} \tag{5.42}$$

After collecting steady state operation data for different conditions, the points are regressed to fit the expression in 5.40. The result, with a value for the coefficient of determination of $R^2 = 0.9888$, is illustrated in Figure 5.23. The regression is valid for the range $\dot{m}_{sw} = [7.079 \cdot 10^3, 1.2274 \cdot 10^4]\ kg/s$
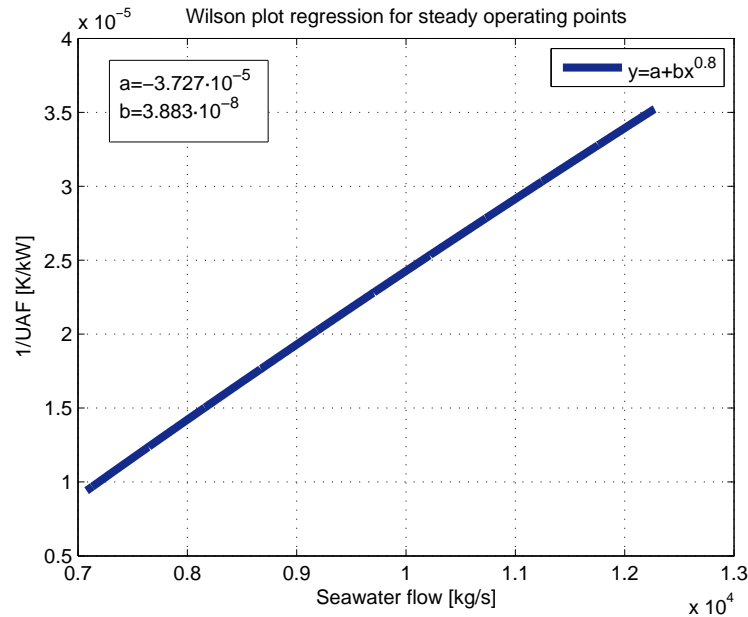

Figure 5.23. Steady state data regression to Equation 5.40.

5.3.3 Model Implementation Analysis and Problematic

There are, however, a number of issues associated with the practical implementation of this approach that will be discussed hereafter.

One of the parameters present in the Equations 5.26 is the overall heat transfer coefficient, whose theoretical calculation and regression was presented in Section 5.3.2. The fitting was performed for steady state operating data. However, this is generally not the case at the Studstrup power plant. The value of UA undergoes continuous and substantial variations and its value will not match the theoretical value given by the curve in Figure 5.23, resulting in an incorrect prediction of the pressure in the condenser. This affects the UA of the total condenser, as well as that of the individual sections in the seawater side.

Another issue affecting Equation 5.25 is the weak correlation between the input variables and the observed output. In order to test the correlation between the variables, the following test is considered:

- H_0: There exists no correlation between the variables
- H_1: There is a correlation between the variables

The correlation coefficient between two variables i and j is defined as follows:

$$R(i,j) \; = \; \frac{C(i,j)}{\sqrt{C(i,i)C(j,j)}} \tag{5.43}$$

where:

$C(i,j)$ Covariance between the i and j variables

Taking the equation presented in Equation 5.25:

$$\dot{T}_{sat} \; = \; k_1 \cdot \underbrace{\dot{m}_{steam}\lambda(T_{sat})}_{x_{data}} + k_2 \cdot \underbrace{U_{tot}AF\Delta T_{tot}}_{y_{data}} \tag{5.44}$$

The correlation coefficient matrices for the output $\dot{T}_{sat}$ with each of the input variables x_{data} and y_{data} are:

$$R_{x_{data},\dot{T}_{sat}} \; = \; \begin{bmatrix} 1 & 0.0747 \\ 0.0747 & 1 \end{bmatrix} \tag{5.45}$$

$$R_{y_{data},\dot{T}_{sat}} \; = \; \begin{bmatrix} 1 & 0.0971 \\ 0.0971 & 1 \end{bmatrix} \tag{5.46}$$

The p-value in both cases is very small, several orders of magnitude below a significance level of 0.05. Therefore, the null hypothesis is rejected ('There exists no correlation') and it is reasonable to assume a correlation between each of the variables and $\dot{T}_{sat}$. The values of the correlation coefficients are, however, very close to zero, meaning that the correlation may be too weak to obtain a good fit. Attempts to achieve a good fit for the system dynamics using this equation and thereby predict the behavior of the system have shown that the model is not capable of predicting the saturation temperature in the condenser.

As a consequence of both factors (the uncertainty in the value of UA and the poor goodness of the fitting), it is decided to abandon this model in favor of other models that can model and predict the behavior of the system more reliably and accurately. The next section will present an alternate method to achieve these goals, not based on a thermodynamic model of the system, but on the statistical analysis of the data.

5.4 Data-Driven Model of the Condenser

This section proposes a statistical approach to modeling the steam condenser in the plant. The goal is to achieve a mathematical model that describes the input-output static and dynamic behavior of the system accurately and reliably. First, the variables involved in the modeling will be introduced and analyzed. The statistical model that produces the best simulation results will be chosen.

5.4.1 Motivation. Static vs Dynamic Model

The thermodynamic model proposed in Section 5.3 could not simulate the behavior of the real system, as explained in Section 5.3.3. It is therefore decided to identify the parameters that are most relevant to the process through a statistical analysis. These parameters are used to develop a general model that will be fitted according to the available data.

Unlike in Section 5.4, where T_{sat} was chosen as output variable and later converted to pressure via steam tables, the analysis will consider the pressure level in the condenser as output directly, since this is the output of interest. In order to choose the input variables, a correlation analysis of the possible variables involved in the process will be performed, and the best descriptors of the process will be chosen for the model.

The model proposed in Section 5.3 was a dynamic one. However, the model that will be proposed is static. This is possible thanks to the very fast dynamics of the system, due to the rapid heat transfer between seawater and steam sides. The mass flow of seawater remains above 100 times (and up to 500 times) the flow of steam coming into the condenser. The conductivity and convection heat transfer coefficients of the condenser pipes through which the seawater circulates are very high (high U). The heat exchange area is as well very high (12844 m^2). All these factors contribute to a very large heat flow relative to the flow of steam, and therefore a very fast dynamics of the steam side of the condenser. Thus, the seawater dynamics are regarded as the dominant dynamics of the overall system.

5.4.2 Dependence Analysis

A first step towards developing a model that describes the behavior of the system will be to find the process variables that determine the output of the system. In order to do this, it will be studied how each of the variables relates to the output, p_{cond}. The candidate variables for the analysis will be those that are theoretically related to the model output through 5.26. A first step will be to show what variables show the strongest correlation to the output. However, correlation does not imply dependence, which is necessary for the model to predict the output of the system given only the inputs. Therefore, a dependence test will be performed on the variables.

The correlation between each of the variables of study and the pressure in the condenser is denoted as R_{i1} and is shown in Table 5.1.

	R_{i1}	p-value	Correlation at $\alpha = 0.05$
x_{data}	-0.1984	0 $(1.87 \cdot 10^{-70})$	Yes
y_{data}	-0.0914	0 $(5.2 \cdot 10^{-16})$	Yes
ΔT_{tot}	0.5542	0	Yes
$\dot{m}_{steam}$	-0.1816	0 $(3.63 \cdot 10^{-59})$	Yes
$\dot{m}_{sw}$	0.648	0	Yes
$T_{sw,in}$	0.8523	0	Yes

Table 5.1. Correlation of each variable with the pressure in the condenser.

From Table 5.1, the variables that show the maximum correlation with the pressure level in the condenser are Tsw, in, $\dot{m}_{sw}$ and ΔT_{tot} on the seawater side and x_{data} on the steam side (where $x_{data} = \dot{m}_{steam} \cdot \lambda$). As explained before, these variables still need to be tested for dependence. The dependence tests are based on [A Gretton, 2008] and use an equiprobable space partitioning ($L1$ method) and a distribution-free test threshold. The hypotheses of the test are the following:

- H_0: The input variable is independent from the output variable.
- H_1: There exists a dependence relationship between the input and output variables.

For each case, the threshold is computed independently and the test statistic is compared to the threshold. If the value of the statistic is larger than the threshold, the null hypothesis (independence) is rejected. The tests were performed for a confidence level of $\alpha = 0.05$, which is used within the test algorithm to determine the threshold. The results of the test are presented in Table 5.2

	Threshold	Value of the Test Statistic	Action	Dependence
x_{data}	0.047	0.5148	Reject H_0	Yes
ΔT_{tot}	0.047	0.5377	Reject H_0	Yes
$\dot{m}_{sw}$	0.047	0.7511	Reject H_0	Yes
$T_{sw,in}$	0.047	0.8103	Reject H_0	Yes

Table 5.2. Dependence of the output with each of the proposed variables.

Therefore, the output is dependent on the four input variables proposed. The next section will fit a linear model using x_{data}, ΔT_{tot}, $\dot{m}_{sw}$ and Tsw, in to the available operational data from the plant.

5.4.3 Model Fitting

The four variables mentioned previously can be fitted through a multiple linear regression to an equation in the form:

$$p_{cond} = a_0 + a_1 x_1 + a_2 x_2 + a_3 x_3 + a_4 x_4 \tag{5.47}$$

The expression in Equation 5.47 shows the relationship between each of the variables and the pressure inside the steam condenser. Each of these variables is considered as input to the system, two of them being uncontrollable but measurable disturbances (those will be the flow of steam and the inlet temperature of seawater), another parameter that is computed (the average temperature difference) and the last of them, the flow of seawater given by the hydraulic model. The variables, chosen from the dependence analysis, are:

x_1	x_2	x_3	x_4
$\Delta T_{tot}(t)$	$x_{data}(t)$	$\dot{m}_{sw}(t)$	$T_{sw,in}(t)$

It has been observed, however, that there exists a delay between some of the inputs and the output. The delay between the variations in the mass flow of steam and its derived parameter xdata and the variations in the pressure level in the condenser (θ_{steam}) has been estimated to be 9 samples at a sampling time of 66.005, or 594.045 seconds. In the case of the flow of seawater, the delay (θ_{sw}) has been estimated to be of 15 samples or 990.075 seconds. Fitting equation 5.48 has yielded the results specified in Appendix C.

Substituting the input variables in Equations 5.47, the final expression for the model is:

$$p_{cond}(t) \;=\; a_0 + a_1\Delta T_{tot}(t) + a_2 x_{data}(t - \theta_{steam}) + a_3\dot{m}_{sw}(t - \theta_{sw}) + a_4 T_{sw,in}(t) \quad (5.48)$$

The model has been tested against validation data from the plant operation. The result is shown in Figure 5.24. The model shows a spike at approximately $3.6 \cdot 10^4$ s, which is not reflected in the measurements. This is due to an increase in the temperature of the hotwell. This increase should translate into an increase of the condensation pressure, since both parameters are directly related through the steam tables. This mismatch could be due to a fault in either the hotwell temperature sensor or the pressure sensor. Unfortunately, no third measurement is available to determine the source of the error.
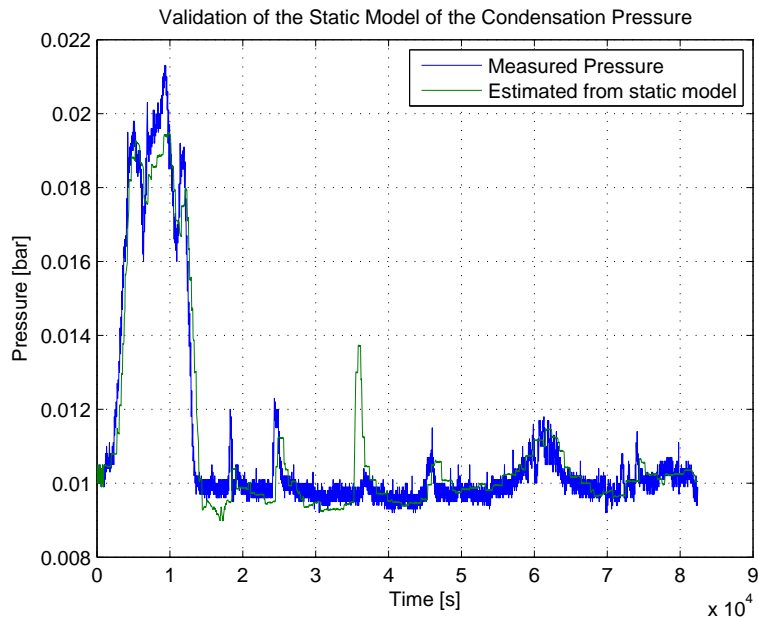

Figure 5.24. Measured condensation pressure against the pressure predicted by the model.

As it can be seen in Figure 5.24, the simulated pressure response is less noisy than the actual measured output, even though real, noisy measurements have been used in the simulation. A probable source is measurement noise from the pressure sensor, which will be added for the control simulations in order to achieve a more realistic environment to test the controller.

Notes and Limitations of this Model

This model simulates the output of the condenser in relation to the inputs. However, it should be noted that there are limitations to its applicability that must be taken into account when performing a simulation.

The regression was performed with the available data from the plant operation. The range of validity for the model is therefore the range of the data used in the regression. There is no guarantee for the accuracy or reliability of the estimates outside these boundaries. The validity range is:

$$
\begin{aligned}
p_{cond} &= [0.008,\ 0.022]\ \ bar \\
T_{sw,in} &= [1.71,\ 9.54]\ \ °C \\
m_{sw} &= [3.2264 \cdot 10^3,\ 1.4492 \cdot 10^4\ \ kg/s \\
\Delta T_{tot} &= [0.2153,\ 11.5838]\ \ °C \\
m_{steam} &= [0.1411,\ 187.3014]\ \ kg/s
\end{aligned}
\tag{5.49}
$$

One of the regression variables (which greatly improves the accuracy of the simulation) is ΔT_{tot}, which is given by 5.31. This parameter depends on the outlet temperature of the water. This variable, while considered as output in the thermodynamic model of the condenser, is being monitored in Studstrup (as mentioned previously, it is necessary to comply with the environmental regulations by ensuring that the temperature increase of the seawater does not exceed the limit). Therefore, it can be used in the control of the pumps, but in order to have an estimation of this value, a model describing its behavior will be proposed.

Furthermore, the model from Equation 5.48, in spite of being a linear combination of each of its parameters, contains the term x_{data}. This term is in itself nonlinear, since $x_{data} = \dot{m}_{steam}\lambda$, with λ having a nonlinear relation to the pressure. λ can be computed from the condensation pressure through the enthalpy of the steam in saturation conditions via steam tables. The linearization of this equation will be further discussed in Section 6.2.

5.4.4   Outlet Temperature Model

As explained before, the model requires knowledge of the outlet temperature of the water leaving the condenser. Even though this measurement is available in the plant, knowledge of this parameter is required for simulation purposes. For the same reasons as in the case of the saturation temperature, the model proposed in Section 5.3 does not fit the actual values or dynamics of the outlet seawater temperature. This section proposes a simple static model that can estimate the current outlet temperature based on input data.

The proposed model for the outlet temperature is a linear relationship between the parameters involved in the thermodynamic model of the condenser and the outlet. The parameters employed as inputs to the model are the inlet temperature of the water $T_{sw,in}$, the incoming flow of seawater $\dot{m}_{sw}$, the pressure level of the steam in the condenser at the previous time sample p_{cond} and the

measured temperature in the hotwell $T_{hotwell}$. The focus of the model is to obtain an approximate value of $T_{sw,out}$, even though it is not possible to reproduce its dynamic behavior since the model is purely static.

The outlet temperature will be fitted to a linear multi-input model in the form:

$$T_{sw,out} = f_1 + f_2 T_{sw,in} + f_3 \dot{m}_{sw} + f_4 T_{hotwell} + f_5 p_{cond} \tag{5.50}$$

It has been observed that there is a delay between the inputs and the output. This can be seen for example in the operational data shown in Figure 5.25, where each of the variables has been normalized with respect to their means for better visibility and the variable T_{out} has been scaled accordingly. It can be seen that the changes in $T_{sw,out}$ lag behind the changes in each of the inputs with similar pure delays. Time constants have not been taken into account in the model because of the difficulty in their calculation (due to the impossibility of generating steps for each of the inputs). It can be seen in Figure 5.25 that T_{out} follows the dynamics of the inputs (after a delay) and additional dynamics are not necessary to explain the variations in T_{out}. From the data it has been inferred that there is a dead time of 50 samples at a sampling rate of 66.005 seconds, which is equivalent to 55 minutes. This is a very large delay, but is, however, the delay that is observed in the data. This delay is of least significance in the case of the inlet temperature of the seawater, since this parameter tends to remain constant throughout long periods of time and experiments only seasonal variations.
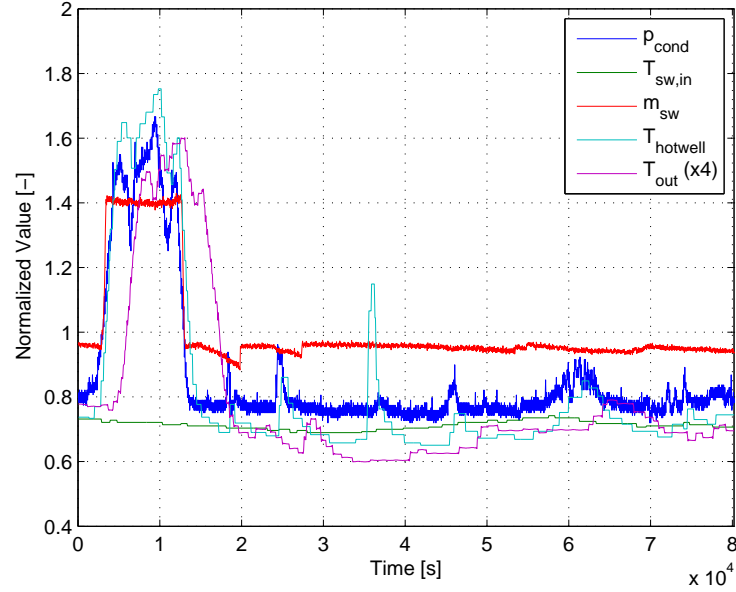

Figure 5.25. Sample of input and output values of the parameters involved in Equation 5.50. All values have been normalized with respect to their means.

The model from Equation 5.50 is corrected for the observed delay θ_p. Therefore, the current value of the outlet temperature is computed from the previous observed values of the inputs as in Equation 5.51:

$$T_{sw,out}(t) = f_1 + f_2 T_{sw,in}(t - \theta_p) + f_3 \dot{m}_{sw}(t - \theta_p) + \tag{5.51}$$
$$f_4 T_{hotwell}(t - \theta_p) + f_5 p_{cond}(t - \theta_p)$$

49

This model has been fitted to the available data from the plant. The model tested against validation data is shown in Figure 5.26. The value of the parameters found after the fitting process can be found in Appendix C.
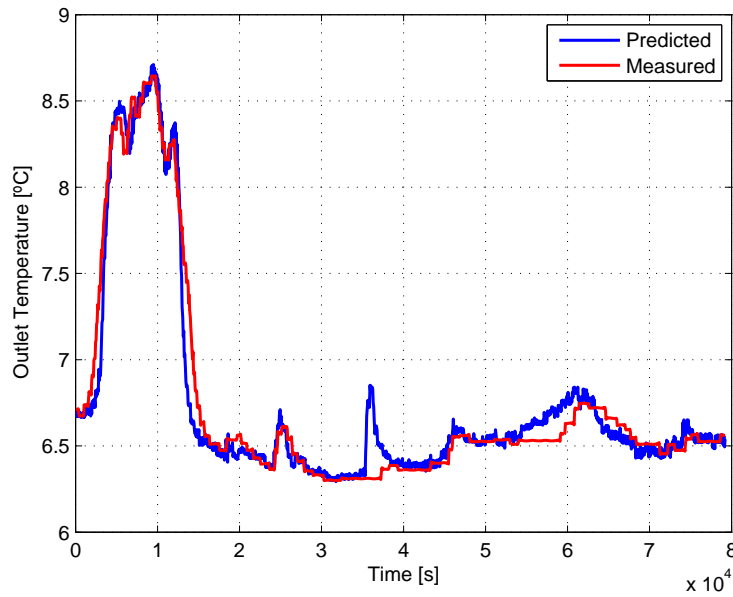

Figure 5.26. Outlet temperature computed from the model (in blue) and measured values of the temperature (red).

This model depends on the pressure level in the condenser and on the saturation temperature of the steam (which in turn depends on the pressure inside the condenser through the saturation properties of the steam). However, it does not depend on the current output but on older ones, due to the delay in the system.

In this chapter, the model of the system has been presented. First, a dynamic model of the hydraulics involved in the system was introduced. Later, a thermodynamic model of the system was presented. Due to the inability of the model to simulate the behavior of the real condenser, the model was abandoned. Instead, a data-driven model was developed. The static model will serve as output equation for the dynamic model of the hydraulics.

Linearized Model 6

In this chapter a linearized model of the main cooling system will be presented. The model presented in the previous chapter is used in the linearization.

6.1 Linearized Hydraulic Model

In order to simplify the linearization, it is assumed that both pumps are running with the same speed and the flow in both condensers are the same at all time. Thereby only one line will be linearized. The linearized model will only be valid, when both pumps are running with the same speed and the flow in both condensers are the same. If there are small deviations, that makes the flow in the two lines different from each other, it can be seen as a disturbance in the model. In Equation 6.1 the non-linear model of line 1 is shown. The pump head function is added to the equation, such that the input is RPM instead of differential pressure.

$$\dot{q}_{line1} \; = \; -\frac{K_{line1}}{J_{line1}} \cdot q_{line1}^2 + \frac{g \cdot \rho}{J_{line1}} \cdot H(n_{line1}, q_{line1}) \tag{6.1}$$

where:

q_{line1}	Volumetric flow	$[m^3/s]$
K_{line1}	Total fluid resistance in line 1	$[kg/m^7]$
J_{line1}	Total fluid inertance in line 1	$[kg/m^4]$
g	Gravity acceleration	$[m/s^2]$
ρ	Density of fluid	$[kg/m^3]$
$H(n_{line1}, q_{line1})$	Head function of pump	$[m]$
n_{line1}	Revolutions per minute	$[RPM]$

By using a slow ramp as RPM input, the steady state values of the flow, at a given RPM, is shown. In Figure 6.1 the steady state values of the flow at a given RPM is shown.
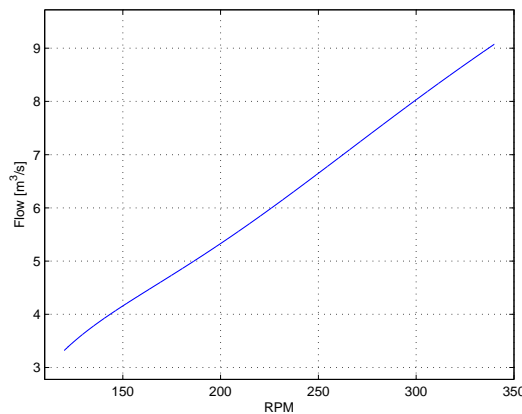

Figure 6.1. Steady state values of RPM and Flow in non-linear model.

The minimum RPM is 120 and the maximum RPM is 340 for the pumps. The model is linearized at the point, where the number of RPM is 230, as this is in between maximum and minimum RPM. The steady state value of the flow, when the RPM is 230, is 6.104 m^3/s. In Equation 6.2 the model of line 1 is linearized. The value of a_{l1} and b_{l1} can be found in Appendix C on page 119.

$$\dot{q}_{l1} \;=\; a_{l1} \cdot q_{l1} + b_{l1} \cdot n_{l1} \tag{6.2}$$

$$a_{l1} \;=\; \left(-\frac{2 \cdot K_{line1}}{J_{line1}} \cdot q_0 + \frac{g \cdot \rho}{J_{line1}} \cdot \left.\frac{\partial H(n,q)}{\partial q}\right|_{n=n_0,q=q_0} \right)$$

$$b_{l1} \;=\; \left(\frac{g \cdot \rho}{J_{line1}} \cdot \left.\frac{\partial H(n,q)}{\partial n}\right|_{n=n_0,q=q_0} \right)$$

In Figure 6.2 the non linear and linear model of line 1 is plotted, where a given RPM and flow will lead to a given flow acceleration. The plot of the non linear model is the left side of the figure and the plot of the linear model is the right side of the figure. The two models seams similar, except in the region where the flow is high and the RPM is low. As this is a region, where the system is assumed to never or rarely go, the linear model is assumed valid in the entire range of operation.
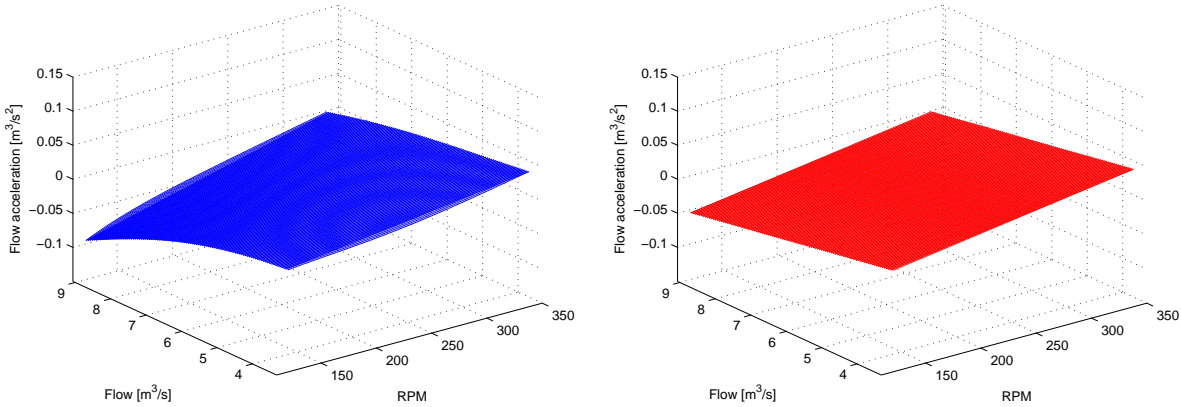

Figure 6.2. From RPM and flow to flow acceleration, where the graph to the left shows the points from the non linear model of line 1 and the graph to the right is the linear model of line 1.

In Figure 6.3 a slow ramp is used as RPM input and the steady state values of the flow, at a given RPM, is shown.
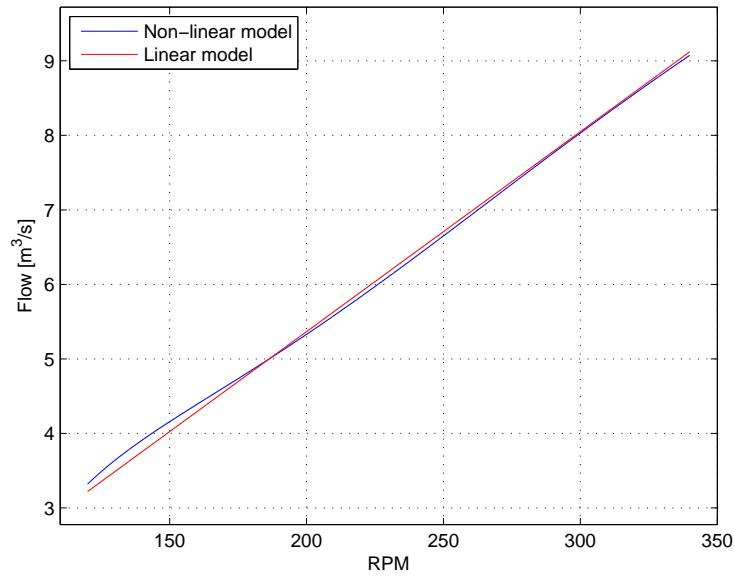

Figure 6.3. Steady state values of RPM and Flow for line 1.

In Equation 6.3 the linearized model is extended, such that it contains both lines.

$$\dot{q}_{lin} \;=\; A \cdot q_{lin} + B \cdot n_{lin} \tag{6.3}$$

As both lines have the same dynamic properties, the parameters from line 1 is used in line 2.

$$A \;=\; \begin{bmatrix} a_{l1} & 0 \\ 0 & a_{l1} \end{bmatrix} \;,\; B = \begin{bmatrix} b_{l1} & 0 \\ 0 & b_{l1} \end{bmatrix}$$

$$q_{lin} \;=\; \begin{bmatrix} q_{line1} \\ q_{line2} \end{bmatrix} \;,\; n_{lin} = \begin{bmatrix} n_{line1} \\ n_{line2} \end{bmatrix}$$

where:

q_{line1}	Flow in condenser 1	$[m^3/s]$
q_{line2}	Flow in condenser 2	$[m^3/s]$
n_{line1}	Revolutions per minute in pump 1	$[RPM]$
n_{line2}	Revolutions per minute in pump 2	$[RPM]$

6.2 Linearized Condenser Model

As stated in Section 5.4, the static model from Equation 5.48 on page 47 will be used in the control design. However, the model is not completely linear, but presents a nonlinearity in the x_{data} term, which follows the expression $x_{data} = \lambda \cdot m_{steam}$, λ being the latent heat of condensation of the steam. This can be seen in equation 6.4.

$$p_{cond} = a_0 + a_1 \Delta T_{tot} + \underbrace{a_2 \lambda(p) \cdot m_{steam}}_{nonlinearity} + a_3 \dot{m}_{sw} + a_4 T_{sw,in} \qquad (6.4)$$

The model will be linearized for a certain operating point as an example. However, the linearization point will depend on the target condenser pressure that Studstrup desires to keep. The first step towards linearizing the model will be to substitute λ by its linearized expression, which in turn depends on the pressure level of the condenser. The new λ will be given by Equation 6.5:

$$\lambda = \lambda_0 + \dot{\lambda} \cdot (p_{cond} - p_{cond,0}) \qquad (6.5)$$

where:

λ_0	=	2506.3	[kJ/kg]
$\dot{\lambda}$	=	-2412.8	[kJ/(kg bar)]
p_0	=	0.011	[bar]

Figures 6.4 and 6.5 show the linearization of λ around the operating point $p = 0.014\ bar$. The relative error in the operating range of interest ($[0.008 : 0.022]$) remains below 0.2%.

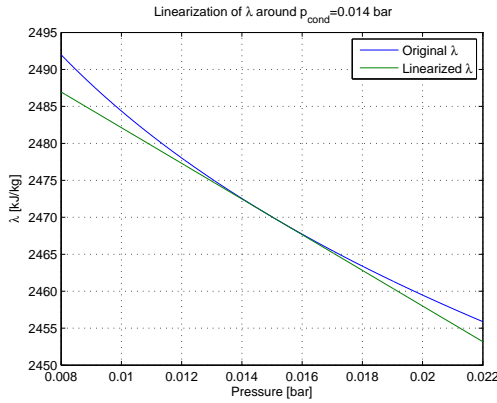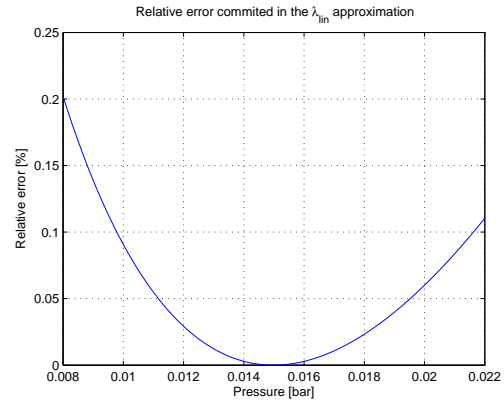**Figure 6.4.** Linearized λ

Figure 6.5. Linearization error

Substituting the new expression for λ in 6.4 yields:

$$p_{cond} = a_0 + a_1 \Delta T_{tot} + a_2 \dot{m}_{steam}(\lambda_0 + \dot{\lambda} \cdot (p_{cond} - p_{cond,0})) + a_3 \dot{m}_{sw} + a_4 T_{sw,in} \qquad (6.6)$$

Isolating the variable p_{cond} on the left side:

$$p_{cond}(1 - a_2 \dot{m}_{steam} \dot{\lambda}) = a_0 + a_1 \Delta T + a_2 (\lambda_0 - \dot{\lambda} \cdot p_{cond,0}) \dot{m}_{steam} + a_3 \dot{m}_{sw} + a_4 T_{sw,in} \qquad (6.7)$$

The linearization point is denoted as OP_0. Finally, taking the derivative with respect to the input that needs to be linearized, m_{steam}, and simplifying:

$$\left.\frac{dp_{cond}}{dm_{steam}}\right|_{OP_0} = \frac{a_2(a_1\Delta T\dot\lambda) + a_3\dot m_{steam,0}\dot\lambda + a_0\dot\lambda + a_4 T_{sw,in,0}\dot\lambda - p_{cond,0}\dot\lambda + \lambda_0}{(1 - a_2\dot m_{steam,0}\dot\lambda)^2} \quad (6.8)$$

Finally, a linear model is available for the thermodynamic part. Its expression is:

$$p_{cond} = p(\Delta T, \dot m_{sw}, T_{sw}, \dot m_{steam,0}) + \left.\frac{dp_{cond}}{dm_{steam}}\right|_{OP_0} (\dot m_{steam} - \dot m_{steam,0}) \quad (6.9)$$

$$p_{cond} = a_0 + a_1\Delta T + a_2 m_{cond,0}\lambda_0 + a_3\dot m_{sw} + a_4 T_{sw,in} +$$
$$\left.\frac{dp_{cond}}{dm_{steam}}\right|_{OP_0} (\dot m_{steam} - \dot m_{steam,0}) \quad (6.10)$$

Let us denote $\left.\frac{dp_{cond}}{dm_{steam}}\right|_{OP_0} (\dot m_{steam} - \dot m_{steam,0})$ as d_{lin}. The numerical value of d_{lin} and d_0 from Equation 6.11 can be found in the Appendix C. Equation 6.10 can be re-expressed as:

$$p_{cond}(t) = d_0 + a_1\Delta T(t) + a_3\dot m_{sw}(t - \theta_{sw}) + a_4 T_{sw,in}(t) + d_{lin}\dot m_{steam}(t - \theta_{steam}) \quad (6.11)$$

where:
θ_{sw} Delay from m_{sw} to p_{cond} [s]
θ_{steam} Delay from m_{sw} to p_{cond} [s]

Since it is a 4-input-1-output model it is not possible to represent it graphically in a 3D plot like the previous hydraulic model. Instead, the linearized model has been tested against validation data from the plant operation. The result can be seen in Figure 6.6.
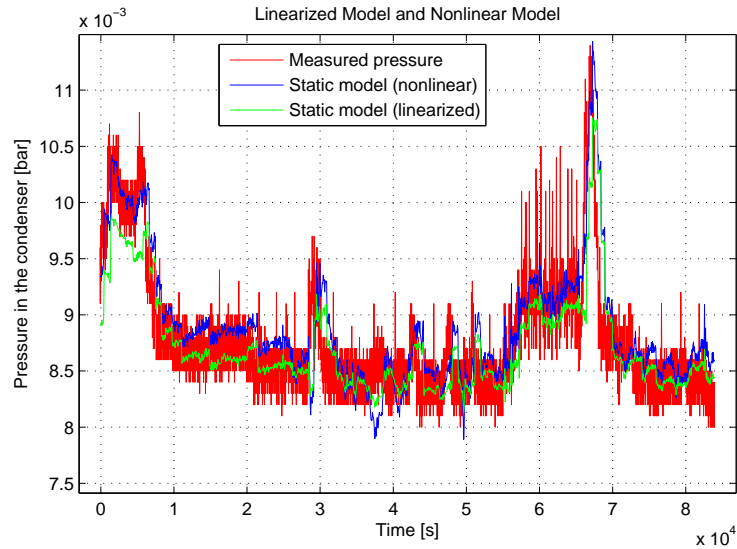

Figure 6.6. Validation of the linearized model for historical operation data.

6.3   Simulation of the Linearized System

The linear model presented in this chapter has been implemented and simulated using MATLAB. The input is maintained constant at the beginning and later subject to a ramp. The disturbances to the system, namely the inlet temperature of the water and the flow of steam are kept constant plus an additive Gaussian noise with variance 0.1 for the seawater temperature and of 2 for the flow of steam. Process noise is simulated as well in the hydraulic system, with a variance of 0.002. The sampling time used in the simulations was $T_s = 66.005\ s$. Both pumps and both parts of the condenser are assumed to operate under the same conditions. The outlet temperature of the seawater is estimated using the linear model derived in Section 5.4.4.

6.3.1   Simulation of an Input Ramp

The response of the system to a ramp in the rotational speed of the pumps (both of which are assumed equal) has been simulated with the available model. The speed of the pumps should never vary too abruptly, but respect the slew rate limitation of the pumps. When the speed of the pumps is lowered from 200 rpm to 150 rpm (see Figure 6.7), the flow of seawater that is circulated decreases, as can be seen in Figure 6.8. Note that Figure 6.8 shows the flow for one pipeline. The flow through the second pipeline is assumed to be equal at all times. If the inlet temperature of the seawater is assumed constant (see Tin Figure 6.9), this means that in order to condense the same amount of steam, the seawater will experience a higher temperature increase, and hence the outlet temperature increases (see Tout in Figure 6.9). The lower rate of condensation of the steam, however, causes the pressure in the condenser to increase (see Figure 6.11). The increase in the condensation pressure results directly in an increase of the saturation temperature of the steam (see Tsat in Figure 6.9). The result of this is that, in spite of the outlet seawater temperature increasing (which results in an increase of the average temperature of the seawater in the condenser), the increase in the saturation temperature compensates this effect and results finally in a higher mean temperature difference between the steam and the seawater (see Figure 6.10). The flow of steam is kept constant (with noise) during the simulation, as shown in Figure 6.12. In order to have a better overview of the dynamics of the system and the effect of the delays, the input (rotational speed of the pump), state (flow of seawater through the hydraulic cooling circuit) and the main output (pressure level inside the condenser) have been normalized with respect to their means in Figure 6.13.
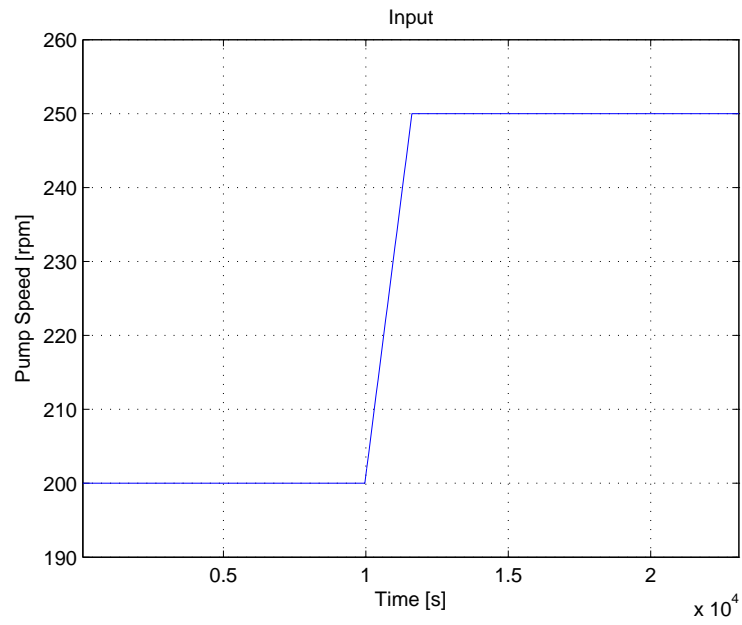
Figure 6.7. The rotational speed of the pumps is the input to the system. Both pumps are assumed to operate at the same conditions.

Figure 6.8. The flow of the seawater through one pipeline as the state.

Figure 6.9. Temperatures in each of the sides of the condenser. Saturation temperature of the steam and inlet and outlet temperatures of the cooling seawater.
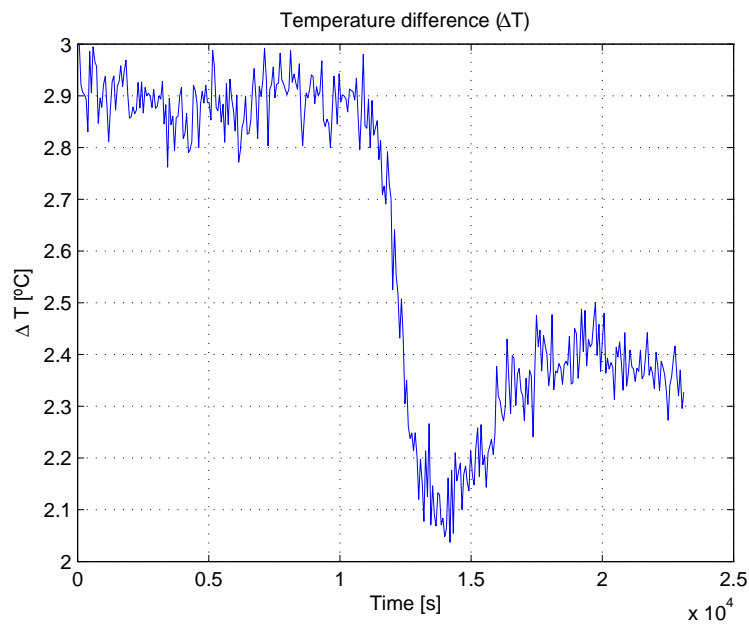
Figure 6.10. Average temperature difference in the condenser.
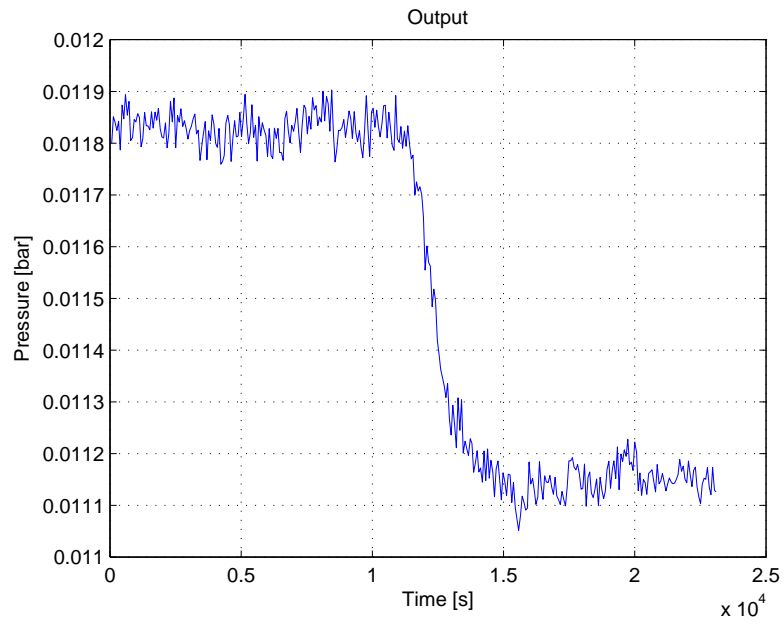
Figure 6.11. The output of the system is the pressure level of the steam inside the condenser.
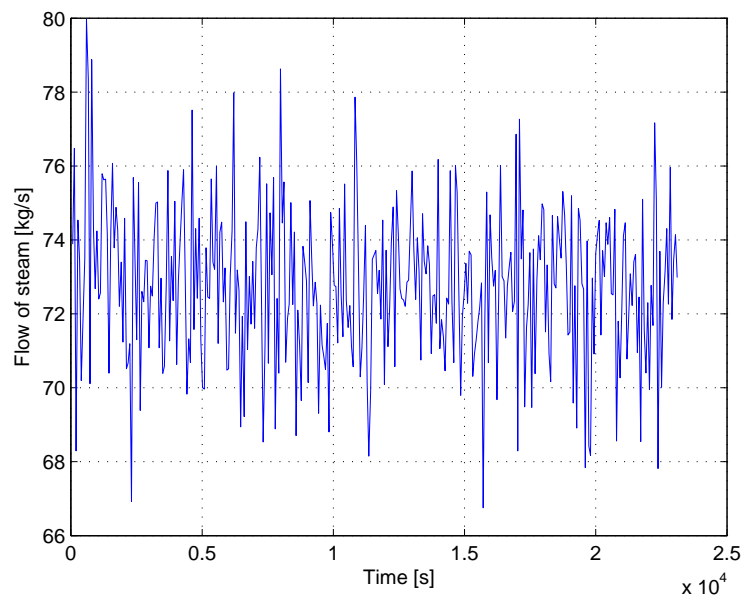
Figure 6.12. Flow of steam during the simulation
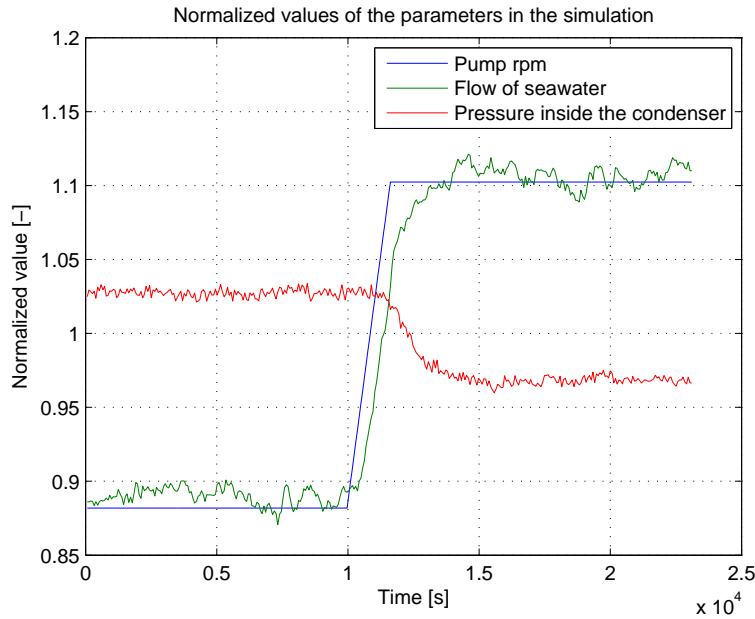
Figure 6.13. Mean-normalized values of the input, state and output of the system

6.3.2 Simulation of a Disturbance on the System

One of the main input disturbances that drives the variations of the condensation is the amount of steam arriving to the condenser. A surge in the flow of steam will cause a rise in the pressure, shifting the operating point of the plant. In this simulation, an increase in the mass flow of steam is simulated while keeping a constant input speed to the pumps. It is expected that the pressure will increase, dragging the saturation temperature to a higher value as well, and increasing the outlet temperature of the seawater.

The input to the system is constant, as shown in Figure 6.14, which results in a (roughly) steady flow, disturbed by the process noise (Figure 6.15). The inlet temperature is again considered constant and only subject to seasonal variations (see Figure 6.16). The flow of steam is increased from an initial average value of $72.81kg/s$ to a final value of $97.81kg/s$, as shown in Figure 6.19. As expected, the increase in the flow of steam leads to an increase in the condensation pressure (Figure 6.18), the saturation temperature and the outlet seawater temperature (Figure 6.16). It can be seen in Figure 6.17 that the increase of the saturation temperature causes a higher mean temperature difference, though the delayed increase in the outlet temperature causes a small decrease in its value. As in the previous simulation, input, state and outlet, along with the flow of steam, are represented normalized with respect to their means in Figure 6.20.
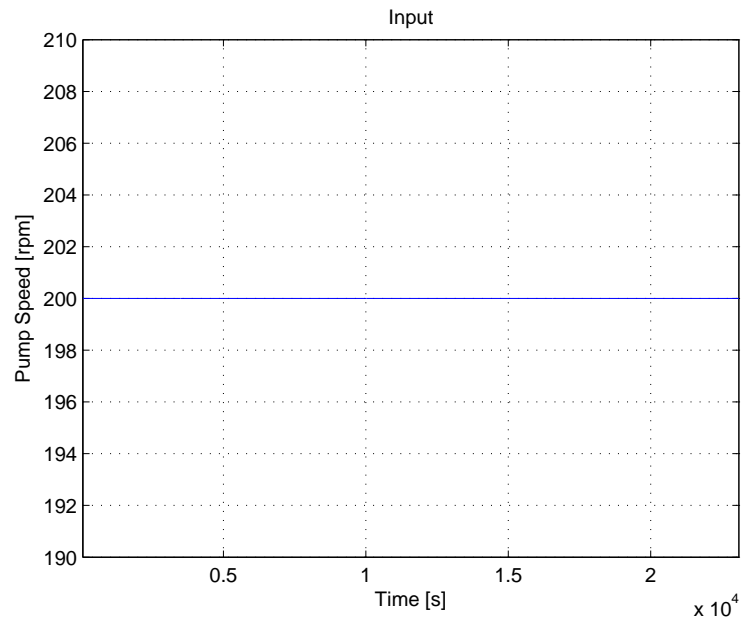
Figure 6.14. The rotational speed of the pumps is the input to the system. Both pumps are assumed to operate at the same conditions.
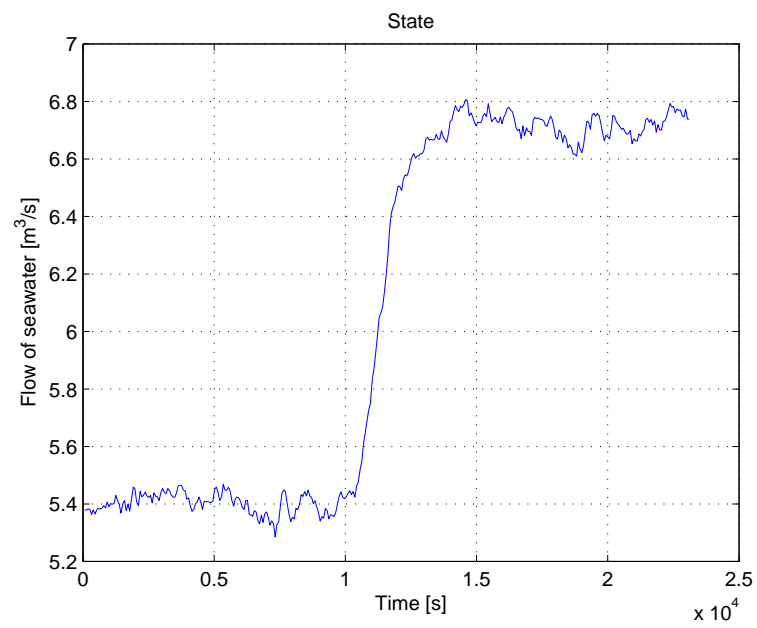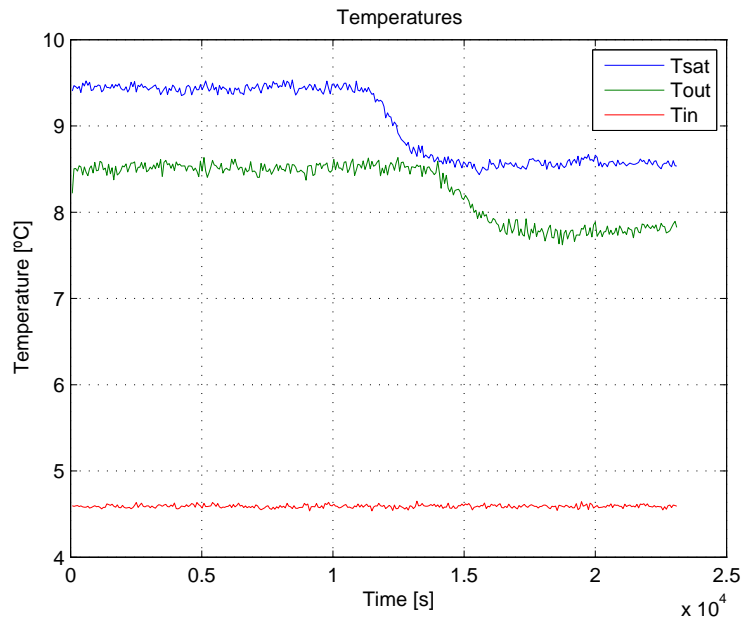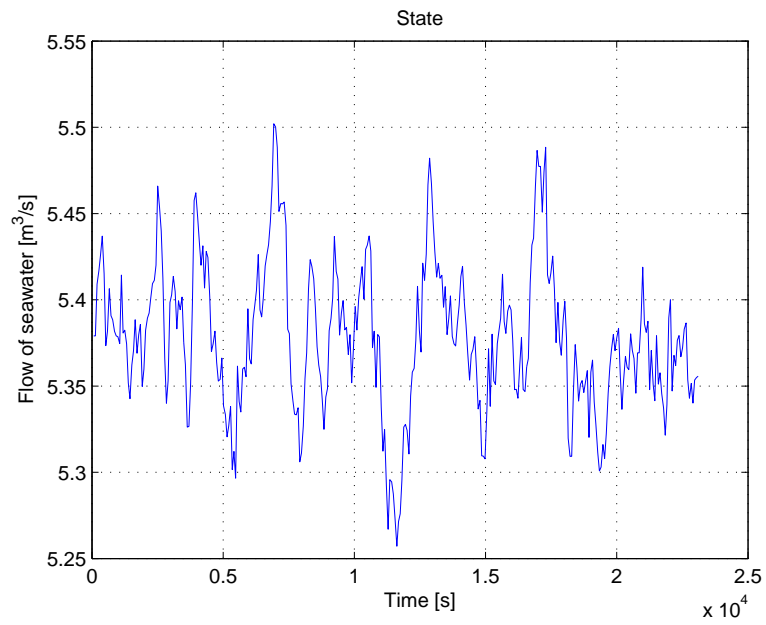

Figure 6.15. The flow of the seawater through one pipeline as the state.
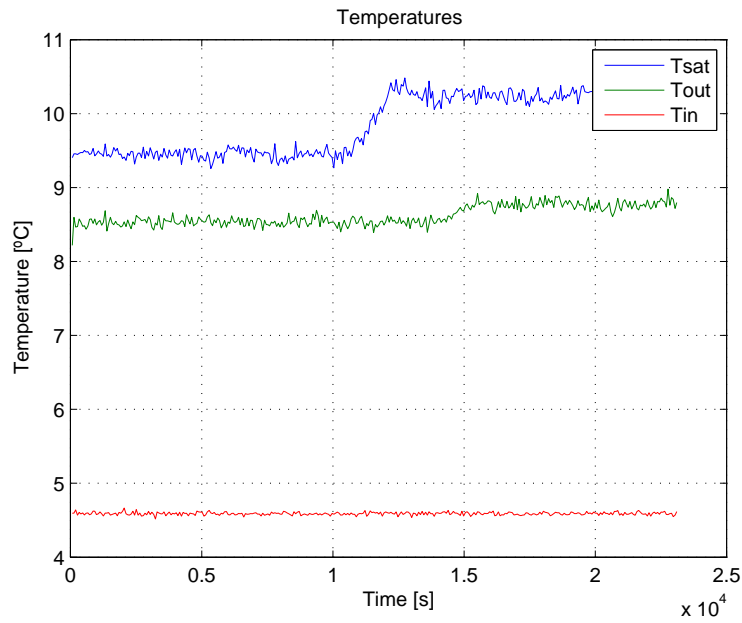
Figure 6.16. Temperatures in each of the sides of the condenser. Saturation temperature of the steam and inlet and outlet temperatures of the cooling seawater.
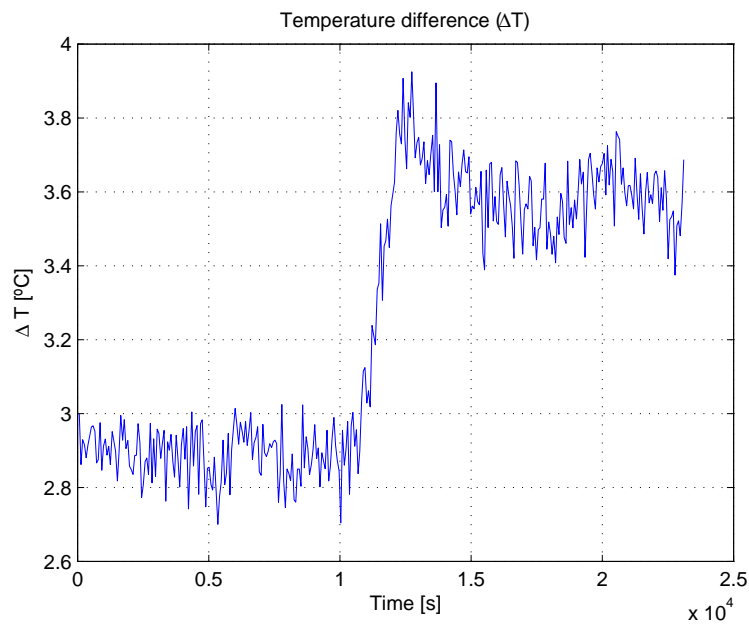
Figure 6.17. Average temperature difference in the condenser.
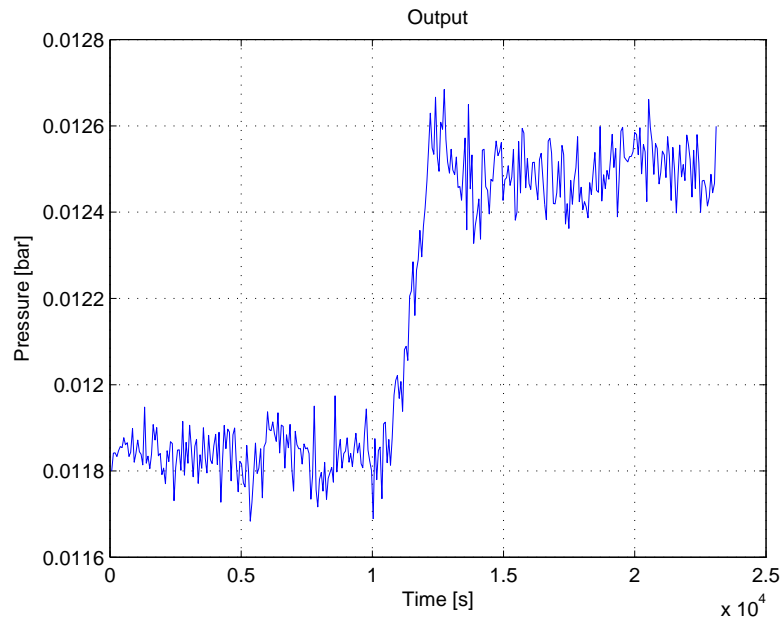
Figure 6.18. The output of the system is the pressure level of the steam inside the condenser.
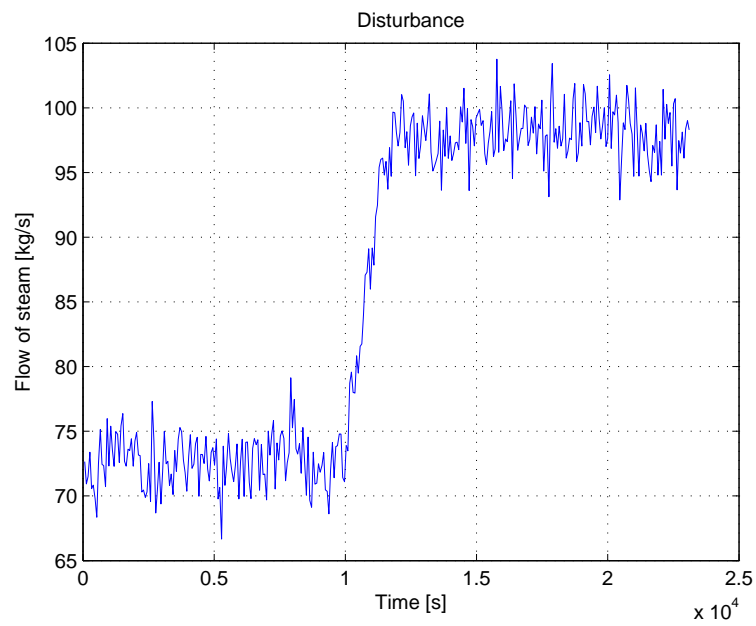
Figure 6.19. Flow of steam during the simulation
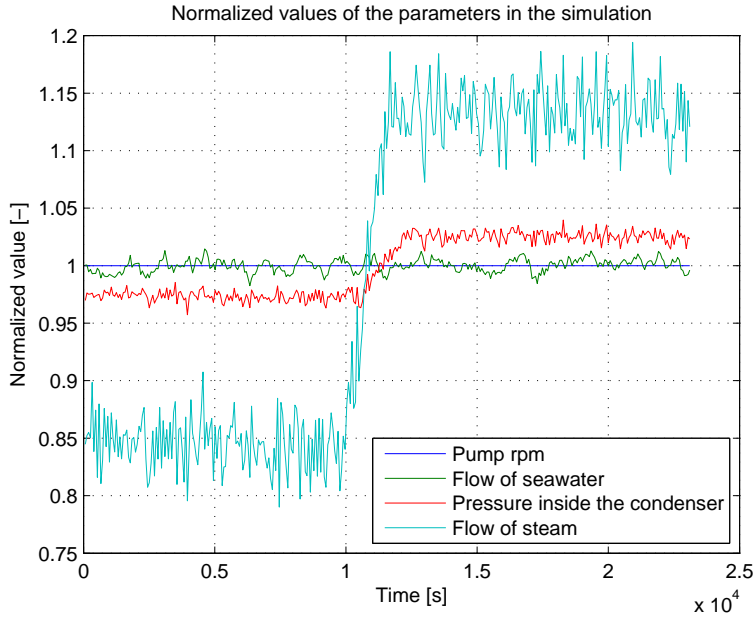
Figure 6.20. Mean-normalized values of the input, state and output of the system

6.3.3 Interpretation of the Results

In this Section, simulations of the model have been shown. It is of particular interest to observe the behavior of the mean temperature difference, ΔT, and how it relates to the condensation pressure. In Section 6.3.1, the flow of seawater was increased, causing two opposing effects on ΔT: an decrease in the saturation temperature (and pressure), which tends to decrease ΔT and a decrease in the outlet temperature of seawater, which causes ΔT to increase. The result of both effects combined is an overall decrease in ΔT. The average temperature difference is positively related to the heat transfer rate in a heat exchanger, in steady state the heat transfer would be given by Equation 6.12.

$$Q \;=\; UAF \cdot \Delta T \tag{6.12}$$

Therefore, in order to achieve a lower pressure, the flow of seawater can be increased (by increasing the speed of the pump), but that will cause a drop in the mean temperature difference, which hinders the heat transfer, such that the larger flow of seawater is required for the steady operation of the condenser. In addition, varying the pressure level in the condenser affects the latent heat of condensation of the water, and thereby the amount of heat that needs to be extracted from the steam. Figure 6.21 shows the relation between the latent heat of condensation λ and the pressure level in the condenser. The plot was made using XSteam, a MATLAB implementation of the steam tables. It can be seen that the value of λ is monotonously decreasing with the pressure. Hence, a higher cooling capacity is needed to condense the steam at lower pressure than at a higher one.
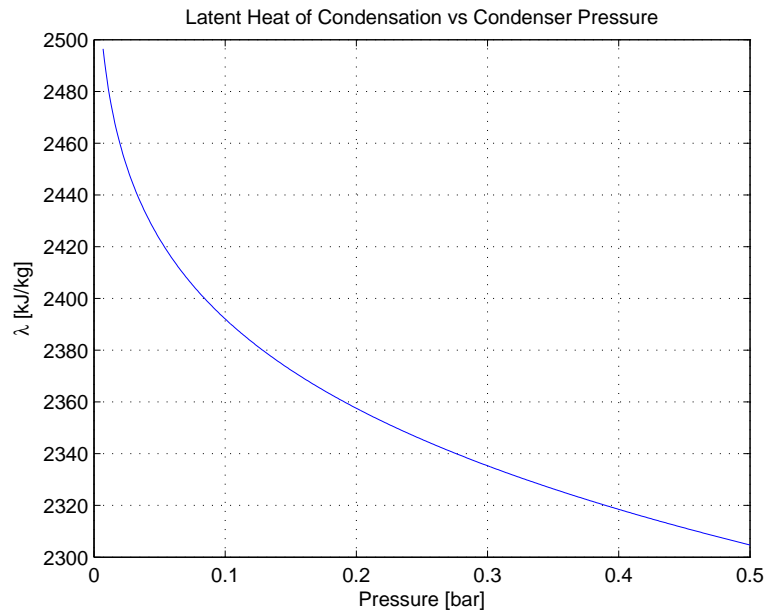
Figure 6.21. At lower pressure, the amount of heat that needs to be extracted in order to condense the fluid is larger.

On the other hand, the effect of increasing the mass flow of steam into the condenser is the opposite. Both the steam saturation temperature and the outlet seawater temperature increase, ultimately increasing the value of ΔT and improving the heat transfer, such that the cooling demand is met without increasing the flow of seawater.

This chapter has presented the linearized model for both the hydraulic circuit and the thermodynamic system. Its response has been simulated for changes in the input (speed of the pumps) and disturbances (inlet flow of steam). However, before proceeding with suggesting a control strategy for the system, an improved way of estimating the flow of seawater will be proposed.

Estimation 7

In the Studstrup CHP power plant not all the relevant system states can be measured directly. It is therefore necessary to estimate the value of some of them in order to generate the appropriate set point for the pumps. This section will analyze the possible methods that can be used to estimate these sates using the available data and discuss their advantages and drawbacks.

Seawater Flow

The flow of seawater, which is needed for condensing the steam, is not measured directly, but estimated through the differential pressure across the condenser. In case of fouling in the condenser, the pressure will increase and thereby the estimation of flow will show increasing flow, where the flow is decreasing. In order to make the estimation more reliable then the present flow estimation at Studstrup power plant, other possible estimators are considered. There are three different differential pressures in the pipeline system, that are of interest in the creation of an alternative flow estimator. There is the differential pressure across the pumps, the mussel filters and the TAPROGGE filters. From the differential pressure across the mussel filters and the TAPROGGE filters, it is possible to estimate the flow of seawater in the same manner as with the present flow estimation at the power plant. The differential pressure across the pumps can be used in an estimator including the pipeline model or the pump model. This leads to three different approaches to estimate the flow of seawater:

- Estimation from the overall Head-Flow curve of the system
- Estimation from the pressure loss in the mussel or TAPROGGE filter
- Estimation from the characteristic curve of the pump

This section will analyze each of the possibilities and assess their advantages and drawbacks in order to choose the most reliable method to estimate this parameter.

7.1 Flow Estimation from The Overall Head-Flow Curve of The System

For a target flow, the pumps need to provide a certain level of head in order to overcome the resistance of the system. By knowing the curve of the system and the current rotational speed of the pumps, it is possible to know the operating point and thus the flow. The head-flow curve of the system is not static, as it has to be taken into account that fouling can have an effect on the resistance of the pipes. As a result, the parameter of the curve can vary. The curve of the system will in case of fouling change as shown in Figure 7.1, as the fluid resistance will increase.
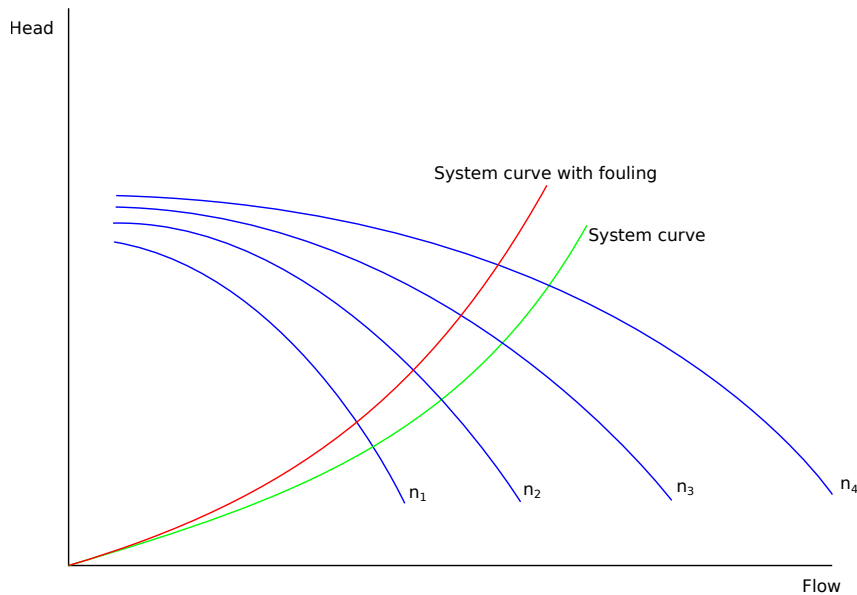
Figure 7.1. Head-Flow curves with different working conditions.

In case the pipeline model from RPM to flow is used, the misbehavior in the system such as fouling will not be shown in the output. In case the pipeline model from differential pressure to flow is used, the misbehavior in the system will be shown. In case of fouling the pressure after the pump will increase, which will increase the differential pressure across the pumps. An increasing differential pressure will in the pipeline model produce an increasing flow, where in case of fouling the flow is decreasing. Thereby this approach contains the same issues, as the estimation already in use at Studstrup power plant and will therefore not be used.

7.2 Flow Estimation from The Pressure Loss in The Mussel or TAPROGGE Filter

In order to know whether or not the differential pressure across the mussel or the TAPROGGE filter can be used in an estimator to calculate the flow of seawater, the pressure across the condenser, mussel filter and the TAPROGGE filter are compared. In Figure 7.2, 7.3 and 7.4 the differential pressure across the condenser, mussel filter and the TAPROGGE filter are shown.

In Figure 7.2 the differential pressure across the condenser is shown. The data shown is from a day where the flow of seawater is quite steady. The differential pressure across the the condenser is with only minor changes. In Figure 7.3 the differential pressure across the mussel filter is shown. The measurement of the differential pressure across the mussel filter is noisy and contains a sawtooth signal with a relatively high amplitude. The pressure across the mussel filter is therefore assumed a too noisy signal to use in a flow estimator.
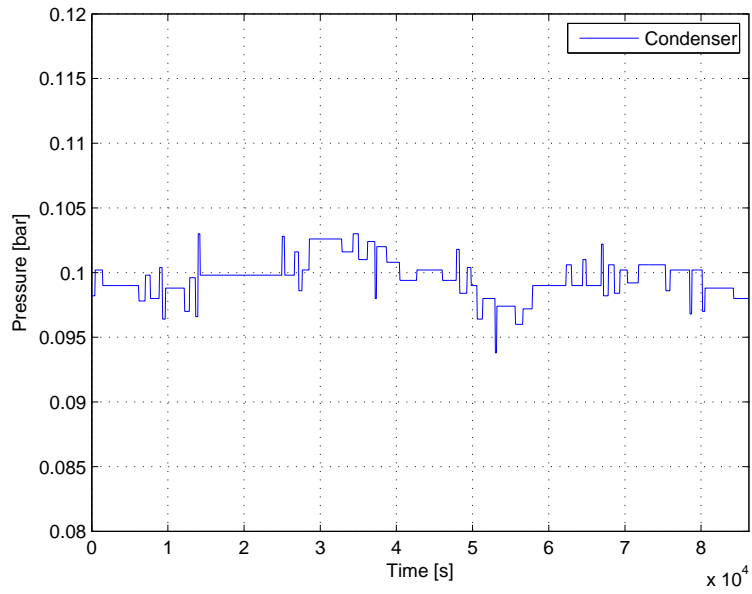
Figure 7.2. Pressure across the condenser.
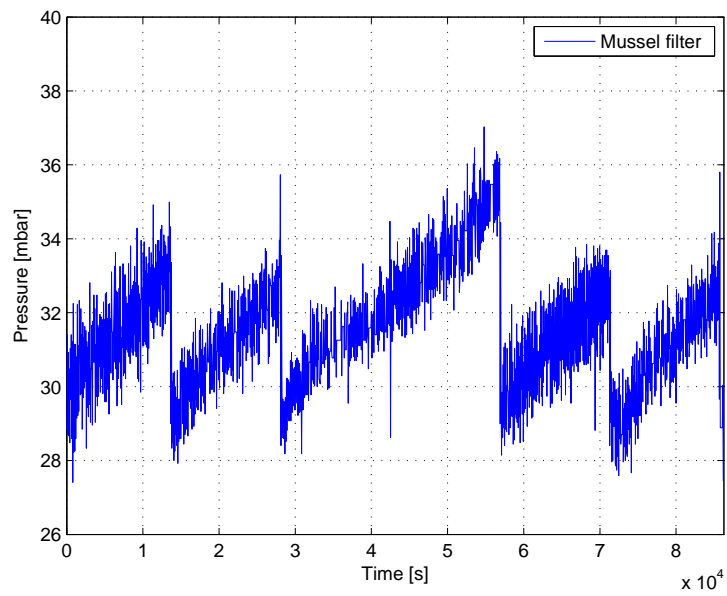
Figure 7.3. Pressure across the mussel filter.

In Figure 7.4 the differential pressure across the TAPROGGE filter is shown. The differential pressure measurement is noisy, but the mean value seams quite steady.
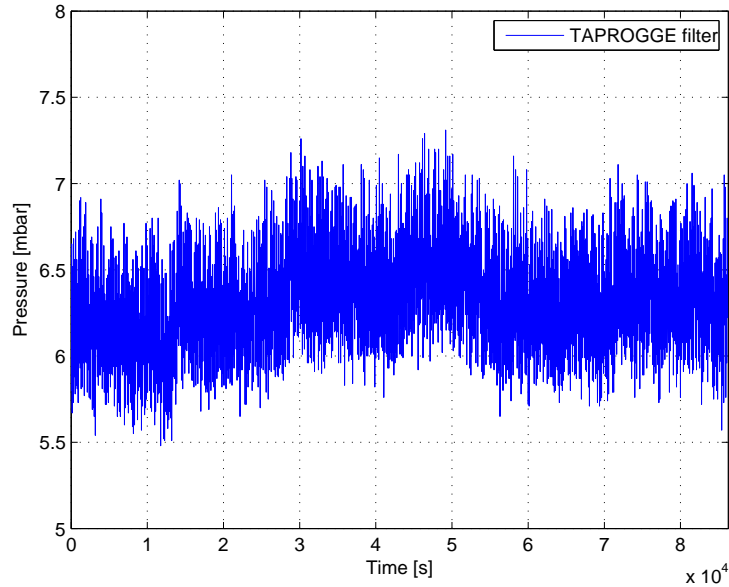
Figure 7.4. Pressure across the TAPROGGE filter.

The flow estimation is calculated in the same manner as the flow estimation from the differential pressure across the condenser. The calculation of the seawater flow is shown in Equation 7.1, where the value of K_{filter} is chosen from fitting the flow estimation through the TAPROGGE filter to the estimation through the condenser. The value of K_{filter} can be found in Appendix D on page 123.

$$q_{filter} \;=\; \sqrt{\frac{\Delta p_{filter}}{K_{filter}}} \tag{7.1}$$

where:

q_{filter}	Volumetric flow through TAPROGGE filter	$[m^3/s]$
K_{filter}	Fluid resistance coefficient in TAPROGGE filter	$[kg/m^7]$
Δp_{filter}	Pressure drop across the TAPROGGE filter	$[kg/m \cdot s^2]$

In Figure 7.5 the flow at the 10th of February 2014 is shown. The flow estimation from the differential pressure across the TAPROGGE filter is following the flow estimation from the differential pressure across the condenser. The influence of the noise in the flow estimation can be reduced by using a Kalman filter containing the model of the linearized pipeline model, where the input is the RPM and the differential pressure across the TAPROGGE filter.
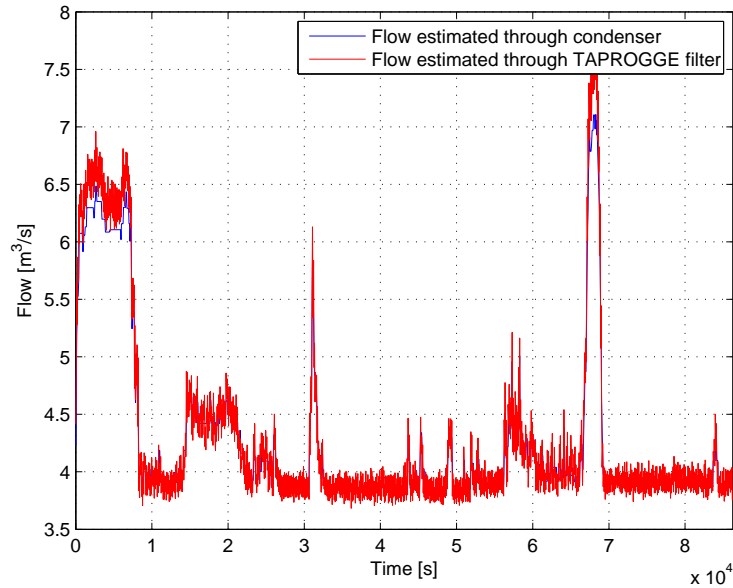
Figure 7.5. Flow estimation from the differential pressure.

7.3 Flow Estimation from The Characteristic Curve of The Pump

As both the Head and Power curves of the pumps are available, either of them can be used to estimate the flow of seawater for a certain rotational speed of the pumps. The characteristic curve of the pump provides a static map from the flow to the head or the power given a rotational speed. One possible approach to estimate the flow of seawater is to fit a function to the characteristic curve of the pump, where the RPM and differential pressure or power are inputs and the flow of seawater is the output. In Figure 7.6 the fitted function of RPM and differential pressure is used to estimate the flow of seawater. In the figure both the flow estimation through the fitted function and the flow estimation through the condenser are plotted. The flow estimation from the fitted function is following the estimation from the condenser, but the estimation is noisy.

In Figure 7.7 the fitted flow estimation function with RPM and power as inputs is used. The plot contains both the flow estimation from the fitted function and the condenser. The function estimation is following the estimation from the condenser, but is more noisy than the flow estimation through the fitted function with RPM and differential pressure as inputs. Both fitted functions are a polynomial with the degree in both variables of five. The functions can be found in Appendix D on page 123.

70
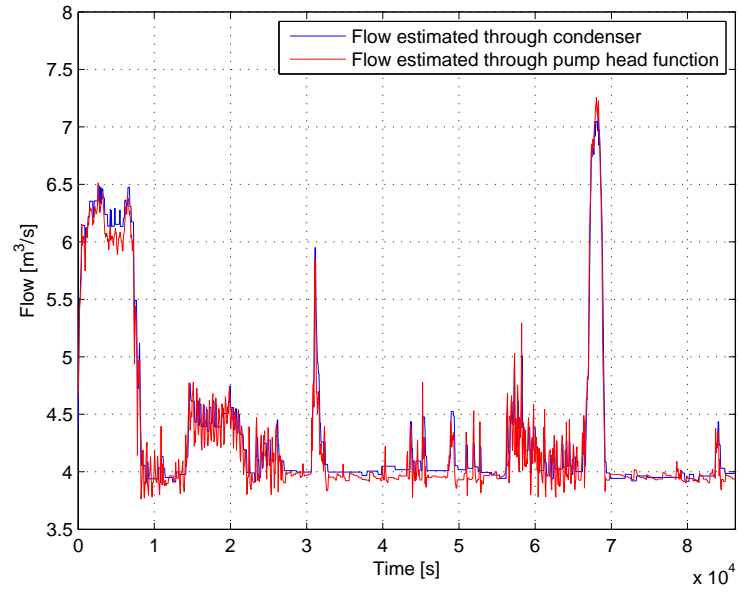
Figure 7.6. Flow estimation from the pump head curve.
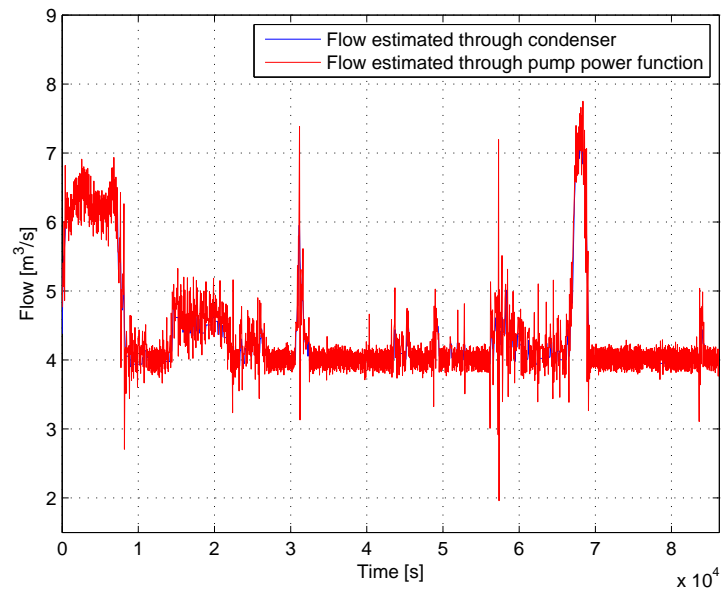
Figure 7.7. Flow estimation from the pump power curve.

Like in the case with the TAPROGGE filter, the influence of the noise can be reduced by a Kalman filter.

7.4   Flow Estimation Using A Kalman Filter

The flow estimation through the TAPROGGE filter, pump pressure and pump power are all noisy. As they all contribute with information of the system behavior, they are all used as measurement inputs to a Kalman filter. As the hydraulic model is nonlinear an Extended Kalman Filter (EKF) is used. To make the flow estimation more reliable fouling in the condenser is considered, where it is assumed that fouling is only occurring in the condenser. In Figure 7.8 the parts in the system of interest are shown, where:

- P_{w1}/P_{w2} is the power consumption of pump 1 / pump 2
- $\Delta p_1/\Delta p_1$ is the differential pressure across pump 1 / pump 2
- q_{p1}, q_{p2}, q_{ls1} and q_{ls2} is the flow through pump 1, pump 2, condenser 1 and condenser 2
- $\Delta p_{con1}/\Delta p_{con2}$ is the differential pressure across condenser 1 / condenser 2
- $\Delta p_{filter1}/\Delta p_{filter2}$ is the differential pressure across TAPROGGE filter 1 / filter 2

The flow is modeled by using the nonlinear dynamic model, which is shown in Equation 5.13 on page 26. The differential pressure across the condenser and the TAPROGGE filter are modeled by using a static pipe model. The power consumption of the pump and the differential pressure across the pump are modeled by using the pump functions, which can be found in Appendix C on page 119.
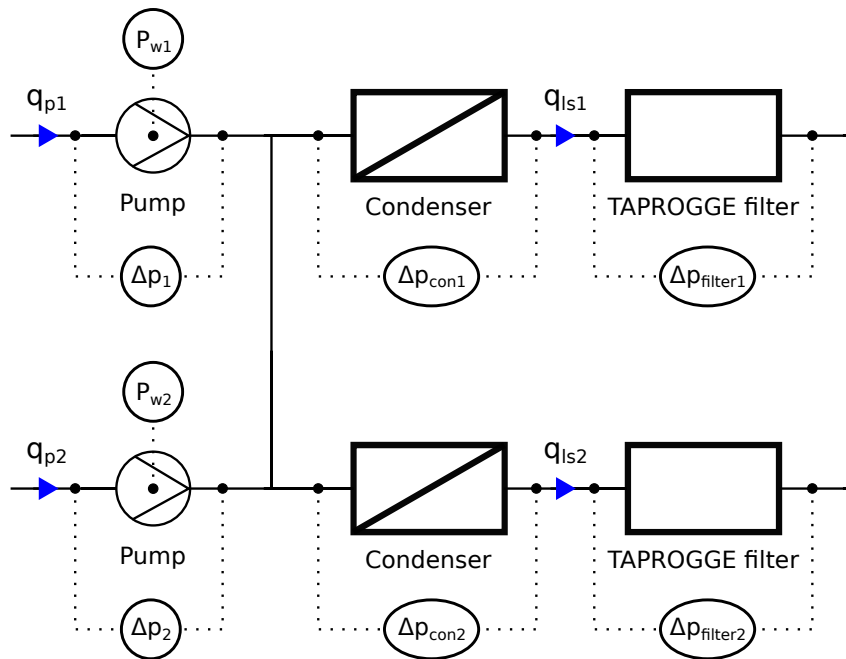
Figure 7.8. Overview of the seawater system, where the shown measurements are used in the construction of the extended Kalman filter.

In Appendix D on page 123 the nonlinear hydraulic model is changed, such that it contains the fouling parameters. Further more the parameters that are, in Appendix C on page 119, equal to zero, are removed from the model. The parameters J_{ls1} and J_{ls2} are equal and therefore the parameter J_{ls} is used instead. The same is the case with the flow resistance K_{ls1} and K_{ls2}, where the parameter K_{ls} is used. Further more the pump head function is added to the model, such that the input is RPM instead of pressure. The model is shown in Equation D.6 on page 125,

where the discretized model is used in the EKF. The discretization is done using forward Euler method. The discretized model is shown in Equation 7.2.

$$q[k+1] = -Ts \cdot \lambda_{KJ1}(q[k], K_{f1}, K_{f2}) - Ts \cdot \lambda_{KJ2}(q[k]) \qquad (7.2)$$
$$+ Ts \cdot \lambda_{pJ}(n[k], q[k]) + q[k]$$

where:

Ts	Sample time	$[s]$
K_{f1}	Fluid resistance coefficient caused by fouling in condenser 1	$[kg/m^7]$
K_{f2}	Fluid resistance coefficient caused by fouling in condenser 2	$[kg/m^7]$

The differential pressure across the condenser and the TAPROGGE filter are modeled by using a static pipe model. The power consumption of the pump and the differential pressure across the pump are modeled by using the pump functions, which can be found in Appendix C on page 119. The output model is given by:

$$\Delta p_{con1}[k] = (K_c + K_{f1}) \cdot q_{p1}[k]^2$$
$$\Delta p_{con2}[k] = (K_c + K_{f2}) \cdot q_{p2}[k]^2$$
$$\Delta p_{filter1}[k] = K_{filter} \cdot q_{ls1}[k]^2$$
$$\Delta p_{filter2}[k] = K_{filter} \cdot q_{ls2}[k]^2$$
$$P_{w1}[k] = P(n_{p1}[k], q_{p1}[k])$$
$$P_{w2}[k] = P(n_{p2}[k], q_{p2}[k])$$
$$\Delta p_1[k] = g \cdot \rho \cdot H(n_{p1}[k], q_{p1}[k])$$
$$\Delta p_2[k] = g \cdot \rho \cdot H(n_{p2}[k], q_{p2}[k])$$

where:

$q_{p1}[k]$, $q_{p2}[k]$	Flow through pumps	$[m^3/s]$
$q_{ls1}[k]$, $q_{ls2}[k]$	Flow through condensers	$[m^3/s]$
$K_{f1}[k]$, $K_{f1}[k]$	Fouling in condensers	$[kg/m^7]$
K_c	Fluid resistance coefficient in condenser	$[kg/m^7]$
K_{filter}	Fluid resistance coefficient in TAPROGGE filter	$[kg/m^7]$
$p_{con1}[k]$, $p_{con2}[k]$	Pressure across condensers	$[kg/m \cdot s^2]$
$p_{filter1}[k]$, $p_{filter2}[k]$	Pressure across TAPROGGE filters	$[kg/m \cdot s^2]$
$P_{w1}[k]$, $P_{w2}[k]$	Power consumption in the pumps	$[kW]$
$\Delta p_1[k]$, $\Delta p_2[k]$	Pressure across the pumps	$[kg/m \cdot s^2]$
$n_{p1}[k]$, $n_{p2}[k]$	RPM in the pumps	$[RPM]$
g	Gravity acceleration	$[m/s^2]$
ρ	Density of fluid	$[kg/m^3]$

The fluid resistance coefficients caused by fouling in the condensers are unknown. In order to estimate the values of the fouling resistance coefficients, two extra states are added to the EKF such that the K_{f1} and K_{f2} are stats. The fouling in the condenser is assumed to contain significantly slow dynamic, therefore the fouling is considered a constant. The state vector (X), output vector (Z) and input vector (n) in the EKF are therefore:

$$\hat{X}[k] \;=\; \begin{bmatrix} \hat{q}_{p1}[k] \\ \hat{q}_{p2}[k] \\ \hat{q}_{ls1}[k] \\ \hat{q}_{ls2}[k] \\ \hat{K}_{f1}[k] \\ \hat{K}_{f2}[k] \end{bmatrix} \;,\quad \hat{Z}[k] \;=\; \begin{bmatrix} \widehat{\Delta p}_{con1}[k] \\ \widehat{\Delta p}_{con2}[k] \\ \widehat{\Delta p}_{filter1}[k] \\ \widehat{\Delta p}_{filter2}[k] \\ \hat{P}_{w1}[k] \\ \hat{P}_{w2}[k] \\ \widehat{\Delta p}_1[k] \\ \widehat{\Delta p}_2[k] \end{bmatrix} \;,\quad n[k] \;=\; \begin{bmatrix} n_{p1}[k] \\ n_{p2}[k] \end{bmatrix}$$

From Equation 7.2 and the output model, the estimation of the state and output can be done as shown in Equation 7.3 and 7.4.

$$\hat{X}[k] \;=\; f\big(\hat{X}[k-1] \,,\, n[k-1]\big) \tag{7.3}$$

$$\hat{Z}[k] \;=\; g\big(\hat{X}[k] \,,\, n[k-1]\big) \tag{7.4}$$

As the fouling in the condenser is assumed constant, the state estimation function is:

$$f\big(\hat{X}[k] \,,\, n[k]\big) \;=\; \begin{bmatrix} Ts \cdot \Big(\lambda_{pJ}(n[k], \hat{q}[k]) - \lambda_{KJ1}(\hat{q}[k], \hat{K}_{f1}[k], \hat{K}_{f2}[k]) - \lambda_{KJ2}(\hat{q}[k]) \Big) + \hat{q}[k] \\ \hat{K}_{f1}[k] \\ \hat{K}_{f2}[k] \end{bmatrix}$$

By using the output model, the output estimation function is given by:

$$g\big(\hat{X}[k] \,,\, n[k]\big) \;=\; \begin{bmatrix} (K_c + \hat{K}_{f1}[k]) \cdot \hat{q}_{p1}[k]^2 \\ (K_c + \hat{K}_{f2}[k]) \cdot \hat{q}_{p2}[k]^2 \\ K_{filter} \cdot \hat{q}_{ls1}[k]^2 \\ K_{filter} \cdot \hat{q}_{ls2}[k]^2 \\ P(n_{p1}[k], \hat{q}_{p1}[k]) \\ P(n_{p2}[k], \hat{q}_{p2}[k]) \\ g \cdot \rho \cdot H(n_{p1}[k], \hat{q}_{p1}[k]) \\ g \cdot \rho \cdot H(n_{p2}[k], \hat{q}_{p2}[k]) \end{bmatrix}$$

In order to calculate the propagation of the covariance in the prediction step in the EKF, the state and output matrix is calculated by linearizing the state estimation function and the output estimation function. In order to construct and test the Kalman filter, a seawater fouling test model are constructed as explained in Appendix E on page 127. The prediction steps of the EKF are shown in Equation 7.5, 7.6 and 7.7 and the updating steps are shown in Equation 7.8, 7.9 and 7.10.

Predict :

$$\hat{X}^-[k] \; = \; f\big(\hat{X}^+[k-1] \; , \; n[k-1]\big) \tag{7.5}$$

$$\hat{Z}[k] \; = \; g\big(\hat{X}^-[k] \; , \; n[k-1]\big) \tag{7.6}$$

$$P^-[k] \; = \; \Phi_h[k-1] \cdot P^+[k-1] \cdot \Phi_h[k-1]^T + Q \tag{7.7}$$

where:
$\hat{X}^-[k]$ Priori state estimation
$\hat{X}^+[k]$ Posteriori state estimation
$n[k]$ Revolutions per minute
$\hat{Z}[k]$ Output estimation
$P^-[k]$ Priori error covariance
$P^+[k]$ Posteriori error covariance
$\Phi_h[k]$ Linearized state matrix
Q Process noise covariance

Update :

$$K[k] \; = \; P^-[k] \cdot H_h[k]^T \cdot (H_h[k] \cdot P^-[k] \cdot H_h[k]^T + R)^{-1} \tag{7.8}$$

$$\hat{X}^+[k] \; = \; \hat{X}^-[k] + K[k] \cdot (Z[k] - \hat{Z}[k]) \tag{7.9}$$

$$P^+[k] \; = \; (I - K[k] \cdot H_h[k]) \cdot P^-[k] \tag{7.10}$$

where:
$K[k]$ Kalman gain
$H_h[k]$ Linearized output matrix
$Z[k]$ Measurement
R Measurement noise covariance

The linearized state and output matrix are calculated in each prediction step, where the predicted state is used as the operating point.

$$\Phi_h[k-1] \; = \; \left.\frac{\partial f(X \; , \; n[k-1])}{\partial X}\right|_{X=\hat{X}^-[k-1]} \quad , \quad H_h[k] \; = \; \left.\frac{\partial g(X \; , \; n[k-1])}{\partial X}\right|_{X=\hat{X}^-[k]}$$

The values of the measurement noise covariance are found by using data, where the RPM is constant. The values of the process noise covariance are found by fitting the flow estimation from the EKF to the flow from the seawater fouling test model. In the fitting $K_{f1} = 1000$, $K_{f2} = 500$ and the input RPM signal used is shown in Figure 7.9. The R and Q matrices can be found in Appendix D on page 123.
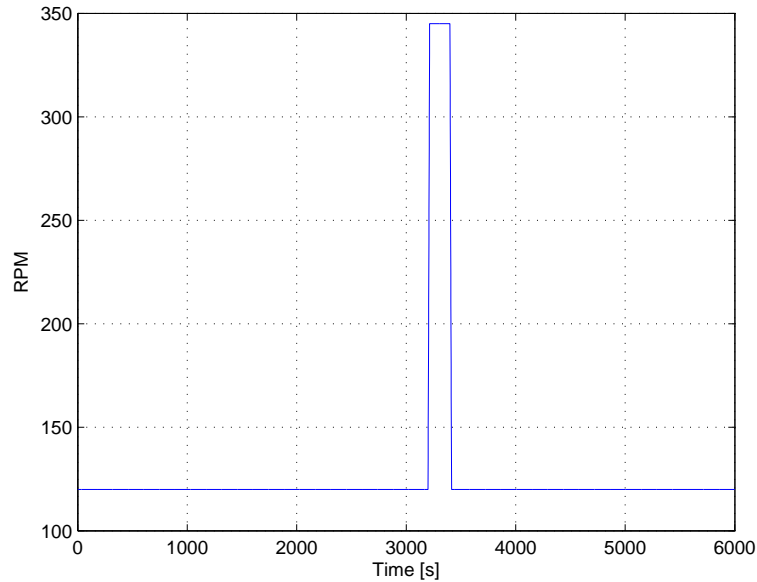
Figure 7.9. The input RPM to the model.

The flow through each pump, caused by the RPM shown in Figure 7.9, is shown in Figure 7.10. As shown the estimated flow converge to the model flow and follows the model flow.
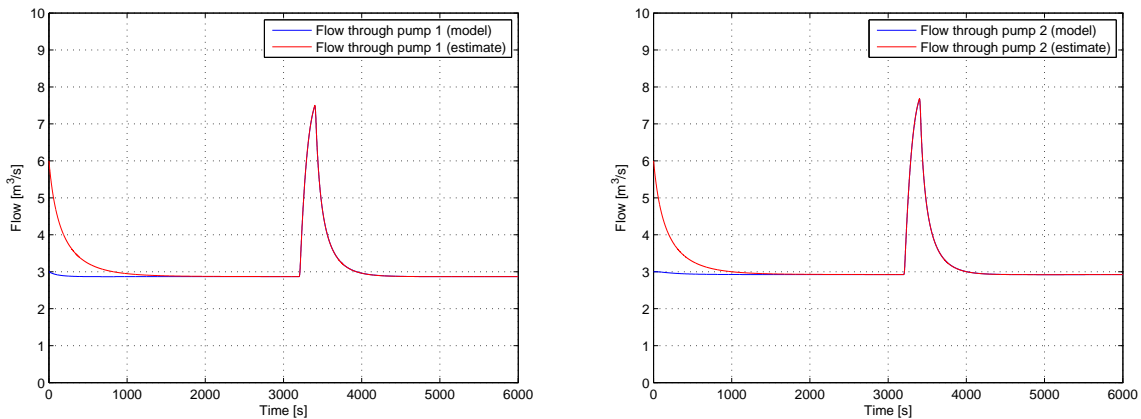
Figure 7.10. The flow through pump 1 to the left and the flow through pump 2 to the right.

The flow through each condense is shown in Figure 7.11. As in the case with the pump flow, the estimated flow converge to the model flow and follows the model flow.
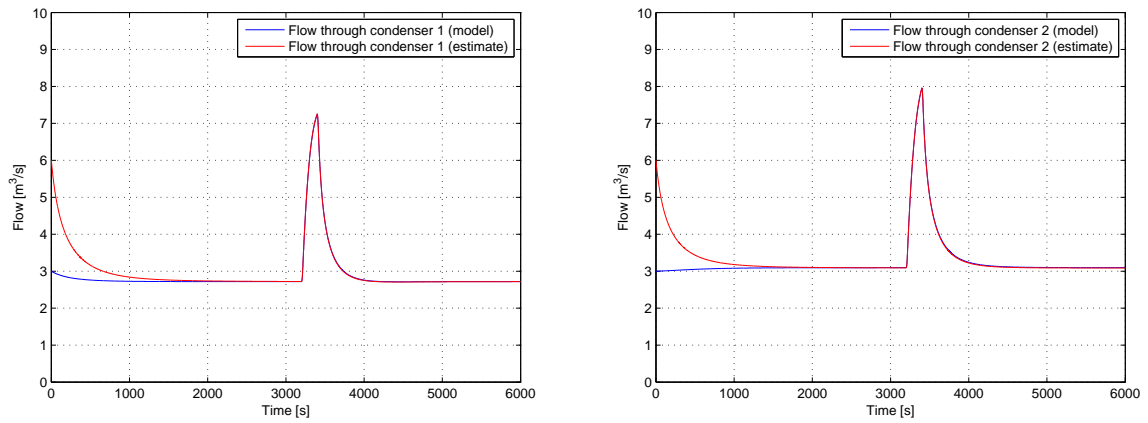
Figure 7.11. The flow through condenser 1 to the left and the flow through condenser 2 to the right.

In Figure 7.12 the estimated fouling is shown. Changes in the input effects the estimation of the fouling, but as the step in the input is a step from the minimum allowed RPM to the maximum RPM used in the power plant, the effect in the estimation is small.
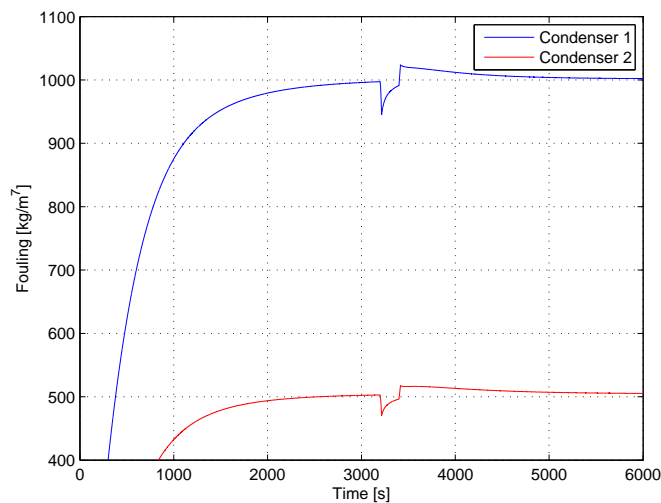
Figure 7.12. The fouling estimated by the EKF.

Four different methods for estimating the flow of seawater has been proposed. The first method uses the model of the system, where due to fact that the method contains the same issues as the method already in use at the power plant, the method was not used. The second method uses the filters before and after the condensers, where the measurements was too noisy to use directly and the method was therefor not used. The third method uses the characteristic curve of the pump to calculate the flow of seawater, but as in the case of the second method, the measurements was too noisy to use and the method was therefor not used. The fourth method combines all the three first methods in an extended Kalman filter, where the fouling can be estimated and thereby used in the calculation of the flow. The fourth method gives a more reliable estimation of the seawater flow than the one already in use at the power plant, as it uses more measurements in the estimation. The fourth method can, unlike the one already in use at the power plant, estimate the flow of seawater when fouling occurs in the condenser.

Part III

Control

Control Strategy 8

This chapter presents the suggested control strategy for the main cooling system of the Studstrup CHP plant. The goal is to maintain a reference level of pressure in the condenser that will maximize the power output of the plant. Two different solutions will be proposed and discussed.

8.1 Aim of the Control

The ultimate goal of control is to maximize the electrical power output of plant. The power output of the plant depends on several factors, such as the power produced by the different stages of the turbine, the power consumption of the seawater pumps and of the feedwater pump, in addition to the auxiliary elements. Therefore, neither operating at the lowest possible pressure nor at the BEP (Best Efficiency Point) of the pumps is a guarantee of optimal efficiency in the cycle. Instead, the best efficiency of the plant can be achieved by maintaining a target condensation pressure [Nedelkovski et al., 2005]. In this project, it will be assumed that the optimal pressure in the condenser is known (it may be computed using software packages such as Turabs) and it will be the target reference for the control loop.

In order to maintain the target pressure, a certain amount of cooling needs to be provided via seawater. The pumps, as explained previously, circulate the seawater by providing the necessary head for the fluid to overcome the resistance of the hydraulic system. The flow of seawater is controlled by varying the rotational speed of the pumps, which is the control input to the system. By varying this speed, the operating point on the system curve is shifted, as explained in Section 3.2.1. An increase in the rotational speed of the pump will mean that the pump is capable of providing greater head and greater flow, hence being able to decrease the condensation pressure.

8.1.1 Choice of a Control Strategy

The choice of a control strategy is influenced by the system to be controlled. In this case, the main cooling system of Studstrup is a large system with large delays. In addition, there are various sources of disturbances acting on the system continuously, which will result in a noisy output. The sources of noise are the inlet temperature of the water, the variations in the amount of steam entering the condenser and the measurement noise in each of the sensors involved. Most importantly, the control must respect the limits imposed by the operation of the pumps and the environmental limit in the inlet and outlet temperatures.

Model Predictive Control (MPC) as a control approach allows to easily incorporate constraints on input, state, output and derived parameters. It will therefore be the preferred approach to the control problem. The MPC solution will be compared against a simple Proportional Integral (PI) and Proportional Integral Derivative (PID) controller structures in terms of performance and robustness.

8.2 Control Using PI/PID Controllers

A PID controller attempts to minimize the reference tracking error by generating an input control signal in order to take the process to the desired setpoint. The input is given by the expression in Equation 8.1. If T_d is set to zero, the controller becomes a PI controller.

$$u(t) \; = \; K_c \left(\epsilon(t) + \frac{1}{T_i} \int\limits_{0}^{t} \epsilon(t)dt + T_d \frac{d\epsilon(t)}{dt} \right) \tag{8.1}$$

where:

K_c Proportional Gain

T_i Integral time

T_d Derivative time

ϵ Error in reference tracking

Two approaches will be proposed in this section. The first one will attempt to control the output directly from the input. The second approach will consist in a cascaded control, with an inner loop PI controlling the flow and an outer loop integral controller ensuring there is no steady state error in the condensation pressure. Both methods will be implemented using the linearized system model and their results, compared.

Direct Pressure Control Using a PID

The overall control problem is considered here where the pressure in the condenser needs to be controlled using the speed of the pumps as manipulated variable. A PID controller will be tuned for that purpose.

There are a number of techniques that may be used to tune a PID controller. A well-known approach is the Ziegler-Nichols rule. However, the Cohen-Coon technique is more appropriate for systems with large delays [W. Y. Svrcek, 2013] and provides a faster response. Cohen-Coon is an offline tuning technique that requires a step to be applied as input to the system.

The Cohen-Coon method requires the system to have a first order response. The proposed linearized model consists of a first order model for the hydraulic system and a static model plus dead time for the thermodynamic model. The resulting model can be regarded as a First Order Plus Dead Time (FOPDT) model. An FOPDT model follows the following expression:

$$G(s) \; = \; \frac{K_g}{\tau_g s + 1} e^{-\theta_g s} \tag{8.2}$$

where:

K_g Static gain

τ_g Time constant

θ_g Dead time

The general response of an FOPDT model to an input step will resemble that in Figure 8.1.
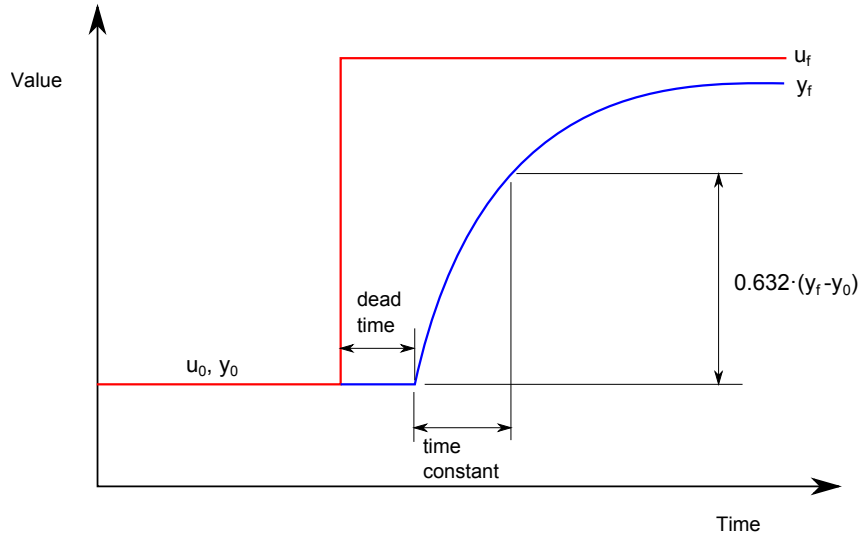
Figure 8.1. Reaction curve of a first order system with dead time.

The Cohen-Coon method can be summarized in the following steps:

- Wait for the process to reach steady state.
- Apply input step to the system. The response of the system is known as the reaction curve.
- Approximate the response to an FOPDT model to obtain the time constant (output reaches 63.2% of its steady state value) and dead time of the process, as well as initial and final values of the input and output. These parameters are represented in Figure 8.1.
- Compute the parameters P, N, L, R. These parameters are given by:

$$P = \frac{u_f - u_0}{u_0} \cdot 100 \tag{8.3}$$

$$N = \frac{y_f - y_0}{y_0} \cdot 100 \cdot \frac{1}{\tau} \tag{8.4}$$

$$L = \theta \quad , \quad R = \frac{\theta}{\tau} \tag{8.5}$$

where:
$u_0, \; u_f$ Initial and final values of the input
$y_0, \; y_f$ Initial and steady state values of the output
τ Time constant
θ Dead time

- Compute the values for the controller gains from P, N, L and R according to the recommended controller settings. The recommended values of these parameters are:

	K_c	T_i	T_d
P	$\frac{P}{NL}(1 + \frac{R}{3})$	-	-
PI	$\frac{P}{NL}(0.9 + \frac{R}{12})$	$L \cdot \frac{30+3R}{9+20R}$	-
PID	$\frac{P}{NL}(0.9 + \frac{R}{12})$	$L \cdot \frac{30+3R}{9+20R}$	$\frac{4L}{11+2R}$

In addition to these parameters, it is necessary to design an anti-windup. The anti-windup will limit the maximum value of the integral term, so the cumulative error that has been integrated does not make the system overshoot too violently, which could cause oscillations and instability of the closed-loop system.

Supervisory Control Using a PI Controller

The first approach presents a number of issues related to the delays in the system. If the delay is estimated incorrectly, the controller will perform poorly and oscillate. It is a requirement of the control (as stated in the problem definition in Chapter 4) that the solution is designed with a focus on robustness.

The system is affected by a number of pure delays in the output (pressure) model, but there is no delay in the flow model. Hence it would be of interest to reach the operating point using a flow setpoint. The suggested solution is illustrated in Figure 8.2. In this section it is proposed to generate the flow reference based on the target pressure using the model, and use a PI controller to generate the appropriate setpoint for the pumps, so that the target flow is met. Additionally, in order to ensure that the reference pressure is achieved in steady state, a slow integrator is placed in the outer loop. This will modify the value of the reference flow q_{ref} to q'_{ref} to ensure there is no steady state error in the condensation pressure.
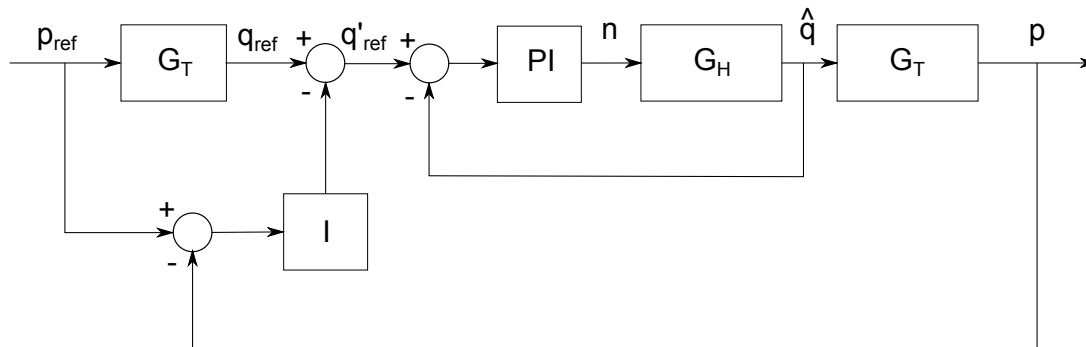
Figure 8.2. Overview of the proposed solution using an inner and outer loop.

The tuning method chosen for the PI controller is Internal Model Control (IMC). This method produces robust controllers and minimizes overshooting and oscillatory behavior. The method becomes simpler if there is no deadtime in the system. Since the process is self-regulating (the output response does not integrate the input), the rules for tuning a PI controller, according to [Ott and Wojsznis, 1995], are the following:

$$ K_c \; = \; \frac{\tau}{K_g(\tau_f + \theta_g)} \qquad\qquad T_i \; = \; \tau \qquad\qquad (8.6) $$

where:
τ Time constant of the system
τ_f Time constant of the filter
K_g Static gain of the system
θ_g Deadtime of the system

In equation 8.6, τ_f is a user-defined filter time constant that is used to determine the settings of the controller. Both the PI controller in the inner loop and the integral controller in the outer loop require anti-windup, whose values are specified in Appendix F. In addition, the PI controller in the inner loop is subject to saturation, given by the limits of the pumps speed.

8.2.1 PI/PID Control: Results and Discussion

PID Controller

The Cohen-Coon method has been implemented to design a PID controller. The reaction curve of the system output (the pressure) to an input step in the rotational speed of the pumps is shown in Figures 8.3 and 8.4. Notice that the response is inverted with respect to Figure 8.1, since the input is inversely proportional to the output. The identified paramters for the FOPDT model are presented in Appendix F. The simulation has been performed without noise.
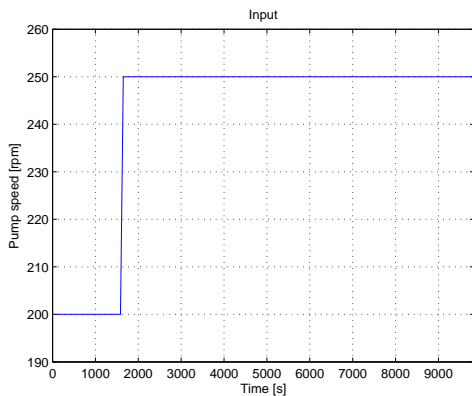
Figure 8.3. Step input to the system.
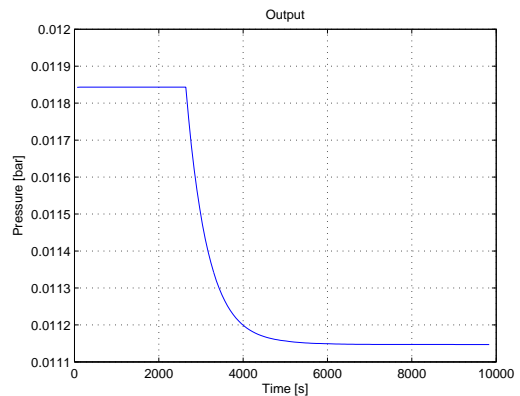
Figure 8.4. Output of the system.

It can be checked in Figure 8.4, that the response of the system to a step does behave as an FOPDT system. The values derived from the step test can be found in Appendix F. The tuned controller has been tested for reference tracking (incorporating noise into the simulation). The results can be seen in Figures 8.5 and 8.6.

83
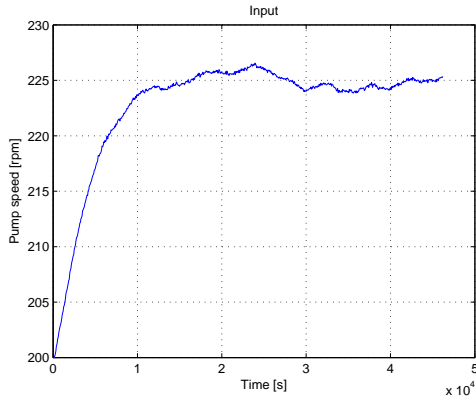
Figure 8.5. Control input to the system.
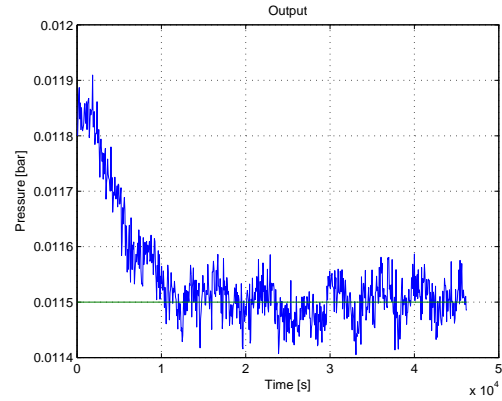
Figure 8.6. Output of the system.

The PID controller leads the system to the desired reference, but produces oscillations in steady state. The controller is, in addition, very slow. Increasing the integral gain or reducing the anti-windup cap would cause the system to converge faster to the reference, but it would also increase the amplitude of the unwanted oscillations. The constraints on the speed of the pumps can be respected by saturating the output of the controller. It is, however, not possible to directly incorporate constraints on the flow of seawater, whose value is not known to the controller, or to the outlet temperature of seawater.

It is therefore necessary to propose a different kind of control strategy to improve the robustness and to incorporate the constraints into the control strategy.

Supervisory Control

Similarly to the previous case, the system is identified from its reaction curve, which can be seen in Figures 8.7 and 8.8. The results of the tuning method are presented in Appendix F.
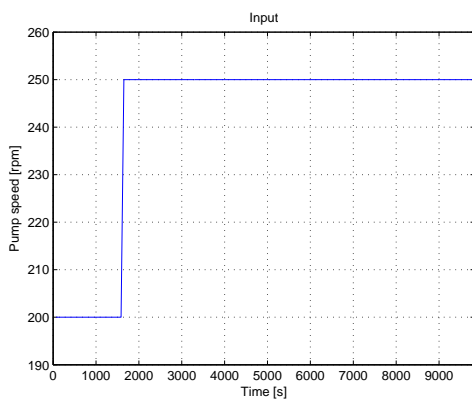
Figure 8.7. Step input to the system.
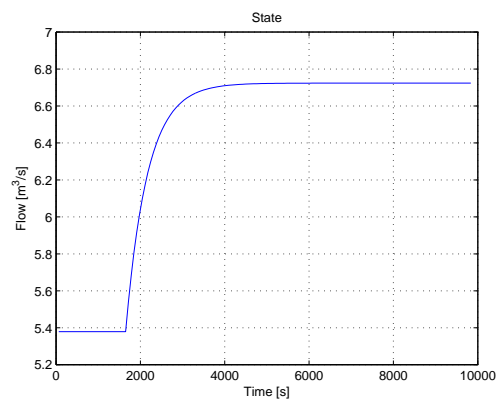
Figure 8.8. State of the system.

Two tests have been performed on this control structure. The first one is identical to the test performed on the PID controller: the system starts at the same initial conditions and takes the system to the desired reference. This is shown in Figures 8.9, 8.11 and 8.10.
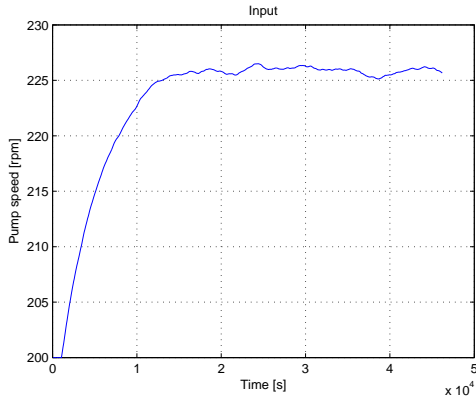
Figure 8.9. Input: rotational speed of the pumps
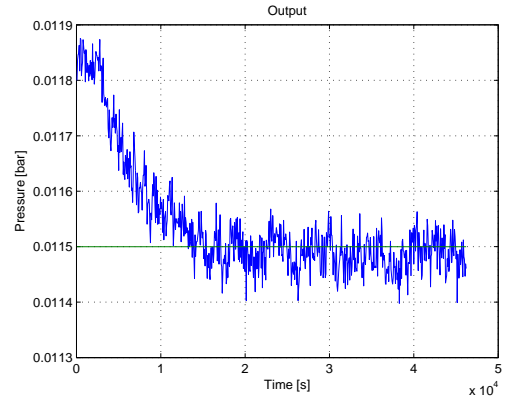
Figure 8.10. Output: condensation pressure
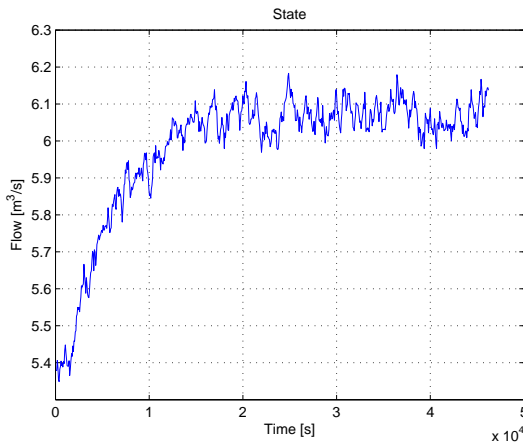
Figure 8.11. State: flow of seawater

The response is similar to the one provided by the PID controller tuned by the Cohen-Coon method, but it shows fewer oscillations and takes less time to reach the reference.

In order to test the action of the outer loop, another simulation is presented. This time, the output model is assumed inaccurate. This means that the flow reference generated from the pressure reference is incorrect and will take the system to an operating point that is not exactly the desired one. The slow integrator in the outer loop should correct the offset and eliminate the steady state error. This is shown in Figures 8.12, 8.13 and 8.14.
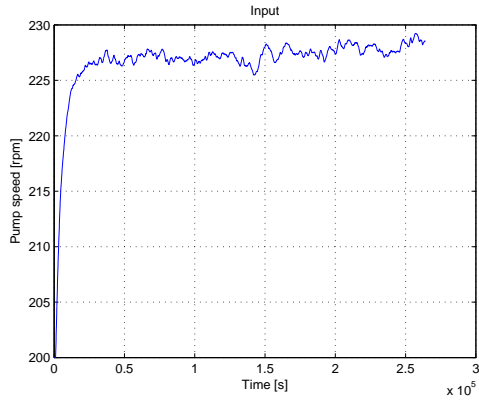
Figure 8.12. Input: rotational speed of the pumps
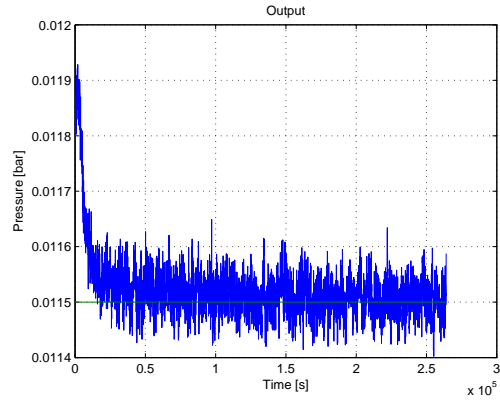
Figure 8.13. Output: condensation pressure
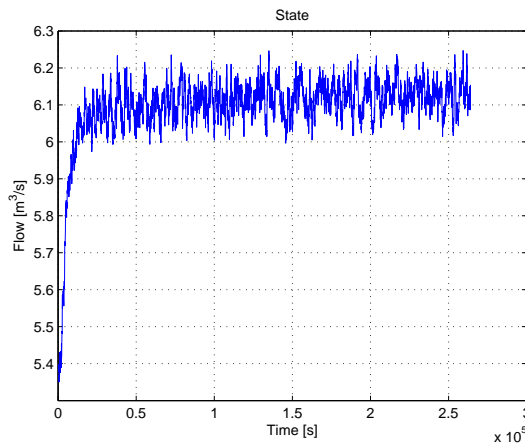
Figure 8.14. State: flow of seawater

It can be seen in Figure 8.13 that the controller initially takes the system to an operating point that is not the reference pressure. The integral control on the outer loop slowly corrects the offset and takes the pressure to the actual reference by varying the flow reference to the inner loop (see Figure 8.14). This simulation, however, assumes that the exact value of the delay is known. If the delay estimation is incorrect, especially if the system is slower than expected, the controller can be too fast and cause the pressure to overshoot. Figures 8.15 and 8.16 show the output of the controlled system when the delay has been misestimated. In Figure 8.15, all deadtimes of the system are 50% higher than the delays used in the design of the controllers. A very slight overshoot can be seen, but no oscillations or steady state error. In Figure 8.16, the delays are 5 times higher than in the original system. The overshoot of the system becomes obvious and the plant takes longer to reach the reference, but causes no instability or oscillations in steady state.
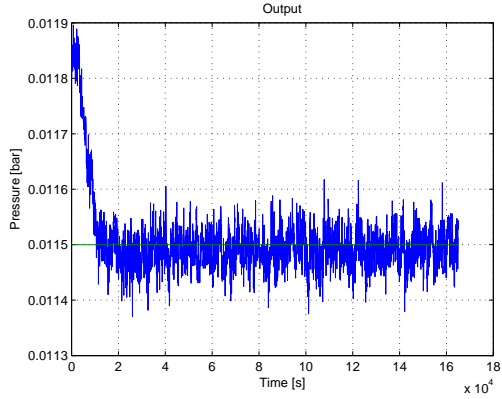
Figure 8.15. Response with +50% deadtime.
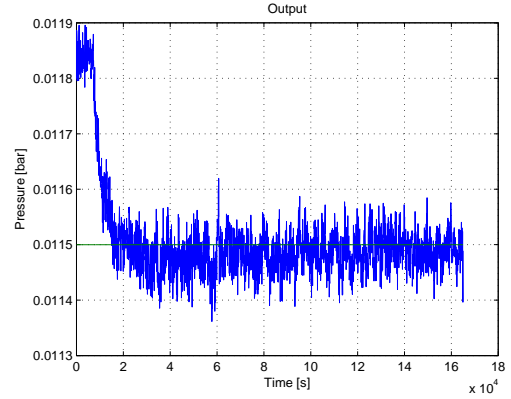
Figure 8.16. Response with +400% deadtime.

8.3 Model Predictive Control of the System

The previous section has presented a control solution based on simple PI and PID controllers. However, as discussed in Section 8.1.1, MPC is an interesting control strategy for its capability to incorporate constraints and good performance.

8.3.1 General Theory Behind MPC

MPC is a control technique based on iterative, finite horizon optimization of a plant model. The algorithm generates the control inputs that minimize a given cost function over a time horizon in the future. After every iteration, only the first input is applied to the system. The inputs are determined within a control horizon N_u so the system fits the reference as closely as possible over a prediction horizon of N_p. For the next iteration, the prediction and control horizons are shifted forward and the optimization is performed again. This is usually known as receeding horizon. The optimization process can be subject to a number of constraints and, therefore, MPC is not optimal in general (unlike a Linear Quadratic Regulator (LQR)), but still produces near-optimal results that can handle the constraints of a real system and actuators.

For a prediction horizon of length N, the cost function for MPC can be expressed as:

$$J \;=\; \sum_{i=t}^{t+N_p} ((r_i - \hat{y}_i)^T Q(r_i - \hat{y}_i)) + \sum_{i=t}^{t+N_u} (\Delta u_i^T R \Delta u_i) \tag{8.7}$$

where:
J	Total cost of the strategy
r	Reference
$\hat{y}$	Output. Estimated using the model
u	Input
N	Length of prediction horizon
N_u	Length of control horizon
Q	Weight on reference tracking
R	Weight on input variations

Subject to a set of constraints. These constraints can be, e.g. on the control moves or on the limit values of the actuator.

There are several parameters that need to be tuned in order to implement a model predictive controller. The prediction horizon, the control horizon and the weights of the cost function need to be chosen. The tuning procedure followed is the one proposed by [Ralph F. Hinde, 1994]. This method relies on several assumptions. Therefore, it will be assumed that:

- The system dynamics can be approximated by an FOPDT
- The system is Single-Input-Single-Output (SISO)
- The system is open loop stable
- The system is minimum phase
- The system is non-integrating

Then the length of the prediction horizon will be given by Equation 8.8:

$$N_p = \frac{5\tau_g + \theta_g}{T_s} \tag{8.8}$$

where:
τ_g Time constant
θ_g Dead time
T_s Sampling time

The length of the control horizon is given by Equation 8.9:

$$N_u = \frac{\tau_g}{T_s} \tag{8.9}$$

In addition, it should be checked that the prediction horizon is larger than the delay in the outlet temperature model, so the system does not violate the constraint on the maximum seawater temperature increase.

The cost function is then set up as follows:

$$J = \sum_{i=t}^{t+N_p} ((r_i - \hat{y}_i)^2) + \sum_{i=t}^{t+N_u} (\Delta u_i^T Q \Delta u_i) \tag{8.10}$$

In Equation 8.10, the parameter Q is referred to as the input suppression weight. According to [Ralph F. Hinde, 1994], Q may be found using Equation 8.11:

$$Q = \Gamma K_g^2 \tag{8.11}$$

Where K_g is the gain of the approximated FOPDT model from 8.2 and Γ is a tunable parameter. In [Ralph F. Hinde, 1994] it is suggested that Γ is adjusted such that the overshoot is 10-15%. However, it is desired that the controller is designed with a focus on robustness over speed, as stated in Section 4 on page 19. Therefore, it is preferred to minimize the overshoot and limit its value to 2% with respect to the initial value of the output. Further decrease is not possible or effective due to the noisy nature of the signal.

MPC Using the Flow of Seawater in the Objective Function

It was discussed in Section 8.2 on page 80 that using the flow to control the system can be an advantage since it is not affected by the large delays in the output model. This is of special importance should there be an inaccuracy in the delay estimation. Therefore, it is proposed to use the flow of seawater in the objective function, instead of the condensation pressure. The controller will then follow a flow reference that is generated through the model. The new cost function for the MPC controller is:

$$
J \;=\; \sum_{i=t}^{t+N_p} ((q_{ref,i} - \hat{q}_i)^2) + \sum_{i=t}^{t+N_u} (\Delta u_i^T Q \Delta u_i) \tag{8.12}
$$

The new objective of the controller is to minimize the error in the flow. However, no direct measurement of the flow is available. This means that, in order to incorporate the measured output into the control, it becomes necessary to estimate the state by observing the output. To this purpose, a Kalman estimator will be proposed.

The delayed model of the system will be re-expressed as a new state space model with a series of consecutive unit delays between each state and the following. For an output y that is delayed by d samples with respect to the state x_1, the model becomes the one in Equation 8.13

$$
\begin{aligned}
x_1(k+1) &= Ax_1(k) + Bu(k) \tag{8.13}\\
x_2(k+1) &= Cx_1(k)\\
x_3(k+1) &= x_2(k)\\
&\vdots \qquad\qquad \vdots\\
x_{d+1}(k+1) &= x_d(k)\\
\\
y(k) &= x_{d+1}(k)
\end{aligned}
$$

Equation 8.13 is an alternate representation of Equation 8.14.

$$
\begin{aligned}
x_1(k+1) &= Ax_1(k) + Bu(k) \tag{8.14}\\
y(k) &= Cx_1(k-d)
\end{aligned}
$$

In the observer design, measured disturbances will be treated as additional inputs. However, some of them have different (smaller) delays than the flow of seawater. When a variable is introduced in the system defined in Equation 8.13, in order to experience a delay θ, it must be introduced in the $(d+2-\theta)^{th}$ state equation.

The system, with a sampling time of $T_s = 66.005\ s$, a delay of 15 samples in the seawater flow and 9 samples in the steam flow (and 1 sample for ΔT and $T_{sw,in}$) follows Equation 8.15. w_i

are the modeled noise values of each of the variables and the original process noise (w_1).

$$
\begin{aligned}
x_1(k+1) &= Ax_1(k) + Bu(k) + w_1 \\
x_2(k+1) &= a_q x_1(k) + w_2 \\
x_3(k+1) &= x_2(k) \\
&\vdots \qquad\qquad \vdots \\
x_7(k+1) &= x_6(k) + a_{steam}\dot{m}_{steam} + w_7 \\
x_8(k+1) &= x_7(k) \\
&\vdots \qquad\qquad \vdots \\
x_{16}(k+1) &= x_{15}(k) + a_{\Delta T}\Delta T(k) + a_{T_{sw,in}}T_{sw,in} + w_{16}
\end{aligned}
\tag{8.15}
$$

$$
y(k) = x_{d+1}(k) + w_{out}
$$

The system can be then described in standard state space notation. This is expressed in Equation 8.16.

$$
\begin{aligned}
x(k+1) &= \Phi x(k) + Gu(k) \\
y(k) &= Hx(k)
\end{aligned}
\tag{8.16}
$$

With the input vector containing the speed of the pumps n, the measured disturbances $\dot{m}_{steam}$, ΔT and $T_{sw,in}$ and an additional constant input of 1 that will be used to obtain the constant value d_0 found in the original output model from Equation 6.11 on page 55:

$$
u(k) = \begin{bmatrix} n(k) \\ 1 \\ \dot{m}_{steam}(k) \\ \Delta T(k) \\ T_{sw,in}(k) \end{bmatrix}
\tag{8.17}
$$

In order to produce an estimate of the flow, a Linear Kalman Filter (LKF) will be used. The objective of the LKF is to estimate the value of the first state of the system x_1 based on the observations of the output. The discrete LKF is given by Equation 8.18:

$$
\textit{Prediction step} \tag{8.18}
$$

$$
\begin{aligned}
\hat{x}_k^- &= \Phi x_{k+1}^+ + Gu_{k-1} \\
\hat{y}_k &= H\hat{x}_k^- \\
P_k^- &= \Phi P_{k-1}^+ \Phi_k^T + Q
\end{aligned}
$$

$$
\textit{Update step}
$$

$$
\begin{aligned}
K_k &= P_k^- H_k^T (H_k P_k^- H_k^T + R)^{-1} \\
\hat{x}_k^+ &= \hat{x}_k^- + K_k(y_k - \hat{y}_k) \\
P_k^+ &= (I - K_k H_k)P_k^-
\end{aligned}
$$

where:

$\hat{x}_k^-$	A priori estimate of the flow at step k
$\hat{x}_k^+$	A priori estimate of the flow at step k
P_k^-	A priori error covariance matrix at step k
P_k^+	A posteriori error covariance matrix at step k
K_k	Kalman gain at step k
Q	Process noise covariance
R	Measurement noise covariance

This method has some similarities with the inner and outer loop control structure that was proposed for the PI regulator. The controller will initially follow a reference flow that is computed from the pressure reference through the system model, using the flow estimate provided by the model. However, a Kalman observer is used to correct the flow estimation (instead of the flow reference) according to the measured output to ensure that the system achieves the reference pressure in the output.

8.3.2   MPC Control: Results and Discussion

The MPC controller has been implemented using MATLAB Convex Optimization Toolbox (CVX). The cost function in Equation 8.10 is minimized for each iteration and only the first input is applied to the system. The optimization process is subject to the following constraints:

- Slew rate constraint. The control move Δu is capped for a maximum variation rate of the speed of the pumps. The variation is considered during the chosen sampling time.
- Absolute maximum and minimum values for the rotational speed of the pumps, as set by the manufacturer.
- Minimum pressure. A too low condensation pressure could potentially lead to the formation of droplets in the last stage of the turbine and have devastating effects on the lifetime of the blades.
- Maximum temperature increase. Using the outlet temperature model, the optimizer chooses a solution that will not cause the temperature difference to increase beyond the environmental limit.
- Maximum NPSH required, so that the available NPSH is above the required value by at least 2 meters. This will prevent any possible occurrence of cavitation, which would reduce the lifetime of the pumps.

The cost function from Equation 8.12 is used with the parameters specified in Appendix F.

Results of the LKF Flow Estimation

The LKF proposed in Section 8.3.1 has implemented and tested for convergence given null initial conditions. The values for the noise covariance matrices Q and R can be found in Appendix F. The simulation was performed for a sampling time of T_s = 66.005 s. All state estimates, output estimate, process covariance matrix and Kalman gain were initialized to zero and the input was kept constant. The results are shown in Figures 8.17 and 8.18.
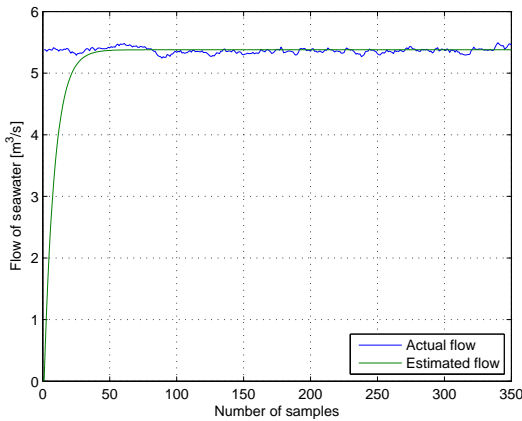
Figure 8.17. State: flow of seawater through the system
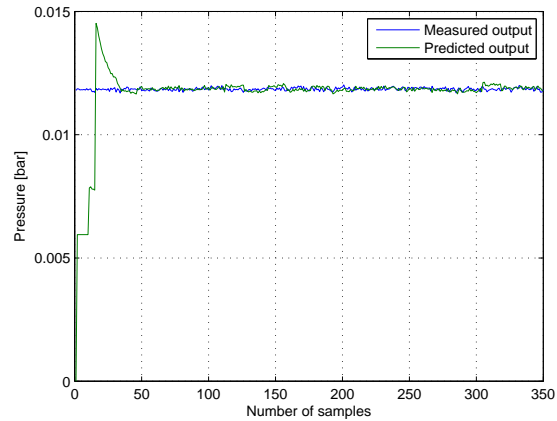
Figure 8.18. Output: condensation pressure

The flow estimation in Figure 8.17 converges to the actual system flow in less than 50 iterations and provides a noise-free value of the seawater flow for the controller to use.

MPC Simulation Results

Simulations have been performed using the cost function from 8.10 with the parameters specified in Appendix F. All simulations have been performed for a sampling time of 66.005 seconds. Constrain values have been chosen to serve as an example but may or may not be the appropriate values for the specific case of Studstrup, except for the maximum and minimum pump speed and the required NPSH, which are obtained from the pump curves. For the simulations, the level of seawater in the basin has been assumed constant, and therefore the available NPSH is also a constant value.

In the next pages, the following simulations will be presented:

- Reaching steady state operation
- Response to a disturbance
- Response to a reference change
- Sensitivity to a delay mismatch between the system and the designed controller

Both the disturbance and the reference change will be applied to the system once it reaches steady state operation.

Reaching Steady State Operation

The system is initialized and a reference pressure is given to the controller, similarly to Section 8.2.1.

Figure 8.19 shows the evolution of the rotational speed of the seawater pumps (input), the flow of seawater (state) and the condensation pressure (output). The system reaches the reference with a measured overshoot of 1.54%. The response is faster than that of the PID controller and does not show oscillatory behavior in steady state.
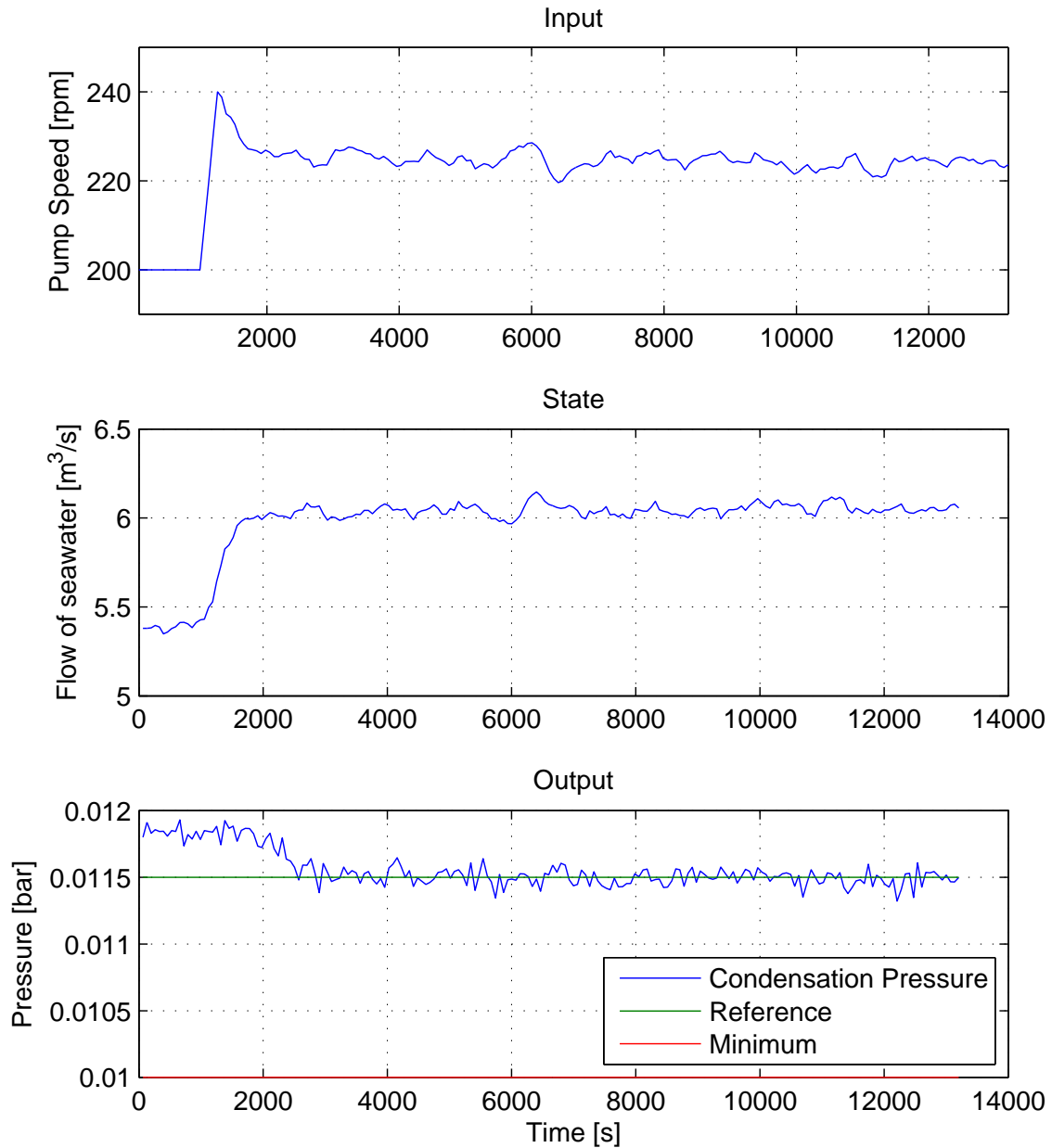
Figure 8.19. Rotational speed of the pumps, seawater flow and condensation pressure.

Figure 8.20 shows the evolution of the inlet and outlet seawater temperatures, the saturation temperature of the steam, the mean temperature difference between the steam and seawater sides and the flow of steam into the condenser. The increase in the temperature difference is caused by the delayed outlet temperature decrease.
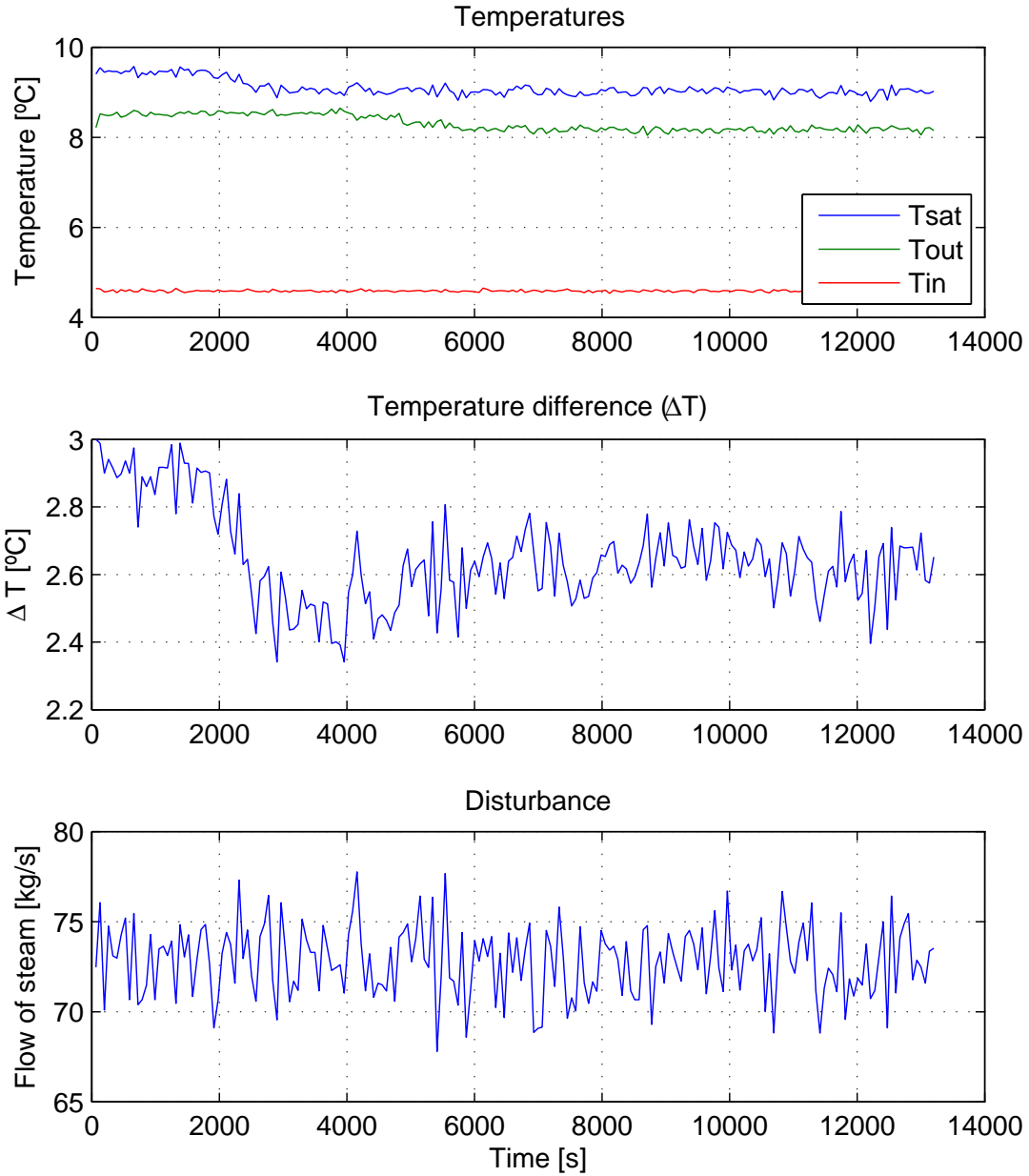
Figure 8.20. Evolution of the temperatures and the flow of steam during the simulation.

In Figure 8.21, other parameters subject to constraints are shown. The constraint on the rate of change in the pump speed becomes active during the approach to steady state operation, so the slope of the input in Figure 8.19 cannot become steeper. This limits how fast the system can converge to steady state. On the other hand, the increase in the seawater temperature and the NPSH (minus safety threshold) remain at all times far from their maximum allowed values.

Figure 8.21. The NPSH, seawater temperature increase and variation rate of the rotational speed of the pumps are subject to constraints that must be respected by the MPC controller.

Controller Response to a Disturbance

In this simulation, the response of the controller to a disturbance in the inlet mass flow of steam is tested. The system is first taken to a steady state operation. Once stable, the mass flow of steam is increased by 25 kg/s within 25 simulation samples (see Figure 8.23).

This will cause the pressure inside the condenser to rise and deviate from the reference (see Figure 8.22). The controller responds by increasing the speed of the pumps, thereby, increasing the flow of seawater to provide the larger cooling capacity required.
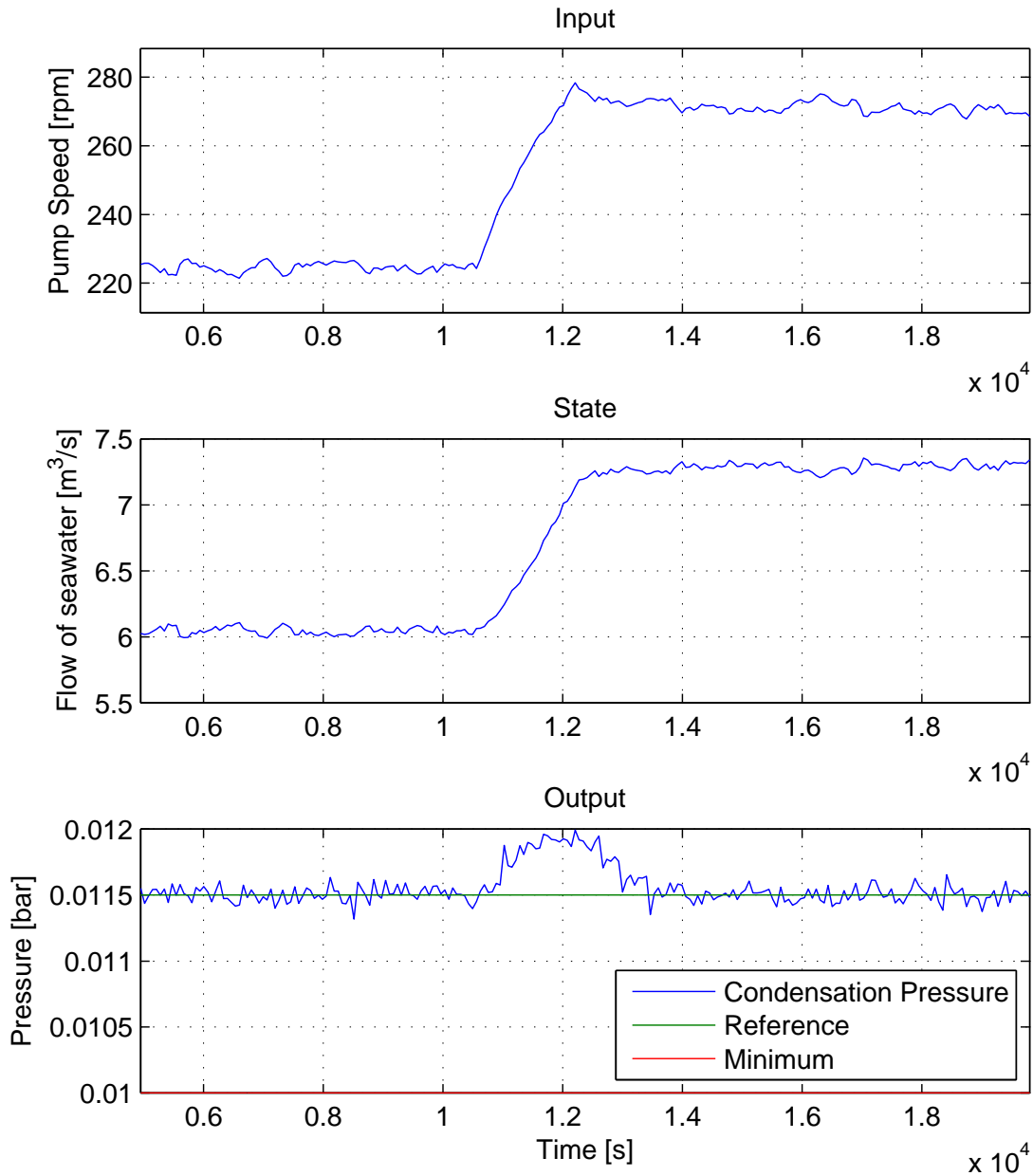
Figure 8.22. Rotational speed of the pumps, seawater flow and condensation pressure.

In Figure 8.23, the disturbance into the system can be appreciated. The increase of the condensation pressure causes an increase in the saturation temperature, which increases the mean temperature difference. Even though the higher flow of steam causes a higher flow of heat towards the condenser, the increase in seawater flow has the opposite effect, being the overall effect a slight decrease in its value.
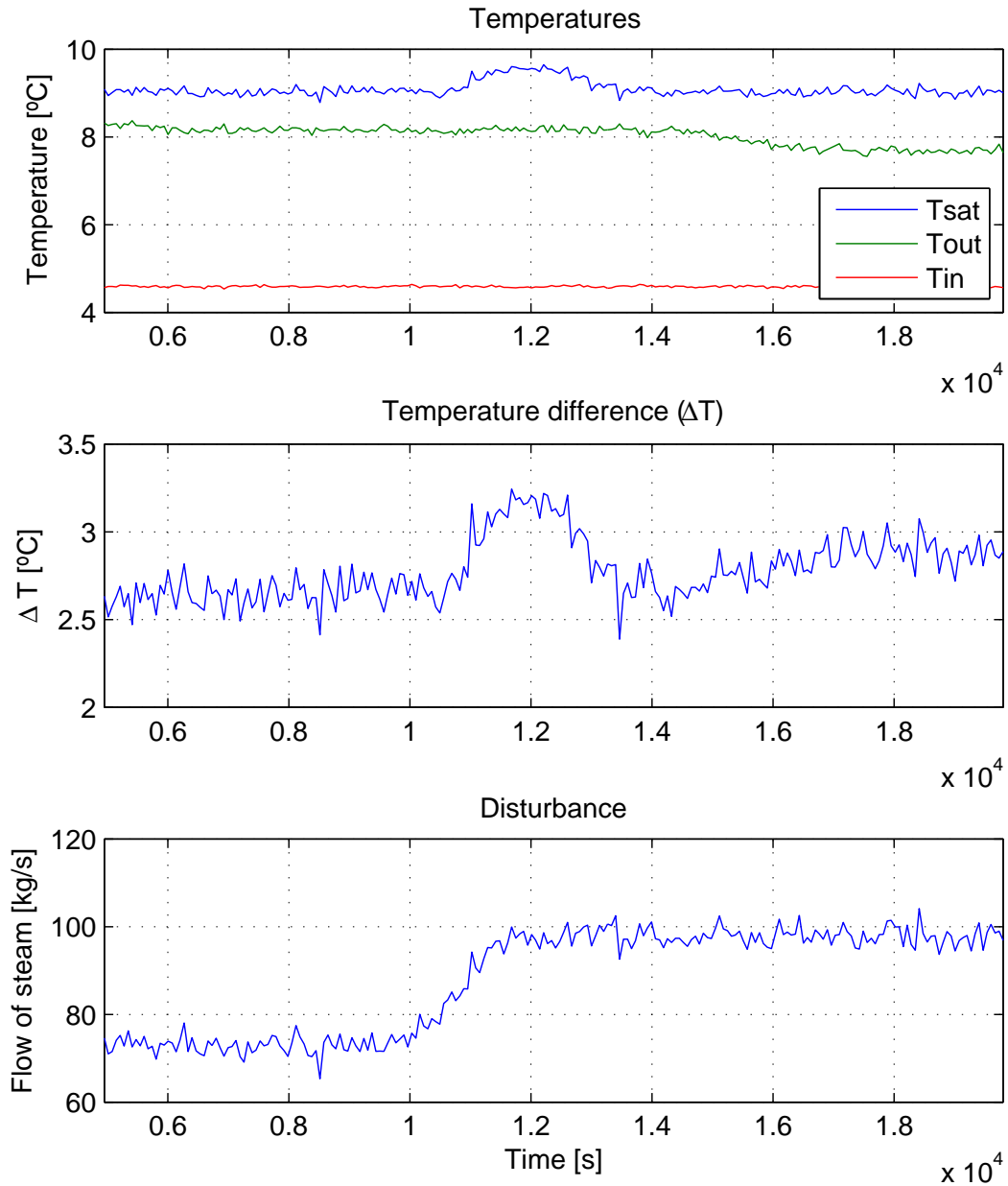
Figure 8.23. Evolution of the temperatures and the flow of steam during the simulation.

In this case, no constraints become active during the control (see Figure 8.24). However, it is worth noting that operating at a higher rotational speed increases the required NPSH considerably.
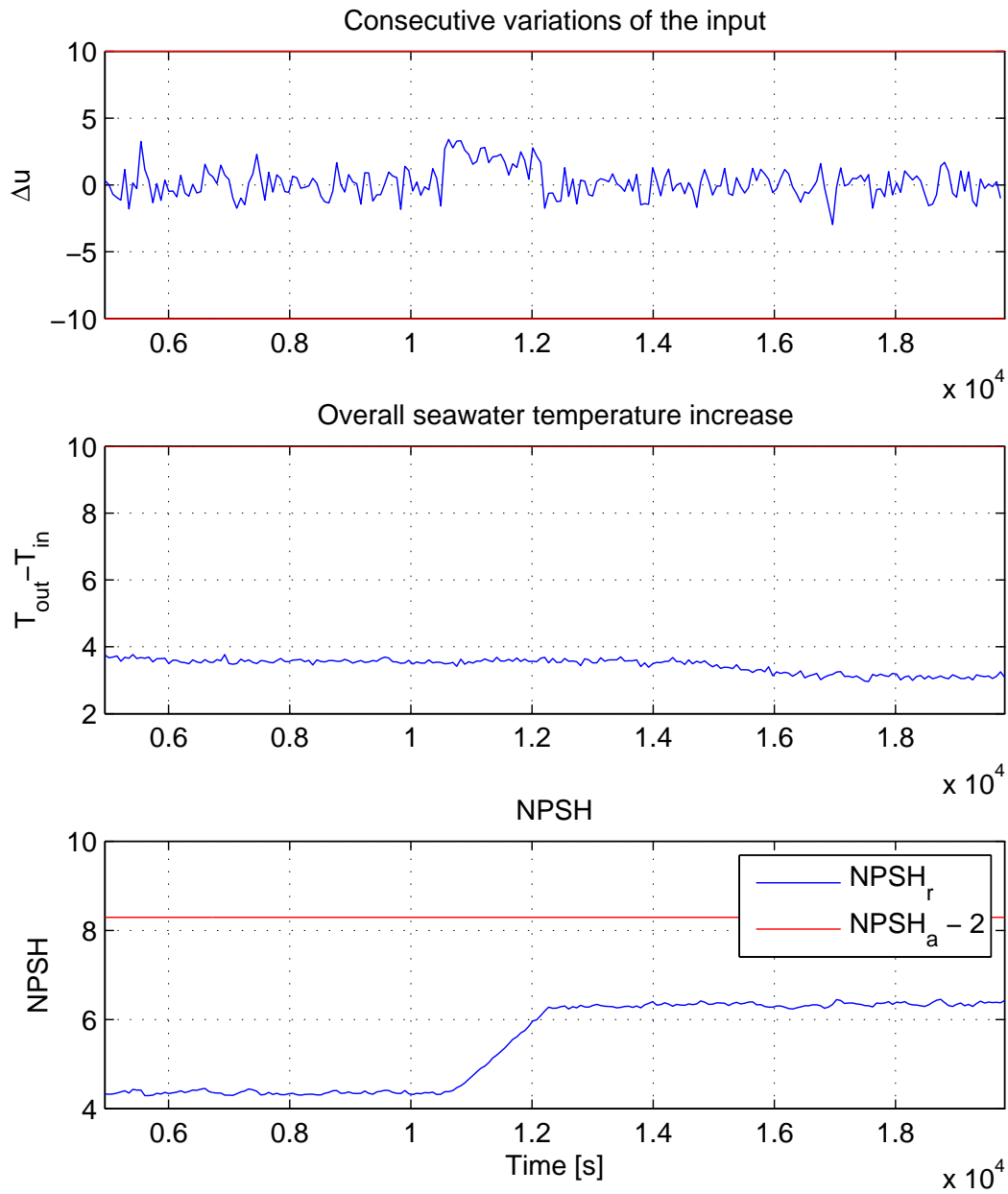
Figure 8.24. NPSH, seawater temperature increase and variation rate of the rotational speed of the pumps, which are subject to constraints that must be respected by the MPC controller.

Controller Response to a Change in the Reference

This simulation analyzes the response of the controller when the condensation pressure reference is varied. This will be the case whenever it is desired to lead the plant to a different operating point. Figure 8.25 shows that the reference is stepped from 0.0115 to 0.0127. The MPC controller is fed future values of the reference and attempts to meet the target value by the time the reference changes. However, the constraint on the minimum pump speed (120 rpm) becomes active during the process, as well as the constraint on the maximum rate of change of the pump speed (Figure 8.27).
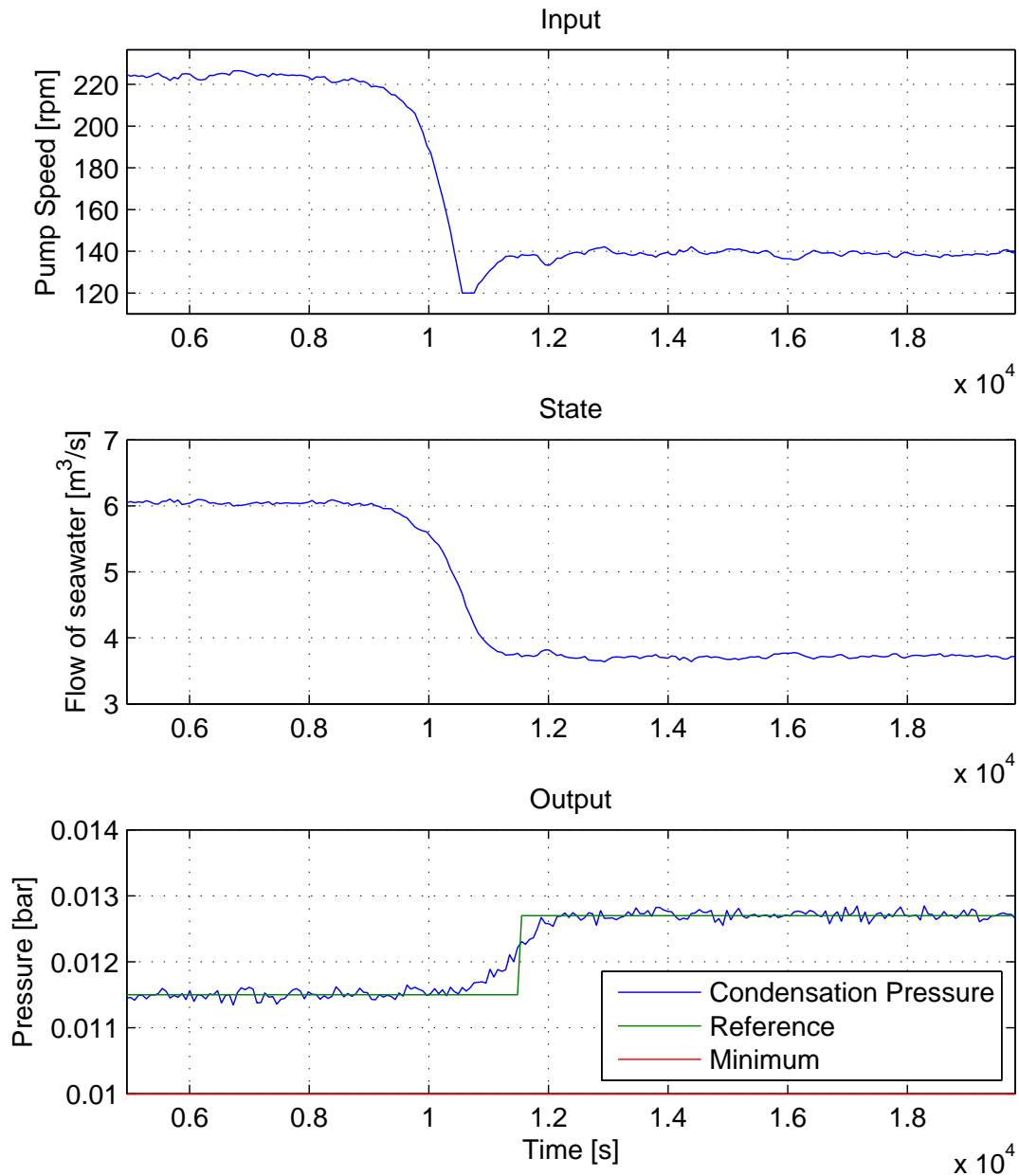
Figure 8.25. Rotational speed of the pumps, seawater flow and condensation pressure.

The higher pressure will result in a higher saturation temperature. At the same time, the lower flow causes the outlet temperature of seawater to decrease. The overall effect on the mean temperature difference is a small increase in its value.
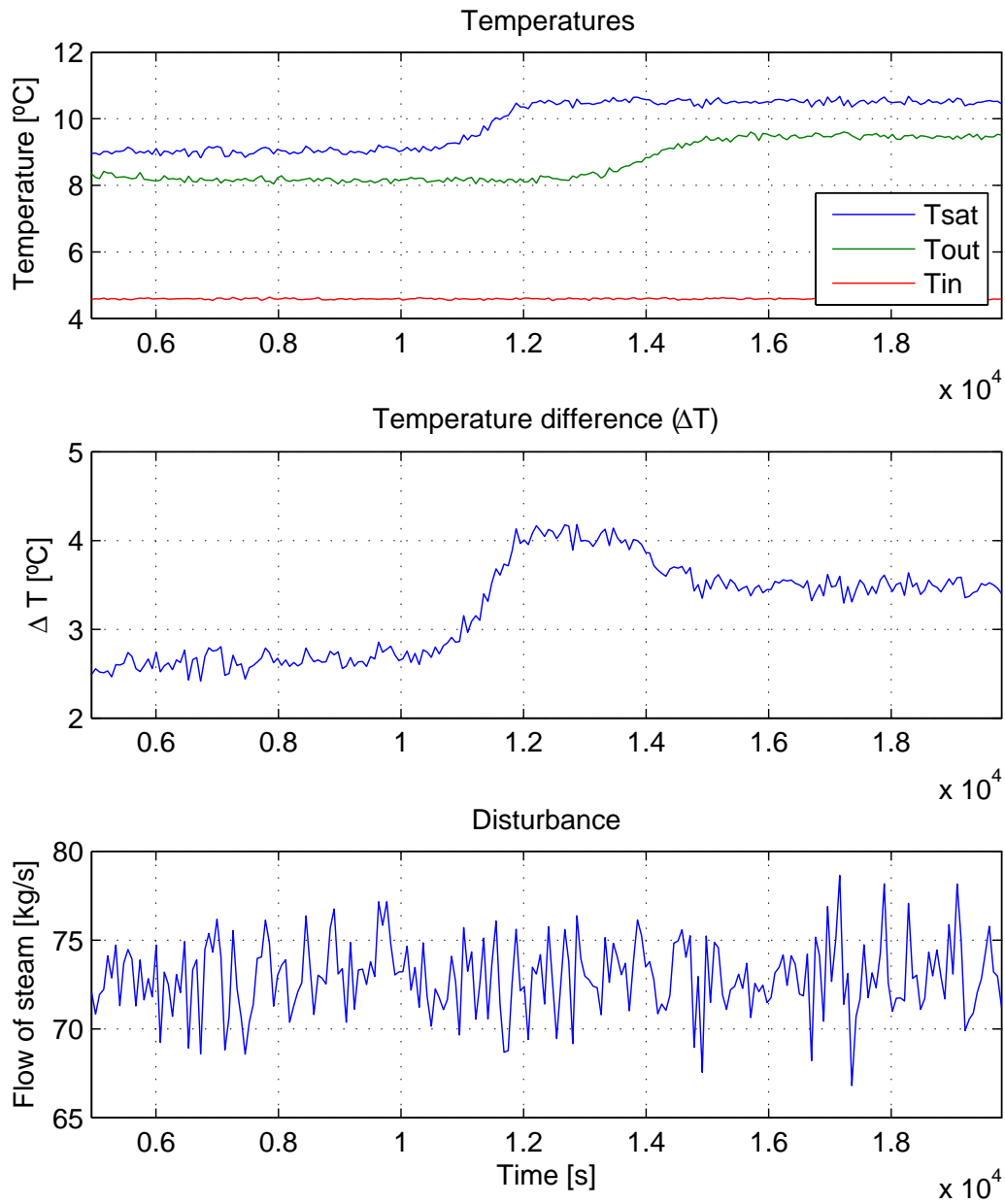
Figure 8.26. Evolution of the temperatures and the flow of steam during the simulation.

As stated previously, the constraint on the variation rate of the pump speed becomes active briefly (Figure 8.21). Other constraints remain far from their maximum values. The value of the required NPSH decreases as the system transitions to a lower flow of seawater.
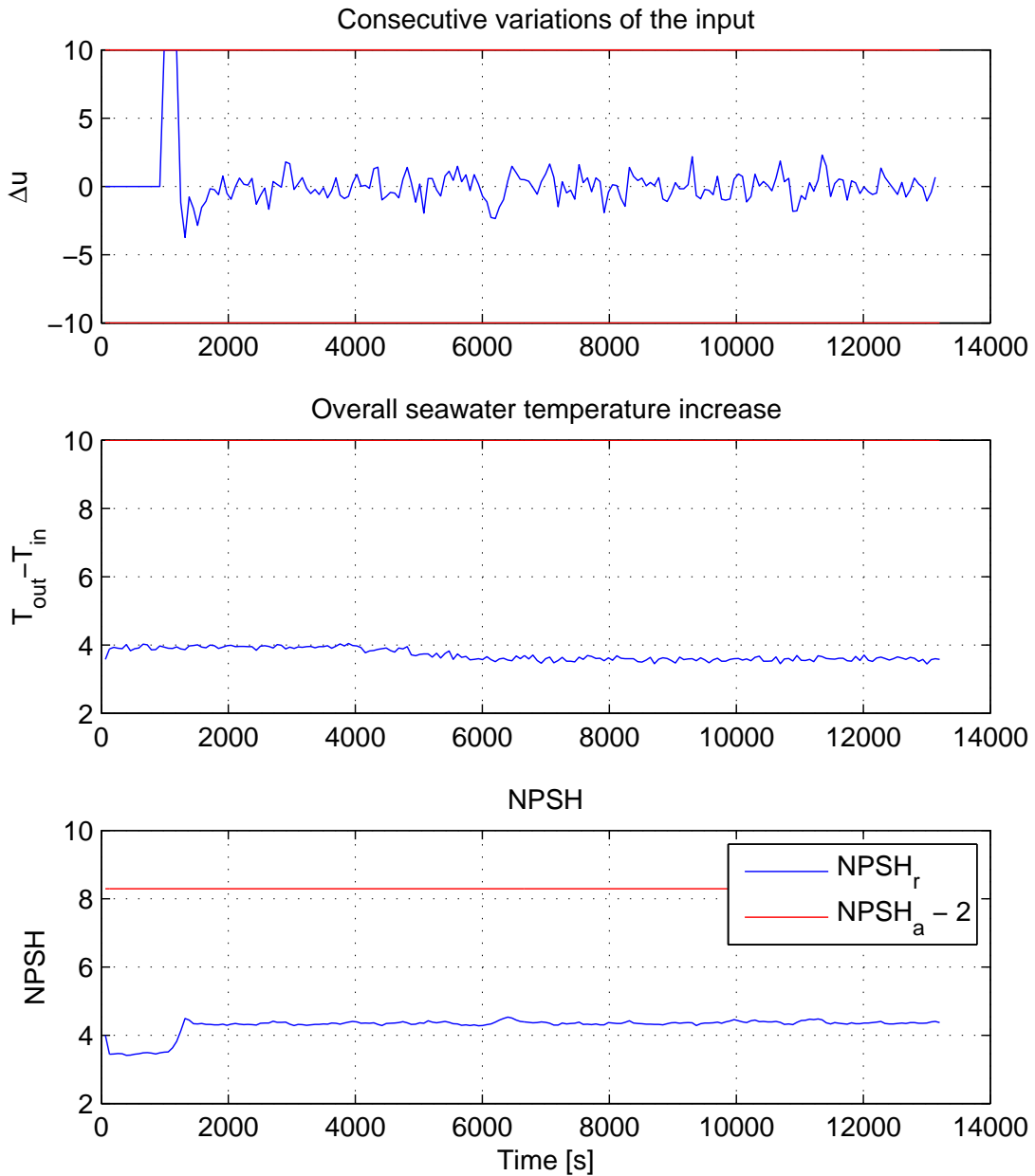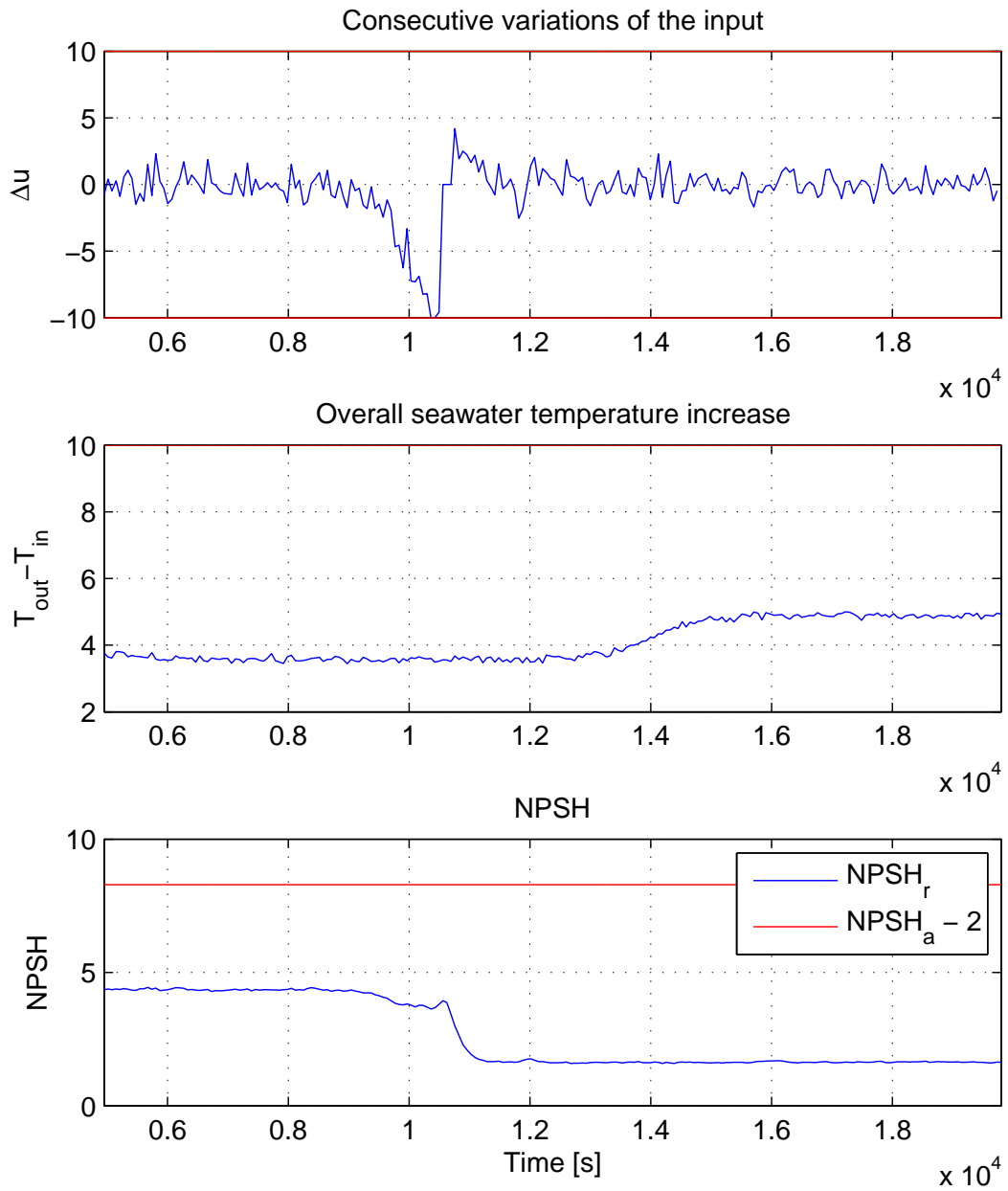

Figure 8.27. NPSH, seawater temperature increase and variation rate of the rotational speed of the pumps, which are subject to constraints that must be respected by the MPC controller.

Controller Sensitivity to a Delay Mismatch

The thermodynamic model is subject to large delays. These delays have been estimated from the available operation data. However, if the delay estimation is incorrect, this may have a great impact on the robustness and stability of the controller. The most critical situation is when the system delay is underestimated, since this means that the designed controller is too fast for the system and can cause overshoot, oscillations or even instability. In this simulation, all delays in the system have been doubled, whereas the controller parameters have been kept constant. The system is subject to a reference change.
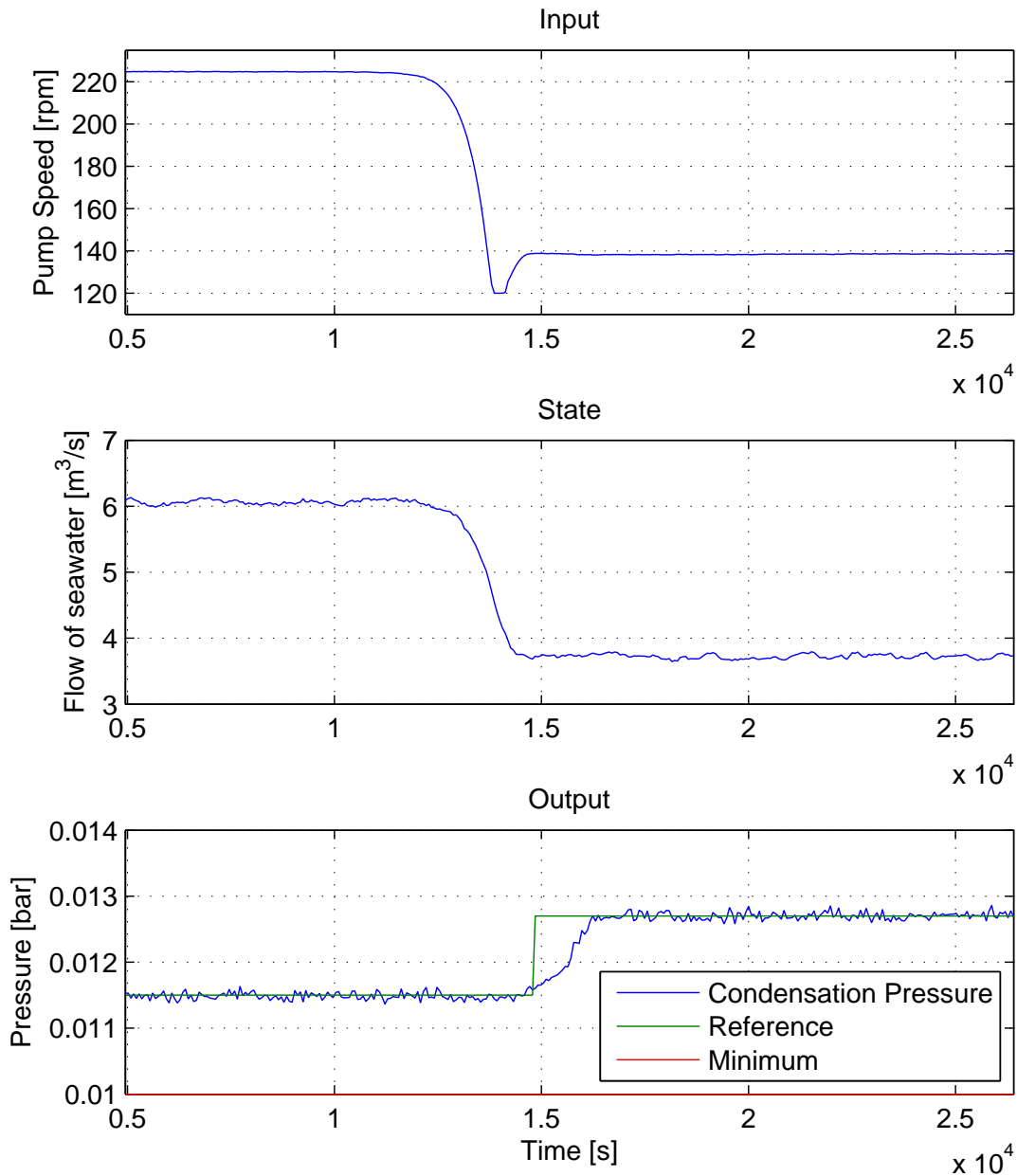
Figure 8.28. Rotational speed of the pumps, seawater flow and condensation pressure.

Figure 8.28 shows the input, output and state of the system. With the new delays, the system fails to meet the reference in advance, since the system takes longer to react to the inputs. However, it does not produce overshoot (1.239 %) or oscillations in steady state. The constraint on the minimum RPM of the pump becomes active during the reference change.

Figure 8.29 shows the evolution of the disturbance, which is kept constant, and the temperatures.
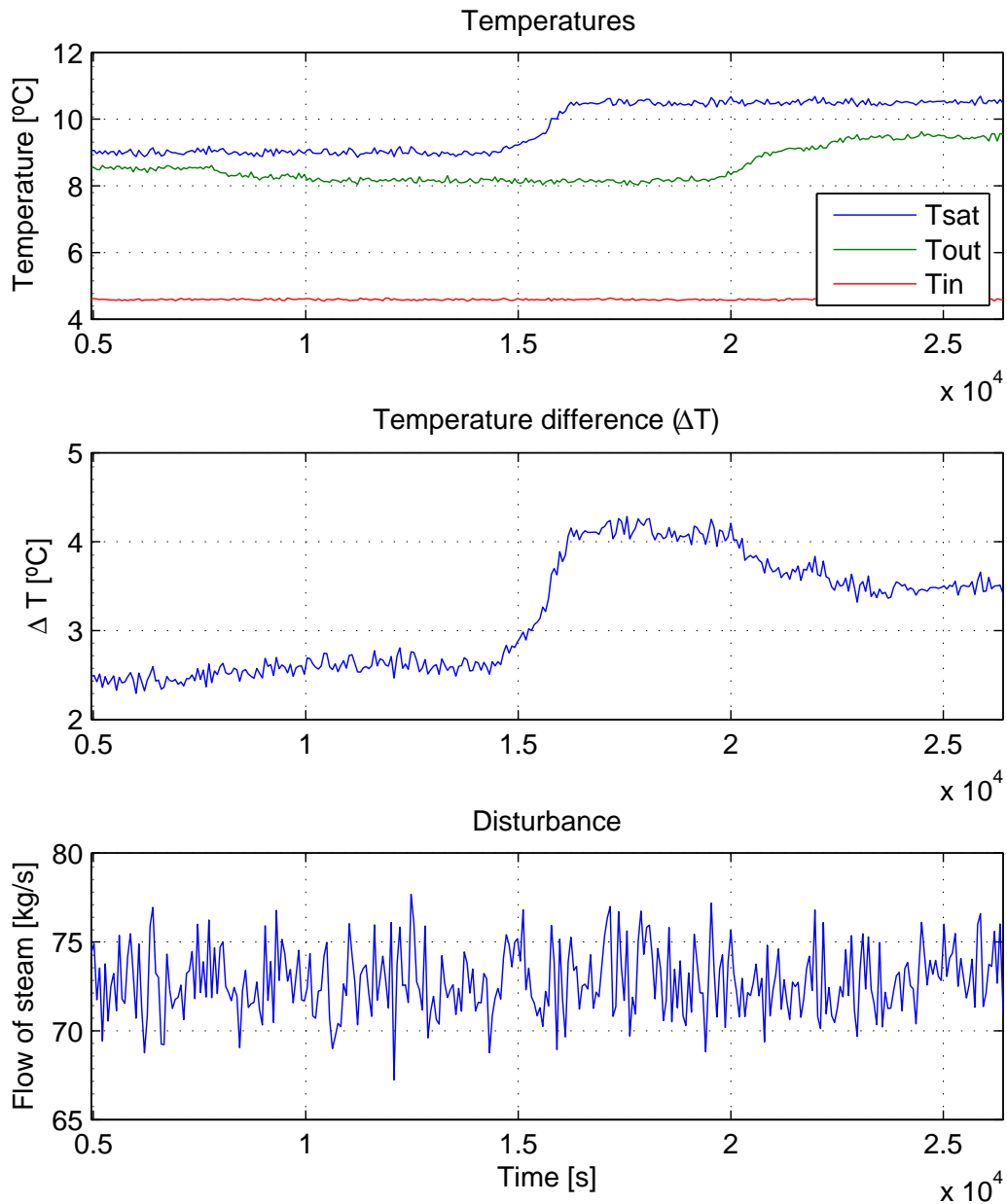
Figure 8.29. Evolution of the temperatures and the flow of steam during the simulation.

Figure 8.30 shows the state of the constraints. Only the constraint on the input variation rate becomes briefly active.
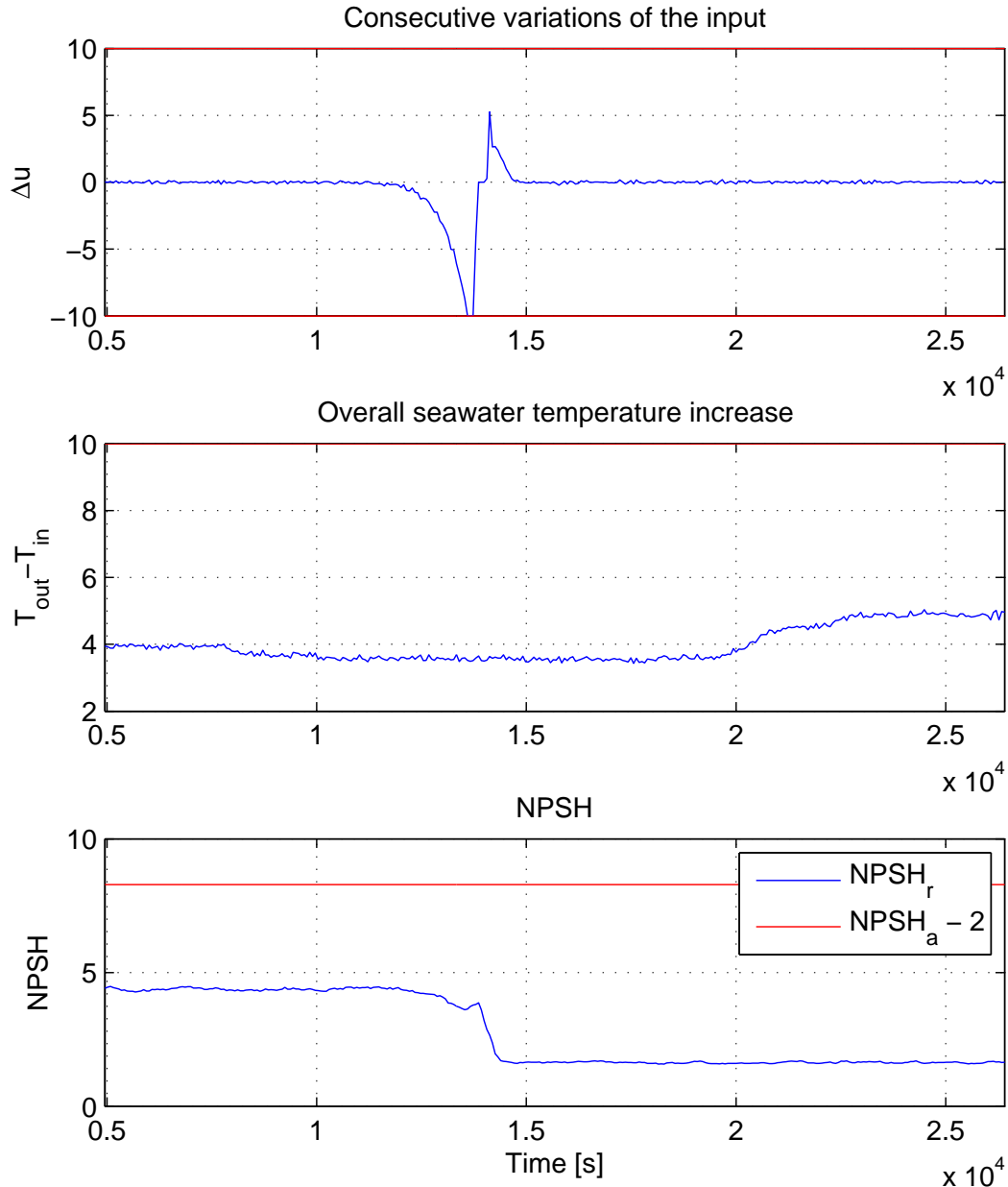
Figure 8.30. NPSH, seawater temperature increase and variation rate of the rotational speed of the pumps, which are subject to constraints that must be respected by the MPC controller.

The impact of the delay on the behavior of the controller is limited when using the flow of seawater used in the cost function. However, the controller can still achieve the target pressure, since the output measurement is used to generate a flow estimate according to the model of the system. This is due to the LKF relying on the model over the measurements.

In this chapter, two main control approaches have been proposed. The first consists of a PI regulator to control the flow of seawater and a slower integral controller to drive the pressure in the outer loop. The second approach uses an MPC controller. While the first solution is simpler, the second solution provides better constraint management and shows better performance in the simulations.

Part IV

Conclusions

Conclusions and Perspective 9

This chapter will analyze how the proposed solution fulfills the primary and secondary goals of the project. It will as well explore the future steps required for the implementation of the solution.

9.1 Conclusions

In this project, the current state of the plant has been described and a series of primary and secondary goals have been set, based on the proposal by Rambøll A/S. Following these objectives:

- Models for the hydraulic and the thermodynamic parts of the main cooling system in Studstrup have been proposed. The relevant parameters involved in the models have been identified.
- The models have been validated using real plant operation data.
- The estimation of the flow of seawater has been improved using an EKF (Extended Kalman Filter).
- A control solution based on an inner and an outer loop control using a PI and an integral controller has been proposed. This solution has the advantage of being simpler and requiring less computational power than the second solution.
- A second control strategy based on MPC (Model Predictive Control) has been proposed. It has the advantage to incorporate constraints in the optimization:

  - Lower pressure limit. This respects the limitations of the turbine by preventing the outlet steam from containing too much liquid. That would lead to the formation of droplets and cause wear in the blades.
  - Maximum seawater temperature increase. This is necessary to comply with the local environmental directives.
  - Pump limits. The controller respects the maximum and minimum allowed RPM and the maximum variation rate of the pumps. It also avoids cavitation by ensuring the availabe NPSH is above the required value by a safety threshold.

- The controllers follow a condensation pressure reference. If determined correctly, this should lead the plant to the operation point that maximizes its efficiency.
- The controllers have been designed with a focus on robustness over speed, minimizing overshoot and oscillatory behavior.
- The solution can be adapted to other similar power plants with similar characteristics. Both tuning methods proposed are online methods. However, MPC relies on a model of the plant and all requirements in Section 8.3.1 must be met if the proposed tuning procedure for MPC is to be implemented.

Therefore, all primary and secondary requirements stated in the Problem Definition have been met. However, there is a number of considerations that need to be taken into account when implementing such solution that will be discussed hereafter.

9.2 Perspective

In this project, a solution to estimate the seawater flow and control the cooling system was proposed. Both require a good model of the system, which can be difficult to achieve online. In order to make the estimation and control solution easy portable to other similar power plants, an online model detection should be made. The detected model can then be used in the construction of the estimator and controller.

The proposed seawater estimator is only considering fouling in the condenser. If fouling occurs in other parts of the hydraulic system, such as the TAPROGGE filter, good estimation of the seawater is not guaranteed. But as the estimator is constructed with respect to sensor fusion, there will only be one measurement out of four that produces inaccurate estimation. It is therefore assumed that the three other measurements will keep the estimation within an acceptable range of the real seawater flow.

The control results presented in this report have been generated using a linearized version of the model of the system. Inaccuracies in both the modeling and linearization of the system may result in a different behavior of the real plant. The validity of the model is also constrained by the available operational data. Only data from October to March was available for modeling and validation purposes. There is no guarantee that the behavior of the plant during the warmer months of summer can be represented by the proposed models and, thus, that the control strategy will perform as desired. This will be especially relevant in the case of the thermodynamic model, since the inlet temperature of seawater and the flow of steam into the condenser (less DH is required during summer) will be different.

Two control solutions have been presented. The first solution is based on an inner loop controller for the flow of seawater and an outer loop controller for the condensation pressurue. The second solution uses MPC to control the flow and uses an LKF to incorporate the delayed output measurements into the control. The first solution has the advantage of being simpler to implement and tune, and requires fewer assumptions on the behavior of the system. The MPC solution, on the other hand, provides better constraint handling and improved performance and robustness, but requires a model of the system and more assumptions on the behavior of the plant. MPC requires as well as a higher computational power to perform the optimization of the cost function.

Bibliography

A Gretton, **2008**. L. Gyorfi A Gretton. *Nonparametric Independence Tests: Space Partitioning and Kernel Approaches*. ALT 19, 2008.

Arthur G.O. Mutambara, **1999**. Marwin S.Y. Al-Haik Arthur G.O. Mutambara. *EKF based Parameter Estimation for a Heat Exchanger*. Proceedings of the American Control Conference, San Diego, CA, 1999.

Danish Energy Agency, **2014a**. Danish Energy Agency. *Large and small scale district heating plants*. URL:`http://www.ens.dk/en/supply/heat-supply-denmark/large-small-scale-district-heating-plants` Copy on the cd 💿 Sources/Large and small scale district heating plants Energistyrelsen.pdf , 2014.

Danish Energy Agency, **2014b**. Danish Energy Agency. *Basic Facts on Heat Supply in Denmark*. URL:`http://www.ens.dk/node/1992` Copy on the cd 💿 Sources/Basic facts on Heat Supply in Denmark Energistyrelsen.pdf , 2014.

DONG Energy, **2014a**. DONG Energy. *The Studstrupværket CHP plant*. URL:`http://ipaper.ipapercms.dk/DONGENERGY/Internet/UK/ThermalPower/SSVbrochure2012UK/` Copy on the cd 💿 Sources/DONG THE STUDSTRUPVÆRKET.pdf , 2014.

DONG Energy, **2014b**. DONG Energy. *District heating: Combined heat and power*. URL:`http://www.dongenergy.com/en/business%20activities/generation/activities/pages/district_heating.aspx` Copy on the cd 💿 Sources/DONG Energy District heating Combined heat and power.pdf , 2014.

European Directive 2004/8/EC, **2004**. European Directive 2004/8/EC. *Directive on the promotion of cogeneration based on a useful heat demand in the internal energy market and amending Directive 92/62/EEC*, 2004.

George Karleskint, Richard Turner. James Small George Karleskint, Richard Turner. *Introduction to Marine Biology*. ISBN: 978-1285402222. Cengage Learning.

Guðmundsson, **2008**. Oddgeir Guðmundsson. Detection of Fouling in Heat Exchangers. Master's thesis, University of Iceland, 2008.

International Energy Agency, **2011**. International Energy Agency. *Energy Policies of IEA Countries: Denmark*, 2011.

Jovic, **2013**. Vinko Jovic. *Analysis and Modelling of Non-Steady Flow in Pipe and Channel Networks*. ISBN: 978-1-118-53214-0. John Wiley & Sons Inc, 2013.

Kreith, **1986**. F. Kreith. *Principles of Heat Transfer*. Harper & Row, 3rd edition, 1986.

Lawson. Thomas B. Lawson. *Fundamentals of Aquacultural Engineering*. ISBN: 978-0412065118. Springer.

Massoud, **2005**. Dr. Mahmoud Massoud. *Engineering Thermofluids: Thermodynamics, Fluid Mechanics, and Heat Transfer*. ISBN: 978-3-540-22292-7. Springer Berlin Heidelberg, 2005.

Michael J. Moran, Howard N. Shapiro, **2005**. Daisie D. Boettner Margaret B. Bailey Michael J. Moran, Howard N. Shapiro. *Fundamentals of Engineering Thermodynamics*. 7th edition, 2005.

Michael R. Lindeburg, **2013**. PE Michael R. Lindeburg. *Mechanical Engineering Reference Manual for the PE Exam*. ISBN: 978-1591264149. Professional Publications, Inc., 13th edition, 2013.

Nedelkovski, Vilos, and Geramitcioski, **2005**. Igor Nedelkovski, Ilios Vilos, and Tale Geramitcioski. *Method for Optimal Control of Power Plant Cooling System*. WEC (5), pages 209–211, 2005.

Ott and Wojsznis, **1995**. Michael G Ott and Willy K Wojsznis. *Auto-tuning: from Ziegler-Nichols to model based rules*. Proceedings of the ISA/95 Conference, pages 323–332, 1995.

Ralph F. Hinde, **1994**. Douglas J. Cooper Ralph F. Hinde. *A Pattern-Based Approach to Excitation Diagnostics for Adaptive Process Control*. Chemical Engineering Science, Vol. 49, No. 9, pp. 1403-1415, 1994.

Steve Wilson, Grundfos A/S. Steve Wilson, Grundfos A/S. *System Curves*. URL:`http://www.grundfos.com/content/dam/CBS/global/whitepapers/Whitepaper%20-%20System%20Curves.pdf`.

TAPROGGE, **2014**. TAPROGGE. *Tube Cleaning for Power Stations and Industry*. URL:`http://www.taprogge.de/products-and-services/in-ta-ctR/tube-cleaning/generating-industry/index.htm` Copy on the cd 💿 Sources/Tube Cleaning for Power Stations and Industry TAPROGGE.pdf , 2014.

W. Y. Svrcek, D. P. Mahoney, **2013**. B. R. Young W. Y. Svrcek, D. P. Mahoney. *A Real-Time Approach to Process Control*. 2nd edition, 2013.

White. Frank M. White. *Fluid Mechanics*. ISBN: 978-0-07-352934-9. McGraw-Hill, 7th edition.

Wilson, **1915**. E. E. Wilson. *A basis for rational design of heat transfer apparatus*. Trans. Am. Soc. Mech. Engrs., 37, 47-70, 1915.

Yanus A. Cengel, **2012**. John M. Cimbala Yanus A. Cengel. *Fundamentals of Thermal-Fluid Sciences*. McGraw-Hill, 5th edition, 2012.

Part V

Appendix

Table of Contents - Appendix

Pipe Dynamics A

The models of the pipes and valves are made for the seawater part. The seawater is assumed incompressible and the pipeline is assumed to consist of rigid pipes. The flow is assumed to be turbulent throughout the pipeline system. In order to derive a mathematical expression of a flow in a pipeline, the conservation of energy is considered. In Equation A.1 the energy balance in a pipeline is shown, where the change in energy in the control volume is the sum of surface forces affecting the control volume [Jovic, 2013].

$$\frac{dU}{dt} + \frac{dE_p}{dt} + \frac{dE_k}{dt} = \frac{d(W_n + W_o)}{dt} \tag{A.1}$$

where:

U	Internal energy of the control volume	$[J]$
E_p	Potential energy of the control volume	$[J]$
E_k	Kinetic energy of the control volume	$[J]$
W_n	Work of normal forces	$[J]$
W_o	Work of resistance forces	$[J]$

Internal Energy

The internal energy is related to the volumetric strain of the seawater. The change in internal energy is expressed as Equation A.2, where the change in the internal forces is the expansion of the control volume [Jovic, 2013].

$$\dot{U} = -\int_{l_1}^{l_2} p \cdot \varepsilon \, dl = -\int_{l_1}^{l_2} p \cdot \left(\frac{\partial A}{\partial t} + \frac{\partial q}{\partial l} \right) dl \tag{A.2}$$

where:

$\dot{U}$	Rate of change in the internal energy of the control volume	$[J/s]$
p	Pressure in the pipeline	$[kg/m \cdot s^2]$
ε	Rate of the volumetric strain	$[m^2/s]$
A	Cross section area of the pipe	$[m^2]$
q	Volumetric flow	$[m^3/s]$

Potential Energy

The change in potential energy is found through the elevation of the fluid and is expressed as Equation A.3 [Jovic, 2013].

$$\dot{E}_p \;=\; \int\limits_{l_1}^{l_2} \rho \cdot g \cdot q \cdot \frac{\partial z}{\partial l} dl \tag{A.3}$$

where:

$\dot{E}_p$	Rate of change in the potential energy of the control volume	$[J/s]$
ρ	Density of fluid	$[kg/m^3]$
g	Gravity acceleration	$[m/s^2]$
q	Volumetric flow	$[m^3/s]$
z	Elevation of fluid	$[m]$

Kinetic Energy

The change in kinetic energy is the change of kinetic energy in the control volume and the change of kinetic energy flow in and out of the control volume through the control cross sections [Jovic, 2013]. The change in kinetic energy is expressed as Equation A.4.

$$\dot{E}_k \;=\; \int\limits_{l_1}^{l_2} \rho \cdot q \cdot \left(\frac{\partial(\beta \cdot v)}{\partial t} + \frac{\partial}{\partial l} \frac{\alpha \cdot v^2}{2} + \zeta \cdot \frac{v^2}{2} \right) dl \tag{A.4}$$

where:

$\dot{E}_k$	Rate of change in the kinetic energy of the control volume	$[J/s]$
ρ	Density of fluid	$[kg/m^3]$
q	Volumetric flow	$[m^3/s]$
v	Mean flow velocity	$[m/s]$
α	Coriolis coefficient	$[-]$
β	Boussinesq coefficient	$[-]$
ζ	Change of friction	$[-]$

The Coriolis and Boussinesq coefficient will in case of turbulent flow be close to one. Change of friction is expressed as Equation A.5 [Jovic, 2013]. As the flow in the pipes is assumed to be turbulent, the change of friction will be close to zero at all time.

$$\zeta \;=\; \frac{1}{\rho \cdot q} \cdot \frac{\partial(\rho \cdot q)}{\partial l} \cdot (\alpha - \beta) \tag{A.5}$$

where:

ζ	Change of friction	$[-]$
ρ	Density of fluid	$[kg/m^3]$
q	Volumetric flow	$[m^3/s]$
α	Coriolis coefficient	$[-]$
β	Boussinesq coefficient	$[-]$

Normal Forces

The change in the work of normal forces is the change in work of the pressure forces at the inlet and outlet. The change in the work of normal forces is expressed as Equation A.6 [Jovic, 2013].

$$\dot{W}_n \;=\; -\int_{l_1}^{l_2} p \cdot \left(\frac{\partial A}{\partial t} + \frac{\partial q}{\partial l} \right) dl - \int_{l_1}^{l_2} q \cdot \frac{\partial p}{\partial l} dl \tag{A.6}$$

where:

$\dot{W}_n$	Rate of change in the work of normal forces of the control volume	$[J/s]$
p	Pressure in the pipeline	$[kg/m \cdot s^2]$
A	Cross section area of the pipe	$[m^2]$
q	Volumetric flow	$[m^3/s]$

Resistance Forces

As the flow is assumed turbulent, the Darcy-Weissbach equation is used to calculate the rate of change in work of resistance forces. Equation A.7 is the calculation of the work of resistance forces in a circular cross section pipe [Jovic, 2013].

$$\dot{W}_o \;=\; -\rho \cdot q \cdot \frac{\lambda \cdot L}{2 \cdot D} \cdot |v| \cdot v \tag{A.7}$$

where:

$\dot{W}_o$	Rate of change in work of resistance forces	$[J/s]$
ρ	Density of fluid	$[kg/m^3]$
q	Volumetric flow	$[m^3/s]$
λ	Friction coefficient	$[-]$
L	Pipeline length	$[m]$
D	Pipe diameter	$[m]$
v	Mean flow velocity	$[m/s]$

Pipe Model

In Equation A.8 the equations from Equation A.1 to A.7 is connected.

$$L \cdot \rho \cdot \frac{\partial v}{\partial t} + \int_{l_1}^{l_2} \rho \cdot \left(g \cdot \frac{\partial z}{\partial l} + \frac{\partial}{\partial l} \frac{v^2}{2} + \frac{\partial}{\partial l} \frac{p}{\rho} \right) dl + \rho \cdot \frac{\lambda \cdot L}{2 \cdot D} \cdot |v| \cdot v \; = \; 0 \qquad \text{(A.8)}$$

where:

L	Pipeline length	$[m]$
ρ	Density of fluid	$[kg/m^3]$
v	Mean flow velocity	$[m/s]$
g	Gravity acceleration	$[m/s^2]$
z	Elevation of fluid	$[m]$
p	Pressure in the pipeline	$[kg/m \cdot s^2]$
λ	Friction coefficient	$[-]$
D	Pipe diameter	$[m]$

The head across the pipe is expressed as Equation A.9 [Jovic, 2013].

$$H \; = \; z + \frac{1}{2 \cdot g} \cdot v^2 + \frac{1}{\rho \cdot g} \cdot p \qquad \text{(A.9)}$$

where:

H	Head	$[m]$
z	Elevation of fluid	$[m]$
g	Gravity acceleration	$[m/s^2]$
v	Mean flow velocity	$[m/s]$
ρ	Density of fluid	$[kg/m^3]$
p	Pressure in the pipeline	$[kg/m \cdot s^2]$

By connecting Equation A.8 and A.9, the dynamic model of the pipe is expressed as Equation A.10.

$$\frac{L}{g \cdot A} \cdot \dot{q} \; = \; - \frac{\lambda \cdot L}{g \cdot 2 \cdot D \cdot A^2} \cdot |q| \cdot q + (H_1 - H_2) \qquad \text{(A.10)}$$

where:

q	Volumetric flow	$[m^3/s]$
$H1$	Head at inlet	$[m]$
$H2$	Head at outlet	$[m]$
L	Pipeline length	$[m]$
g	Gravity acceleration	$[m/s^2]$
A	Cross section area of the pipe	$[m^2]$
λ	Friction coefficient	$[-]$
D	Pipe diameter	$[m]$

In Equation A.11 the head in Equation A.10 is changed to pressure. The J parameter is referred to as the fluid inertance and K is referred to as the fluid resistance coefficient [Michael R. Lindeburg, 2013].

$$J \cdot \dot{q} \;=\; -K \cdot |q| \cdot q + \Delta p \qquad (A.11)$$

$$J \;=\; \frac{\rho \cdot L}{A} \qquad (A.12)$$

$$K \;=\; \frac{\rho \cdot \lambda \cdot L}{2 \cdot D \cdot A^2} \qquad (A.13)$$

where:

q	Volumetric flow	$[m^3/s]$
Δp	Pressure drop across the pipe	$[kg/m \cdot s^2]$
L	Pipeline length	$[m]$
ρ	Density of fluid	$[kg/m^3]$
A	Cross section area of the pipe	$[m^2]$
λ	Friction coefficient	$[-]$
D	Pipe diameter	$[m]$

In Equation A.11 the part Δp is the pressure drop across the pipe and as the fluid can flow in both direction the volumetric flow is not squared, but $(|q| \cdot q)$. Both the J and K_p are depending on the pipe dimensions.

NPSH Available B

The calculation of the available NPSH is given by Equation 3.4 on page 16. This calculation does not consider the situation, where the pump is placed higher or lower than the suction reservoir. By using Bernoulli's equation, the NPSH available at a given pump placement relative to the suction reservoir is given by Equation B.1 [White].

$$NPSH_A \ = \ \frac{p_a}{\rho \cdot g} - z - H_{fi} - \frac{p_v}{\rho \cdot g} \tag{B.1}$$

where:

$NPSH_A$	NPSH available for the pump	$[m]$
p_a	Surface pressure at suction reservoir	$[Pa]$
ρ	Density of fluid	$[kg/m^3]$
g	Gravity acceleration	$[m/s^2]$
z	Elevation of fluid	$[m]$
H_{fi}	Head loss caused by pipe friction	$[m]$
p_v	Vapor pressure of the liquid	$[Pa]$

The Surface pressure at the suction reservoir is assumed atmospheric pressure. The head loss in the pipe from the suction reservoir to the pump is assumed to be so small, that it can be neglected. The elevation of the fluid is measured in the water level measurement. Table B.1 contains the vapor pressure of water at a given temperature and in Equation B.2 the calculation from vapor pressure of water to vapor pressure of seawater is shown [Lawson].

Temperature [$°C$]	Vapor pressure [Pa]
0	611
10	1227
20	2337
30	4242
40	7375

Table B.1. Relation between temperature and the vapor pressure of water [White].

$$p_{vsw} \ = \ (1.000016 - 0.000537 \cdot \rho_{salt}) \cdot p_{vw} \tag{B.2}$$

where:

p_{vsw}	Vapor pressure of seawater	$[Pa]$
p_{vw}	Vapor pressure of water	$[Pa]$
ρ_{salt}	Salinity	$[g/L]$

As the salinity in seawater is approximately 3.5% [George Karleskint], the (ρ_{salt}) is approximately 35. In table B.2 the vapor pressure of seawater at a given temperature is shown.

Temperature [°C]	Vapor pressure [Pa]
0	599.5
10	1204
20	2293.1
30	4162.3
40	7236.5

Table B.2. Relation between temperature and the vapor pressure of seawater.

The highest temperature of the seawater at the inlet is assumed never to exceed 30°C and thereby the highest vapor pressure will never exceed 4162.3 Pa. In Equation B.3 the NPSH available for the pump at a given water level is shown. The equation is derived from Equation B.1, where p_v is 4162.3 Pa, p_a is 101325 Pa and H_{fi} is assumed zero. The z parameter is derived from Equation 2.3 on page 9, where there is an offset in the seawater level measurement, which is 2.58m.

$$NPSH_A \;=\; 12.2902 - WL \tag{B.3}$$

where:

$NPSH_A$	NPSH available for the pump	$[m]$
WL	Water level measured by sensor	$[m]$

Model Fitting Results C

Hydraulic Model

Pipeline Model

The pipeline model is fitted to data from the power plant. The parameters found in the fit are shown in Table C.1 and C.2. The values of the fluid inertance in the table is used, when the input to the model is pressure. When the pipeline model is including the pump model and the input thereby is RPM, the values of the fluid inertance is multiplied by 4.5 in order to fit the model.

$K_{line1} = 10.1382 \cdot 10^2$	$K_{p1} \approx 0$	$K_{ls1} = 10.1382 \cdot 10^2$
$K_m = 340.9848$	$K_{p2} \approx 0$	$K_{ls2} = 10.1382 \cdot 10^2$

Table C.1. The values of the fluid resistance coefficients

$J_{line1} = 32.8091 \cdot 10^5$	$J_{p1} \approx 0$	$J_{ls1} = 32.8091 \cdot 10^5$
$J_m = 16.21 \cdot 10^5$	$J_{p2} \approx 0$	$J_{ls2} = 32.8091 \cdot 10^5$

Table C.2. The values of the fluid inertance

Linearized Pipeline Model

The parameters of the linearized pipeline model is found in table C.3.

$a_{l1} = -91.2273 \cdot 10^{-4}$	$b_{l1} = 24.4814 \cdot 10^{-5}$

Table C.3. Parameters for the linearized pipeline model

Pump Model

The pump head function is fitted to the pump head curve. The function is given by Equation C.1 and the parameters to the function are shown in Table C.4.

$$
\begin{aligned}
H(n, q) &= H_1(n) + H_2(q) + H_3(n, q) & \text{(C.1)} \\
H_1(n) &= ph_{00} + ph_{10} \cdot n + ph_{20} \cdot n^2 + ph_{30} \cdot n^3 + ph_{40} \cdot n^4 + ph_{50} \cdot n^5 \\
H_2(q) &= ph_{01} \cdot q + ph_{02} \cdot q^2 + ph_{03} \cdot q^3 + ph_{04} \cdot q^4 + ph_{05} \cdot q^5 \\
H_3(n, q) &= (ph_{11} \cdot q + ph_{12} \cdot q^2 + ph_{13} \cdot q^3 + ph_{14} \cdot q^4) \cdot n \\
&\quad + (ph_{21} \cdot q + ph_{22} \cdot q^2 + ph_{23} \cdot q^3) \cdot n^2 \\
&\quad + (ph_{31} \cdot q + ph_{32} \cdot q^2) \cdot n^3 + (ph_{41} \cdot q) \cdot n^4
\end{aligned}
$$

where:

$H(n,q)$	Head function of pump	$[m]$
n	Revolutions per minute	$[RPM]$
q	Volumetric flow	$[m^3/s]$

$ph_{00} = -21.64$	$ph_{01} = -0.1252$	$ph_{02} = -0.0442$
$ph_{03} = -0.08837$	$ph_{04} = -0.006856$	$ph_{05} = 0.0007432$
$ph_{10} = 0.4966$	$ph_{11} = -0.001028$	$ph_{12} = 0.004182$
$ph_{13} = 0.000748$	$ph_{14} = -4.009 \cdot 10^{-5}$	$ph_{20} = -0.004045$
$ph_{21} = -6.887 \cdot 10^{-5}$	$ph_{22} = -2.385 \cdot 10^{-5}$	$ph_{23} = 1.186 \cdot 10^{-7}$
$ph_{30} = 1.714 \cdot 10^{-5}$	$ph_{31} = 2.981 \cdot 10^{-7}$	$ph_{32} = 2.162 \cdot 10^{-8}$
$ph_{40} = -3.287 \cdot 10^{-8}$	$ph_{41} = -3.478 \cdot 10^{-10}$	$ph_{50} = 2.41 \cdot 10^{-11}$

Table C.4. The parameters to the pump head function

The pump power function is fitted to the power curve. The function is given by Equation C.2 and the parameters to the function are shown in Table C.5.

$$
\begin{aligned}
P(n,q) &= P_1(n) + P_2(q) + P_3(n,q) & \text{(C.2)} \\
P_1(n) &= pP_{00} + pP_{10} \cdot n + pP_{20} \cdot n^2 + pP_{30} \cdot n^3 + pP_{40} \cdot n^4 + pP_{50} \cdot n^5 \\
P_2(q) &= pP_{01} \cdot q + pP_{02} \cdot q^2 + pP_{03} \cdot q^3 + pP_{04} \cdot q^4 + pP_{05} \cdot q^5 \\
P_3(n,q) &= (pP_{11} \cdot q + pP_{12} \cdot q^2 + pP_{13} \cdot q^3 + pP_{14} \cdot q^4) \cdot n \\
&\quad + (pP_{21} \cdot q + pP_{22} \cdot q^2 + pP_{23} \cdot q^3) \cdot n^2 \\
&\quad + (pP_{31} \cdot q + pP_{32} \cdot q^2) \cdot n^3 + (pP_{41} \cdot q) \cdot n^4
\end{aligned}
$$

where:

$P(n,q)$	Power function of pump	$[kW]$
n	Revolutions per minute	$[RPM]$
q	Volumetric flow	$[m^3/s]$

$pP_{00} = -865.3$	$pP_{01} = 0.2798$	$pP_{02} = 1.823$
$pP_{03} = -1.058$	$pP_{04} = -0.3024$	$pP_{05} = 0.02096$
$pP_{10} = 19.57$	$pP_{11} = -0.06067$	$pP_{12} = 0.01114$
$pP_{13} = 0.01526$	$pP_{14} = -0.001096$	$pP_{20} = -0.1698$
$pP_{21} = 0.0002347$	$pP_{22} = -5.747 \cdot 10^{-5}$	$pP_{23} = 1.83 \cdot 10^{-5}$
$pP_{30} = 0.0007673$	$pP_{31} = -4.564 \cdot 10^{-6}$	$pP_{32} = -3.979 \cdot 10^{-7}$
$pP_{40} = -1.561 \cdot 10^{-6}$	$pP_{41} = 9.485 \cdot 10^{-9}$	$pP_{50} = 1.305 \cdot 10^{-9}$

Table C.5. The parameters to the pump power function

The pump NPSH function is fitted to the NPSH curve. The function is given by Equation C.3 and the parameters to the function are shown in Table C.6.

$$NPSH_R(n,q) = pNPSH_{00} + pNPSH_{10} \cdot n + pNPSH_{01} \cdot q + pNPSH_{20} \cdot n^2 \quad \text{(C.3)}$$
$$+ pNPSH_{11} \cdot n \cdot q + pNPSH_{02} \cdot q^2$$

where:

$NPSH_R(n,q)$	NPSH required by pump	$[m]$
n	Revolutions per minute	$[RPM]$
q	Volumetric flow	$[m^3/s]$

$pNPSH_{00} = -4.446 \cdot 10^{-2}$	$pNPSH_{01} = 0.01823$	$pNPSH_{02} = 1.118$
$pNPSH_{10} = -2.235 \cdot 10^{-4}$	$pNPSH_{11} = -0.0541$	$pNPSH_{20} = 7.322 \cdot 10^{-4}$

Table C.6. The parameters to the pump NPSH function

Thermodynamic Model

Condenser Pressure Model

The data-driven condenser model has given the following results for the operating conditions analyzed:

Static model:

$$p_{cond}(t) = a_0 + a_1 \Delta T_{tot}(t) + a_2 x_{data}(t - \theta_{steam}) + a_3 \dot{m}_{sw}(t - \theta_{sw}) + a_4 T_{sw,in} \quad \text{(C.4)}$$

a_0	0.0029	$[bar]$
a_1	0.0011	$[bar/°C]$
a_2	$1.4586 \cdot 10^{-9}$	$[bar/kW]$
a_3	$1.2217 \cdot 10^{-7}$	$[bar \cdot s/kg]$
a_4	$9.7473e - 4 \cdot 10^{-3}$	$[bar/°C]$
θ_{sw}	990.075	$[s]$
θ_{steam}	594.045	$[s]$

Linearized Condenser Model

$$p_{cond}(t) = d_0 + a_1 \Delta T(t) + a_3 \dot{m}_{sw}(t - \theta_{sw}) + a_4 T_{sw,in}(t) + d_{lin} \dot{m}_{steam}(t - \theta_{steam}) \quad \text{(C.5)}$$

The parameters obtained from the linearized condenser model (Equation C.5) are :

a_1	$-6.41 \cdot 10^{-6}$	$[bar/°C]$
a_3	$-5.10 \cdot 10^{-7}$	$[bar \cdot s/kg]$
a_4	$1.30 \cdot 10^{-3}$	$[bar/°C]$
d_{lin}	$2.60 \cdot 10^{-5}$	$[bar \cdot s/kg]$
d_0	0.0068	$[bar]$
θ_{sw}	990.075	$[s]$
θ_{steam}	594.045	$[s]$

Condenser: Outlet Temperature Model

The outlet temperature of the seawater leaving the condenser has been fitted to the following expression:

$$T_{sw,out}(t) = f_1 + f_2 T_{sw,in}(t - \theta_p) + f_3 \dot{m}_{sw}(t - \theta_p) \quad \text{(C.6)}$$
$$+ f_4 T_{hotwell}(t - \theta_p) + f_5 p_{cond}(t - \theta_p)$$

f_1	0.1464	$[°C]$
f_2	0.9262	$[-]$
f_3	$9.9078 \cdot 10^{-5}$	$[°Cs/kg]$
f_4	0.0971	$[°C/bar]$
f_5	65.2421	$[°Cs/kg]$
θ_p	3300.25	$[s]$

Estimation of The Seawater Flow D

Pressure to Flow in TAPROGGE Filter

The flow estimation from the differential pressure across the TAPROGGE filter is done as in the case with the condenser. The value of the fluid resistance coefficient in the TAPROGGE filter is chosen by comparing the mean value of the flow estimation from the TAPROGGE filter to the flow estimation from the condenser. The value of the fluid resistance coefficient in the TAPROGGE filter is:

$$K_{filter} \; = \; 41$$

RPM And Head To Flow

The flow estimation from the pump head curve is given by Equation D.1 and the parameters to the pump flow function are shown in Table D.1.

$$
\begin{aligned}
Fh(n, H) \;&=\; Fh_1(n) + Fh_2(H) + Fh_3(n, H) & \text{(D.1)}\\
Fh_1(n) \;&=\; Fh_{00} + Fh_{10} \cdot n + Fh_{20} \cdot n^2 + Fh_{30} \cdot n^3 + Fh_{40} \cdot n^4 + Fh_{50} \cdot n^5\\
Fh_2(H) \;&=\; Fh_{01} \cdot H + Fh_{02} \cdot H^2 + Fh_{03} \cdot H^3 + Fh_{04} \cdot H^4 + Fh_{05} \cdot H^5\\
Fh_3(n, H) \;&=\; (Fh_{11} \cdot H + Fh_{12} \cdot H^2 + Fh_{13} \cdot H^3 + Fh_{14} \cdot H^4) \cdot n\\
&\quad + (Fh_{21} \cdot H + Fh_{22} \cdot H^2 + Fh_{23} \cdot H^3) \cdot n^2\\
&\quad + (Fh_{31} \cdot H + Fh_{32} \cdot H^2) \cdot n^3 + Fh_{41} \cdot H \cdot n^4
\end{aligned}
$$

where:

$Fh(n, H)$	Flow function from pump head curve	$[m^3/s]$
n	Revolutions per minute	$[RPM]$
H	Pump head	$[m]$

$Fh_{00} = -30.34$	$Fh_{01} = -7.664$	$Fh_{02} = 0.2285$
$Fh_{03} = 0.07732$	$Fh_{04} = -0.002082$	$Fh_{05} = -5.149 \cdot 10^{-5}$
$Fh_{10} = 0.83$	$Fh_{11} = 0.09356$	$Fh_{12} = -0.007127$
$Fh_{13} = -8.591 \cdot 10^{-5}$	$Fh_{14} = 1.716 \cdot 10^{-5}$	$Fh_{20} = -0.007763$
$Fh_{21} = -0.000461$	$Fh_{22} = 1.164 \cdot 10^{-5}$	$Fh_{23} = -1.3 \cdot 10^{-6}$
$Fh_{30} = 3.686 \cdot 10^{-5}$	$Fh_{31} = 1.674 \cdot 10^{-6}$	$Fh_{32} = 5.402 \cdot 10^{-8}$
$Fh_{40} = -9.079 \cdot 10^{-8}$	$Fh_{41} = -3.318 \cdot 10^{-9}$	$Fh_{50} = 9.638 \cdot 10^{-11}$

Table D.1. The parameters to the pump flow function, where the function is made from the pump head curve.

RPM And Power To Flow

The flow estimation from the pump power curve is given by Equation D.2 and the parameters to the function are shown in Table D.2.

$$
\begin{aligned}
Fp(n, P) &= Fp_1(n) + Fp_2(P) + Fp_3(n, P) && \text{(D.2)} \\
Fp_1(n) &= Fp_{00} + Fp_{10} \cdot n + Fp_{20} \cdot n^2 + Fp_{30} \cdot n^3 + Fp_{40} \cdot n^4 + Fp_{50} \cdot n^5 \\
Fp_2(P) &= Fp_{01} \cdot P + Fp_{02} \cdot P^2 + Fp_{03} \cdot P^3 + Fp_{04} \cdot P^4 + Fp_{05} \cdot P^5 \\
Fp_3(n, P) &= (Fp_{11} \cdot P + Fp_{12} \cdot P^2 + Fp_{13} \cdot P^3 + Fp_{14} \cdot P^4) \cdot n \\
&\quad + (Fp_{21} \cdot P + Fp_{22} \cdot P^2 + Fp_{23} \cdot P^3) \cdot n^2 \\
&\quad + (Fp_{31} \cdot P + Fp_{32} \cdot P^2) \cdot n^3 + Fp_{41} \cdot P \cdot n^4
\end{aligned}
$$

where:

$Fp(n, H)$	Flow function from pump power curve	$[m^3/s]$
n	Revolutions per minute	$[RPM]$
P	Pump power	$[m]$

$Fp_{00} = -97.58$	$Fp_{01} = -0.829$	$Fp_{02} = -24.43 \cdot 10^{-4}$
$Fp_{03} = -2.439 \cdot 10^{-6}$	$Fp_{04} = -9.159 \cdot 10^{-10}$	$Fp_{05} = -1.099 \cdot 10^{-13}$
$Fp_{10} = 2.828$	$Fp_{11} = 17.15 \cdot 10^{-3}$	$Fp_{12} = 3.581 \cdot 10^{-5}$
$Fp_{13} = 2.34 \cdot 10^{-8}$	$Fp_{14} = 4.398 \cdot 10^{-12}$	$Fp_{20} = -0.03121$
$Fp_{21} = -13.78 \cdot 10^{-5}$	$Fp_{22} = -1.802 \cdot 10^{-7}$	$Fp_{23} = -5.749 \cdot 10^{-11}$
$Fp_{30} = 17.37 \cdot 10^{-5}$	$Fp_{31} = 4.974 \cdot 10^{-7}$	$Fp_{32} = 3.074 \cdot 10^{-10}$
$Fp_{40} = -4.79 \cdot 10^{-7}$	$Fp_{41} = -6.728 \cdot 10^{-10}$	$Fp_{50} = 5.22 \cdot 10^{-10}$

Table D.2. The parameters to the pump flow function, where the function is made from the pump power curve.

Changes in The Flow Model

In order to simplify the calculation of the state and output matrix, the hydraulic model is changed, such that the fluid resistance parameters and fluid inertance parameters that are zero, is removed from the model and those that are equal is using the same parameter name such as $J_{ls} = J_{ls1} = J_{ls2}$ and $K_{ls} = K_{ls1} = K_{ls2}$. Thereby the inverse of the fluid inertance matrix is calculated:

$$
J^{-1} =
\begin{bmatrix}
\frac{1}{J_{ls}} & -\frac{1}{J_m} & \frac{1}{J_m} & 0 \\
-\frac{1}{J_m} & \frac{1}{J_{ls}} & 0 & \frac{1}{J_m} \\
\frac{1}{J_{ls}} & 0 & 0 & 0 \\
0 & \frac{1}{J_{ls}} & 0 & 0
\end{bmatrix}
$$

The $J^{-1} \cdot \lambda_{K1}(K_1, q)$ part of Equation 5.13 on page 26 is changed, such that it contains fouling parameters. With the fouling parameters, the fouling in the condensers are included in the model. It can thereby be calculated in another function:

$$\lambda_{KJ1}(q, K_{f1}, K_{f2}) = \begin{bmatrix} \frac{K_{ls}+K_{f1}}{J_{ls}} \cdot q_{ls1}^2 \\ \frac{K_{ls}+K_{f2}}{J_{ls}} \cdot q_{ls2}^2 \\ \frac{K_{ls}+K_{f1}}{J_{ls}} \cdot q_{ls1}^2 \\ \frac{K_{ls}+K_{f2}}{J_{ls}} \cdot q_{ls2}^2 \end{bmatrix} \qquad (D.3)$$

where:
K_{f1} Fluid resistance coefficient caused by fouling in condenser 1 $[kg/m^7]$
K_{f2} Fluid resistance coefficient caused by fouling in condenser 2 $[kg/m^7]$

The $J^{-1} \cdot \lambda_{K2}(K_2, q)$ part of Equation 5.13 is calculated in another function:

$$\lambda_{KJ2}(q) = \begin{bmatrix} \frac{K_m}{J_m} \cdot |q_{ls1} - q_{p1}| \cdot (q_{ls1} - q_{p1}) \\ -\frac{K_m}{J_m} \cdot |q_{p2} - q_{ls2}| \cdot (q_{p2} - q_{ls2}) \\ 0 \\ 0 \end{bmatrix} \qquad (D.4)$$

The $J^{-1} \cdot \lambda_p(\Delta p)$ part of Equation 5.13 is changed in order to use the head function $H(n, q)$, where the new function is:

$$\lambda_{pJ}(n, q) = \begin{bmatrix} (\frac{g \cdot \rho}{J_{ls}} + \frac{g \cdot \rho}{J_m}) \cdot H(n, q_{p1}) - \frac{g \cdot \rho}{J_m} \cdot H(n, q_{p2}) \\ (\frac{g \cdot \rho}{J_{ls}} + \frac{g \cdot \rho}{J_m}) \cdot H(n, q_{p2}) - \frac{g \cdot \rho}{J_m} \cdot H(n, q_{p1}) \\ \frac{g \cdot \rho}{J_{ls}} \cdot H(n, q_{p1}) \\ \frac{g \cdot \rho}{J_{ls}} \cdot H(n, q_{p2}) \end{bmatrix} \qquad (D.5)$$

where:
g Gravity acceleration $[m/s^2]$
ρ Density of fluid $[kg/m^3]$

The changed model of the hydraulic system is thereby:

$$\dot{q} = -\lambda_{KJ1}(q, K_{f1}, K_{f2}) - \lambda_{KJ2}(q) + \lambda_{pJ}(n, q) \qquad (D.6)$$

Process and Measurement Noise Covariance

The noise in the system is assumed white Gaussian noise with zero mean. In Appendix E on the next page the noise in the different measurements has the following properties:

$$
\begin{aligned}
v_{con1}[k] &\sim \mathcal{N}(0, 0.01) &,& \quad v_{con2}[k] &\sim \mathcal{N}(0, 0.01) \\
v_{filter1}[k] &\sim \mathcal{N}(0, 1200) &,& \quad v_{filter2}[k] &\sim \mathcal{N}(0, 1200) \\
v_{p1}[k] &\sim \mathcal{N}(0, 1600) &,& \quad v_{p2}[k] &\sim \mathcal{N}(0, 1600) \\
v_{w1}[k] &\sim \mathcal{N}(0, 3.7) &,& \quad v_{w2}[k] &\sim \mathcal{N}(0, 3.7)
\end{aligned}
$$

where:

$v_{con1}[k], v_{con2}[k]$	Noise in pressure measurement across condenser	$[kg/m \cdot s^2]$
$v_{filter1}[k], v_{filter2}[k]$	Noise in pressure measurement across TAPROGGE filter	$[kg/m \cdot s^2]$
$v_{p1}[k], v_{p2}[k]$	Noise in pressure measurement across pump	$[kg/m \cdot s^2]$
$v_{w1}[k], v_{w2}[k]$	Noise in power measurement in pump	$[kW]$

The measurement noise covariance is therefore:

$$
R = \begin{bmatrix}
0.01 & 0 & 0 & 0 & 0 & 0 & 0 & 0 \\
0 & 0.01 & 0 & 0 & 0 & 0 & 0 & 0 \\
0 & 0 & 1200 & 0 & 0 & 0 & 0 & 0 \\
0 & 0 & 0 & 1200 & 0 & 0 & 0 & 0 \\
0 & 0 & 0 & 0 & 3.7 & 0 & 0 & 0 \\
0 & 0 & 0 & 0 & 0 & 3.7 & 0 & 0 \\
0 & 0 & 0 & 0 & 0 & 0 & 1600 & 0 \\
0 & 0 & 0 & 0 & 0 & 0 & 0 & 1600
\end{bmatrix}
$$

The process noise covariance is found by fitting the EKF to the seawater fouling test model, which is found in Appendix E on the facing page. The process noise covariance is:

$$
Q = \begin{bmatrix}
10^{-11} & 0 & 0 & 0 & 0 & 0 \\
0 & 10^{-11} & 0 & 0 & 0 & 0 \\
0 & 0 & 10^{-11} & 0 & 0 & 0 \\
0 & 0 & 0 & 10^{-11} & 0 & 0 \\
0 & 0 & 0 & 0 & 5 \cdot 10^{-1} & 0 \\
0 & 0 & 0 & 0 & 0 & 5 \cdot 10^{-1}
\end{bmatrix}
$$

Seawater Fouling Test Model E

The seawater fouling test model is made in order to simulate fouling in the condenser. In the construction of the model only fouling occurring in the condenser is considered. The flow is modeled by using the discretized nonlinear dynamic model, which is shown in Equation 7.2 on page 73. The output model used in Section 7.4 on page 72, is used in the seawater fouling test model, where disturbances are added to make the model respond as the the real plant.

State dynamic :

$$
\begin{aligned}
q[k+1] \;=\; & -Ts \cdot \lambda_{KJ1}(q[k], K_{f1}, K_{f2}) - Ts \cdot \lambda_{KJ2}(q[k]) && \text{(E.1)} \\
& + Ts \cdot \lambda_{pJ}(n[k], q[k]) + q[k]
\end{aligned}
$$

where:

Ts	Sample time	$[s]$
K_{f1}	Fluid resistance coefficient caused by fouling in condenser 1	$[kg/m^7]$
K_{f2}	Fluid resistance coefficient caused by fouling in condenser 2	$[kg/m^7]$

Output :

$$
\begin{aligned}
\Delta p_{con1}[k] \;&=\; (K_c + K_{f1}) \cdot q_{p1}[k]^2 + v_{con1}[k] \\
\Delta p_{con2}[k] \;&=\; (K_c + K_{f2}) \cdot q_{p2}[k]^2 + v_{con2}[k] \\
\Delta p_{filter1}[k] \;&=\; K_{filter} \cdot q_{ls1}[k]^2 + v_{filter1}[k] \\
\Delta p_{filter2}[k] \;&=\; K_{filter} \cdot q_{ls2}[k]^2 + v_{filter2}[k] \\
P_{w1}[k] \;&=\; P(n_{p1}[k], q_{p1}[k]) + v_{w1}[k] \\
P_{w2}[k] \;&=\; P(n_{p2}[k], q_{p2}[k]) + v_{w2}[k] \\
\Delta p_1[k] \;&=\; g \cdot \rho \cdot H(n_{p1}[k], q_{p1}[k]) + v_{p1}[k] \\
\Delta p_2[k] \;&=\; g \cdot \rho \cdot H(n_{p2}[k], q_{p2}[k]) + v_{p2}[k]
\end{aligned}
$$

where:

$q_{p1}[k]$, $q_{p2}[k]$	Flow through pumps	$[m^3/s]$
$q_{ls1}[k]$, $q_{ls2}[k]$	Flow through condensers	$[m^3/s]$
$K_{f1}[k]$, $K_{f1}[k]$	Fouling in condensers	$[kg/m^7]$
K_c	Fluid resistance coefficient in condenser	$[kg/m^7]$
K_{filter}	Fluid resistance coefficient in TAPROGGE filter	$[kg/m^7]$
$p_{con1}[k]$, $p_{con2}[k]$	Pressure across condensers	$[kg/m \cdot s^2]$
$p_{filter1}[k]$, $p_{filter2}[k]$	Pressure across TAPROGGE filters	$[kg/m \cdot s^2]$
$P_{w1}[k]$, $P_{w2}[k]$	Power consumption in the pumps	$[kW]$
$\Delta p_1[k]$, $\Delta p_2[k]$	Pressure across the pumps	$[kg/m \cdot s^2]$
$n_{p1}[k]$, $n_{p2}[k]$	RPM in the pumps	$[RPM]$
g	Gravity acceleration	$[m/s^2]$
ρ	Density of fluid	$[kg/m^3]$
$v_{con1}[k], v_{con2}[k]$	Pressure measurement disturbances in condenser	$[kg/m \cdot s^2]$
$v_{filter1}[k], v_{filter2}[k]$	Pressure measurement disturbances in TAPROGGE filter	$[kg/m \cdot s^2]$
$v_{p1}[k], v_{p2}[k]$	Pressure measurement disturbances across pump	$[kg/m \cdot s^2]$
$v_{w1}[k], v_{w2}[k]$	Power measurement disturbance in pump	$[kW]$

All the disturbances in the system are assumed white Gaussian noise with zero mean. From data with constant RPM the covariances are calculated. The disturbances added to the model has the following properties:

$$v_{con1}[k] \sim \mathcal{N}(0, 0.01) \quad , \quad v_{con2}[k] \sim \mathcal{N}(0, 0.01)$$
$$v_{filter1}[k] \sim \mathcal{N}(0, 1200) \quad , \quad v_{filter2}[k] \sim \mathcal{N}(0, 1200)$$
$$v_{p1}[k] \sim \mathcal{N}(0, 1600) \quad , \quad v_{p2}[k] \sim \mathcal{N}(0, 1600)$$
$$v_{w1}[k] \sim \mathcal{N}(0, 3.7) \quad , \quad v_{w2}[k] \sim \mathcal{N}(0, 3.7)$$

The response of the model is compared with the response of the system, where the fluid resistance coefficient caused by fouling is put to zero. In Figure E.1 the flow through the condenser is shown. The graph to the left is the flow calculated by the model and the graph to the right is the flow estimation in the system. Generally the modeled flow follows the flow estimation at the power plant, but some of the spikes in the measurement shows higher flow than the model flow.
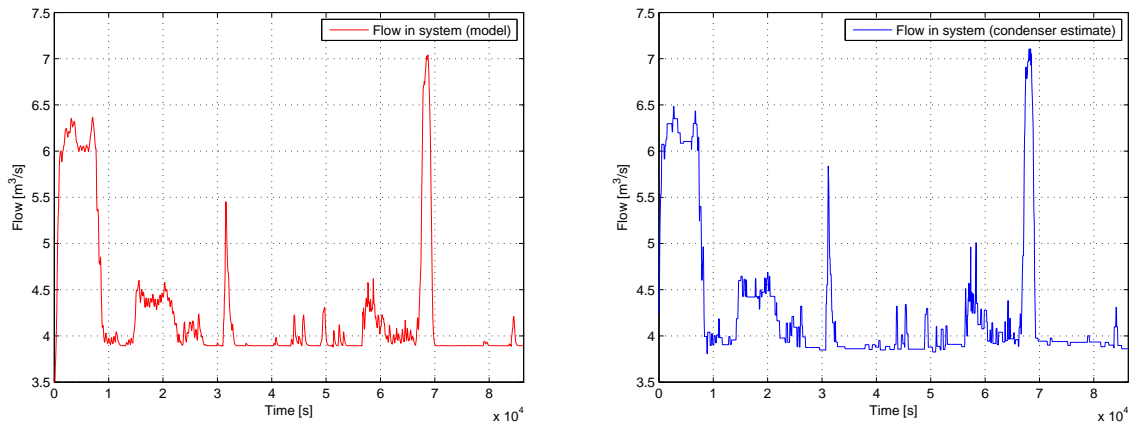
Figure E.1. The seawater flow, where the graph to the left is the flow from the model and the right graph is the flow estimation at the power plant.

In Figure E.2 the pressure across the pump is shown. The extra noise in the graph to the left is assumed to be caused by fast changes in the RPM. The model do not change the flow as fast causing the pressure model to use high flow at low RPM and vise versa.

Figure E.2. Pressure across the pump, where the left graph shows the pressure calculated by model and the right graph is the measured.

In Figure E.3 the power consumption of the pump is shown. The power calculated by the model shows the same behavior as the measured power.
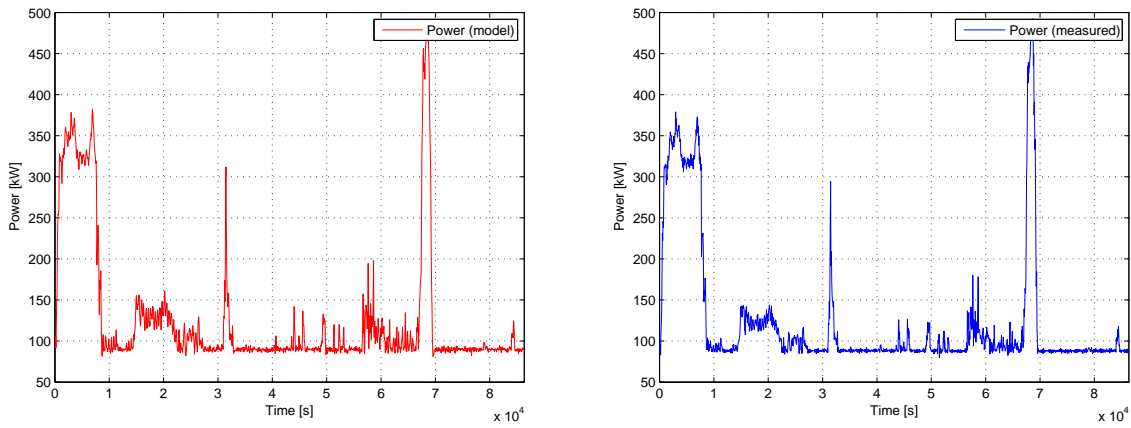
Figure E.3. Power consumption of pump, where the left graph shows the power calculated by model and the right graph is the measured.

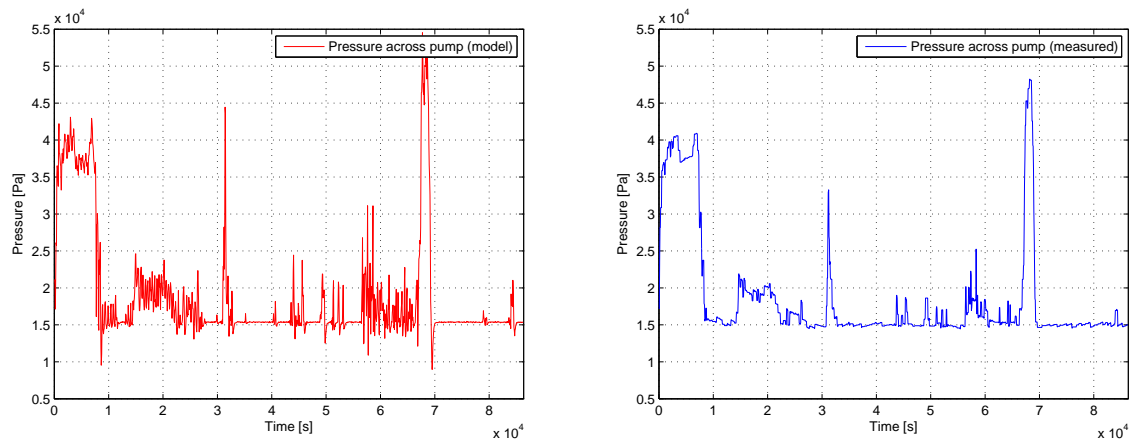The pressure across the condenser is shown in Figure E.4. In general the calculated pressure by the model shows the same behavior as the measured, but some of the spikes in the measurement are showing more pressure than the calculated pressure by the model. As the flow is used to calculate the pressure and the flow model shows the same differences between the estimated flow and the model flow, the flow model is assumed to cause the differences in the calculated and the measured pressure.
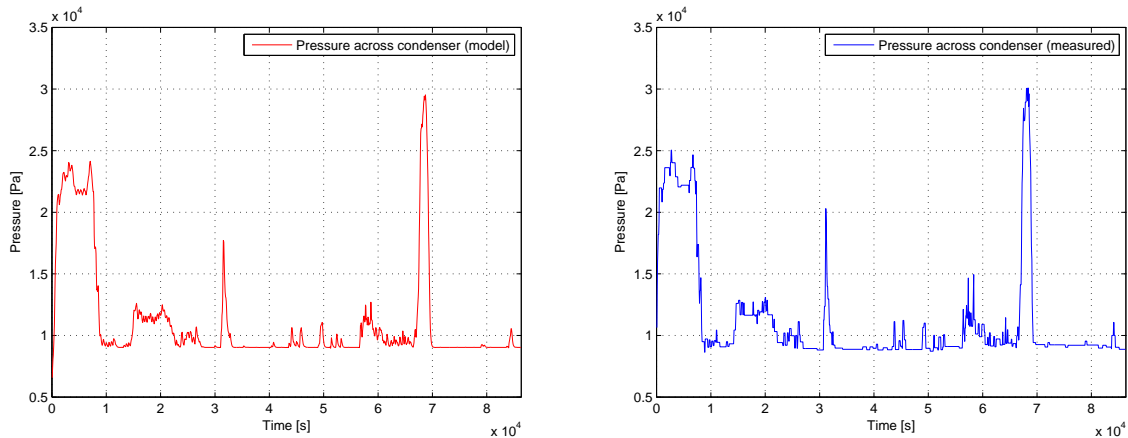
Figure E.4. Pressure across the condenser. The left graph shows the calculated pressure by model and the right graph shows the measured.

Differential pressure in the TAPROGGE filter is shown in Figure E.5. As in the case with the condenser pressure some of the spikes in the measurement are showing more pressure than the calculated pressure by the model. It is assumed that the flow model is causing the differences.

Figure E.5. Pressure across the TAPROGGE filter. The graph to the left shows the calculated pressure by model and the right graph shows the measured.
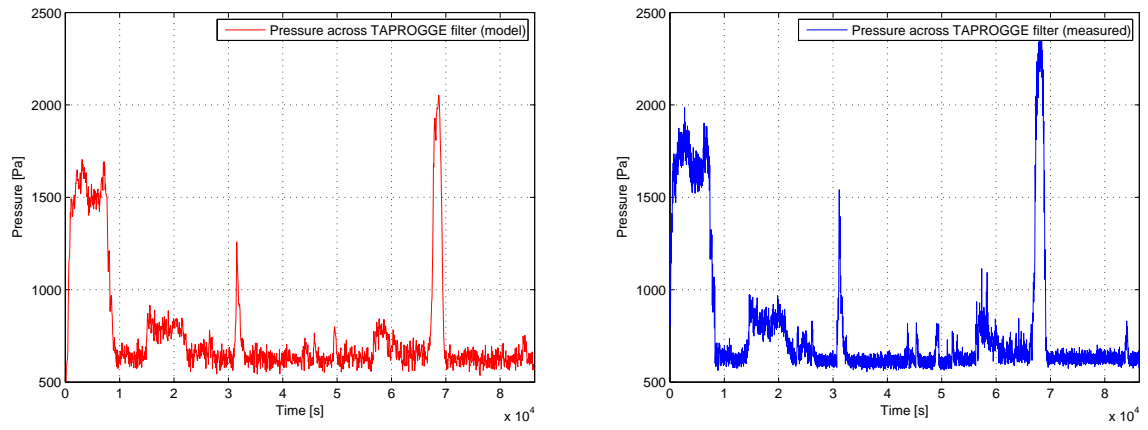
The model shows in general the same behavior as the system, only small differences are observed, which is assumed insignificant. The model is therefore assumed usable to test the EKF.

Controller Tuning Results $\mathbf{F}$

FOPDT Model Paramters

The FOPDT Model, given by:

$$G(s) \;=\; \frac{K_g}{\tau_g s + 1} e^{-\theta_g s} \tag{F.1}$$

has been identified to have the following parameters for the input-output system:

$K_g \;=\; -0.0269$	$\tau_g \;=\; 528.040$	$\theta_g \;=\; 1056.080$

And the following parameters for the input-to-state model:

$K_g \;=\; 0.138$	$\tau_g \;=\; 462$	$\theta_g \;=\; 0$

PID Controller (Cohen-Coon)

The controller is given by the Equation F.2:

$$u(t) \;=\; K_c \left(\epsilon(t) + \frac{1}{T_i} \int_0^t \epsilon(t) dt + T_d \frac{d\epsilon(t)}{dt} \right) \tag{F.2}$$

Where the control parameters K_c, T_i and T_d are computed from:

	K_c	T_i	T_d
PID	$\frac{P}{NL}(0.9 + \frac{R}{12})$	$L \cdot \frac{30+3R}{9+20R}$	$\frac{4L}{11+2R}$

The parameters computed from the reaction curve of the system are:

$P \;=\; 25.0000$	$N \;=\; -0.7288$	$L \;=\; 1056.0800$	$R \;=\; 132.0100$
$K_c \;=\; -1.1152$	$T_i \;=\; 169.8331$	$T_d \;=\; 15.3600$	

The anti-windup has been designed to cap the integral term of the controller at $\pm 10^{-3}$

PI and I controllers: IMC

The PI controller is given by the Equation F.3:

$$u(t) \;=\; K_c \left(\epsilon(t) + \frac{1}{T_i} \int_0^t \epsilon(t) dt \right) \tag{F.3}$$

Where the control parameters K_c and T_i are computed from:

$$K_c \;=\; \frac{\tau}{K_g(\tau_f + \theta_g)} \qquad T_i \;=\; \tau \tag{F.4}$$

132

The parameters used in the simulations are:

$\tau = 462\ s$	$\tau_f = 33000$	$K_c = 0.5204$	$T_i = 462$

The integral controller uses $T_i = 66.005$. The anti-windup limits the integration of the inner loop to 10^{-4} and the outer loop to $5 \cdot 10^{-1}$.

MPC Parameters

Cost function to be minimized:

$$J = \sum_{i=t}^{t+N_p} ((q_{ref,i} - \hat{q}_i)^2) + \sum_{i=t}^{t+N_u} (\Delta u_i^T Q \Delta u_i) \tag{F.5}$$

With:

$$Q = \Gamma K_g^2 \tag{F.6}$$

The tuning procedure has returned the following values:

$N_p = 3696\ s$	$N_c = 528\ s$	$\Gamma = 10^{-2}$

LKF Observer for MPC

The observer uses a sampling time of $T_s = 66.005\ s$. The noise covariance matrices are shown in Equation F.7. Q is a diagonal matrix; thus, all non-diagonal elements are zero. The noise is assumed white and Gaussian.

$$R = \sigma_{w_{out}}^2 \qquad Q = \begin{bmatrix} \sigma_{w_1}^2 & & & & & & \\ & \sigma_{w_2}^2 & & & & & \\ & & 0 & & & & \\ & & & \ddots & & & \\ & & & & \sigma_{w_7}^2 & & \\ & & & & & \ddots & \\ & & & & & & \sigma_{w_{16}}^2 \end{bmatrix} \tag{F.7}$$

The values of the variance of the noise are:

$\sigma_{w_{out}}^2 = 6.76 \cdot 10^{-10}$	$\sigma_{w_1}^2 = 4 \cdot 10^{-4}$	$\sigma_{w_2}^2 = 0.0017$
$\sigma_{w_7}^2 = 3.9737$	$\sigma_{w_{16}}^2 = 0.0068$	